Nonlinear Time History Analysis of Mass Regular and Irregular Multi-Storey Moment Resisting Steel Frames Using Force Analogy Method

A thesis submitted for the degree of

Doctor of Philosophy

by

Ningthoukhongjam Sukumar Singh

Department of Civil Engineering
Indian Institute of Technology Guwahati
Guwahati – 781039, India
December 2019

Nonlinear Time History Analysis of Mass Regular and Irregular Multi-Storey Moment Resisting Steel Frames Using Force Analogy Method

A thesis submitted for the degree of

Doctor of Philosophy

by

Ningthoukhongjam Sukumar Singh

Department of Civil Engineering
Indian Institute of Technology Guwahati
Guwahati – 781039, India
December 2019

DECLARATION

I, **Ningthoukhongjam Sukumar Singh**, a PhD Scholar of Indian Institute of Technology Guwahati declare that the content of this thesis entitled "***Nonlinear Time History Analysis of Mass Regular and Irregular Multi-Storey Moment Resisting Steel Frames Using Force Analogy Method***" submitted here is a partial fulfilment for the requirement of awarding the degree of **Doctor of Philosophy** and submitted in Indian Institute of Technology Guwahati, India. This thesis is the documentation of the research work carried out by me at the institute in a period of December 2012 to December 2019 under the supervision of **Konjengbam Darunkumar Singh**, Professor, Department of Civil Engineering, Indian Institute of Technology Guwahati, India. I certify that the content of this thesis is the original one and has not been used for awarding any other degree. The thesis content has not been published by any other person and the published works by others which I have consulted are always acknowledged in thesis by exact reference.

Date: **Ningthoukhongjam Sukumar Singh**

Place: (Reg. No. 126104038)

CERTIFICATE

This is to certify that the work content in the thesis entitled by "***Nonlinear Time History Analysis of Mass Regular and Irregular Multi-Storey Moment Resisting Steel Frames Using Force Analogy Method***" being submitted here by Mr. **Ningthoukhongjam Sukumar Singh** to Indian Institute of Technology Guwahati, India for the award of degree of **Doctor of Philosophy** is a record of genuine research work carried out by the aspirant being a PhD scholar under my supervision and guidance.

The thesis work, being shown is creditable of considering for the award of degree of **Doctor of Philosophy** in accordance with the regulation of the Institute.

(**Konjengbam Darunkumar Singh**)

Professor
Department of Civil Engineering
Indian Institute of Technology Guwahati

Date:

Place: IIT Guwahati

To the Lord

To my family members:

Ningthoukhongjam Thoibi Devi (Mother)

Ningthoujam Linthoingambi (Wife)

Lingjel Ningthoukhongjam (Daughter)

Athoibi Ningthoukhongjam (Daughter)

ABSTRACT

Building frames constructed in highly seismic zones are vulnerable to severe earthquakes and their susceptibilities to seismic effects are more pronounced if the building frames are 'irregular' in mass (i.e. non-uniform distribution of storey masses along the building height). Irregularity in storey mass may arise due to variation in floor use patterns e.g. residential, parking, commercial/shopping, etc. or due to conversion of existing floor(s) use, for similar requirements. Thus it becomes imperative and pertinent, to conduct detailed seismic analysis of such irregular buildings, before certifying them suitable for use.

In general, seismic analysis of building frames can be performed by using four different methods *viz*., i) Linear Static Procedure, LSP ii) Linear Dynamic Procedure, LDP, iii) Nonlinear Static Procedure, NSP, and iv) Nonlinear Dynamic Procedure, NDP. Among the four aforementioned methods, NDP or more specifically Nonlinear Time History Analysis (NTHA) is generally considered as the most accurate, robust and detailed method of seismic analysis since it can not only takes care of the nonlinear behaviours but also the dynamic behaviour of building frames. Although, NTHA is the preferred choice, for a complete and detailed seismic analysis of frame structures; in practice, the use of this NTHA method is very limited; owing due to the requirement of mainly large computational efforts and convergence issue that may arise in solving non-linear dynamic equations. This may be linked to the conventional Finite Element (FE) based solution technique in the Conventional Structural Dynamic Analysis (CSDA) method, wherein the stiffness matrix needs to be updated as the solution progresses, to capture the force reduction beyond attainment of material yielding. However, with the introduction of Force Analogy Method (FAM) by Wong and Yang (1999), the computation workload and convergence issue for NTHA can now be substantially reduced. FAM has been found to greatly simplify the overall computational time, due to the consistent use of the initial stiffness matrix (which have been computed only once at the beginning of the solution process) throughout the entire nonlinear analysis. Amongst, many advantages, the FAM algorithm has been considered numerically stable because of its ability to handle not only strain-

hardening behaviour, but also elastic-perfectly plastic and strain-softening behaviours, as far as material nonlinearity is concerned. This algorithm is also capable of incorporating geometric nonlinearity using stability functions approach, with better performance in capturing large deformations accurately, than other linearized versions (e.g. P-Δ and geometric stiffness approaches) (see Wong 2014).

In this research, an attempt has been made to perform a detailed systematic NTHA of both mass regular and irregular moment resisting steel frames by considering both material and geometric nonlinearities using FAM methodology. The detailed systematic investigation has been carried out first on regular mid-rise (6, 8 and 10 storey) moment resisting steel frames by considering seven real earthquake accelerations. The results are presented in the form of displacement-based (floor's displacement, storey drift ratio) and energy-based (plastic energy) responses. It has been observed that maximum storey drift ratio occurs within 20% to 40% building height, and dissipation of maximum plastic energy occurs at the location of maximum storey drift ratio. It has also been seen that seismic response decreases when the height of the building frame increases for short period ground motion, on the other hand, seismic response increases when the height of the building frame increases for long period ground excitation. The investigation is further extended to mass irregular moment resisting steel frames, considering the effects of i) number, ii) location and iii) intensity of mass irregular floor. It has been observed that criticality (i.e. storey drift ratio exceeding allowable codal value) of mass irregular frame depends on the criticality of the storey level of reference regular frame. Mass irregular frames have been found to be the most critical when mass irregular floor(s) are located near lower storeys (i.e. 40% building height for 10-storey), and the criticality is seen to decrease when the location of mass irregular floor(s) move away from base towards the top of the building. The criticality of irregular frame increases with the increase in number of mass irregular floor. The criticality has also been seen to decrease when the mass irregular intensity is distributed at multiple floor levels than concentrating at equivalent single floor level. Also, the criticality has been found to increase when the location of multi-masses irregular floor (i.e. single and double mass irregular floors) approaches each other and vice-versa.

ACKNOWLEDGEMENT

The following acknowledgements are an account of the indebtedness I feel towards those who have been a guiding light and source of inspiration towards the completion of this thesis.

I express my deepest sense of gratitude and reverence to my supervisor ***Prof. Konjengbam Darunkumar Singh*** for his constant valuable guidance, enthusiastic involvement and kind help throughout my research work. He has been a constant source of motivation and has treated me as a good friend. I will forever remain indebted to him for his untiring effort and help extended to me that went beyond academics. The extra ordinary experience of working with him would be remembered in my life.

I am thankful to Prof. Baleshwar Singh, Prof. Hrishikesh Sharma and Prof. Satyajit Panda, my doctoral committee members and who has contributed with valuable remarks and ideas from time to time to give a good shape to this thesis.

I would like to thank the Department of Civil Engineering for providing the required facilities for my research work. Cooperation extended by the Head of the Department and office staffs deserves special thanks from my side. I would like to express my sincere thanks to all faculty members who helped me directly or indirectly during my research work.

I would like to express my sincere gratitude for the privilege of support from friends like Maharshi, Sachidananda, Gishan, Vipesh, Jackie, Patil, Narendra, Suman, Prashant and Jyotirmoy during my course of research work.

I am also thankful to Manipur University and Manipur Institute of Technology especially faculty members of civil engineering department for supporting me in completing my research work in time.

The episode of acknowledgement would remain incomplete without the care and support of my parents, wife, daughters, brothers and sisters who are an inseparable part of my life. I owe my gratitude to all of them.

I would express my deepest gratitude to all my well-wishers.

Last but not the least, I express my thanks to Almighty God for his constant guidance and blessing and giving the strength to complete this work.

Ningthoukhongjam Sukumar Singh

CONTENTS

LIST OF FIGURES

LIST OF TABLES

NOTATIONS

a	3×1 input ground motion vector in the three global directions
C	Damping matrix
C_{dd}	Condensed damping matrix
d	Translational Degree of Freedom (DOF)
E	Modulus of elasticity
f_y	Yield force
f_{SR}	Restoring force
f_S	Lateral force
F_a	Additional force due geometric nonlinearity
g	Earthquake ground acceleration vector
g_d	Earthquake ground acceleration vector along translational DOFs
h_i	Storey height
h_N	Normalized building height
I	Moment of inertia
j	n×3 matrix which relates with the directions of each DOF with the global X-, Y-, and Z- directions
K_e	Initial elastic stiffness
K_t	Post-yield stiffness
K	Stiffness that represents the relationship between the force $f_S(t)$ and the displacement $x(t)$
K'	Stiffness that represents the relationship between the restoring force $f_{SR}(t)$ and the plastic rotation $\theta''(t)$
K''	Stiffness that represents the relationship between the residual moment $m_{SR}(t)$ and the plastic rotation $\theta''(t)$
K_a	Stiffness matrix which is a function of the gravity loads on the leaning column
K_L	Elastic stiffness matrix due to the gravity loads
K_G	Stiffness matrix which changes as the axial load on members changes at the time of earthquake loading
K_{dd}, K_{dr}, K_{rd} & K_{rr}	Stiffness sub-matrices partitioned according to the DOFs with mass and those with zero mass

K_d'	K' in translational DOFs
K_r'	K' in rotational DOFs
L	Length of structural member
m	Moment capacity
m_y	Yield moment
m_{SR}	Residual moment
m_S	Moment
m_S'	Elastic moment
m_S''	Inelastic moment
M	Mass matrix
M_{dd}	Condensed mass matrix
n	Degree of freedom (DOF)
p	Plastic hinge location (PHL)
Q_i	Axial force
r	Rotational DOFs
t	Time
x	Total displacement
x'	Elastic displacement component
x''	Inelastic displacement component
x_y	Yield displacement
x_N	Normalized building width
x_d	Total displacement vector in translational DOFs
x_r	Total displacement vector in rotational DOFs
x_d'	Elastic displacement vector in translation DOFs
x_r'	Elastic displacement vector in rotational DOFs
x_d''	Inelastic displacement vector in translation DOFs
x_r''	Inelastic displacement vector in rotational DOFs
$\dot{x}$	Velocity vector
$\dot{x}_d$	Velocity vector in translation DOFs
$\dot{x}_r$	Velocity vector in rotational DOFs

$\ddot{x}$	Acceleration vector
$\ddot{x}_d$	Acceleration vector in translation DOFs
$\ddot{x}_r$	Acceleration vector in rotational DOFs
Z_i	Plastic section modulus
θ''	Plastic rotation

CHAPTER 1

INTRODUCTION

1.1 Background

Building frames constructed in highly seismic zones are vulnerable to severe earthquakes and their susceptibilities to seismic effects are more pronounced if the building frames are 'irregular' in mass (i.e. non-uniform distribution of storey masses along the building height) (Das and Nau, 2003; Choi, 2004). As per UBC (1997) a building is said to be irregular in mass if the effective mass of a storey or storeys are more than 150% of the effective mass of the neighbouring adjacent storeys. Mass irregular building frames have been reported to have resulted into greater seismic responses (and hence critical) as compared to regular counterparts, when excited by the same earthquake force (see e.g. Choi, 2004; Le-Trung *et al*., 2012). Irregularity in storey mass may arise due to variation in floor use patterns e.g. residential, parking, commercial/shopping, heavy machinery floors etc. (e.g. multi-storied residential-

(Courtesy: Avalon Garden City, AGC, 2012) (Courtesy: Spacewizard, SW, 2019)

Figure 1.1 Architectural models of multi-storied residential-cum-shopping complex building structures.

cum-shopping complex building structures (see e.g. Figures 1.1), where lower storeys are used for shopping complex); or due to conversion of existing floor(s) use, for similar requirements. Thus it becomes imperative and pertinent, to conduct detailed seismic analysis of such irregular buildings, before certifying them suitable for use.

In general, seismic analysis of building frames can be performed by using four different methods (FEMA-356, 2000) *viz*., i) Linear Static Procedure, LSP (see e.g. Valmundsson and Nau, 1997; Das and Nau, 2003) ii) Linear Dynamic Procedure, LDP (see e.g. Di Cuia *et al*., 2017; De Domenico *et al*., 2018), iii) Nonlinear Static Procedure, NSP (see e.g. Krawinkler and Seneviratna, 1998; Chopra and Goel, 2002; Kalkan and Kunnath, 2004; Antoniou and Pinho, 2004; Papanikolaou *et al*., 2005 and Pinho *et al*., 2006), and iv) Nonlinear Dynamic Procedure, NDP (see e.g. Wilkinson and Hiley, 2006; Krishnan *et al*., 2006; Krishnan and Muto, 2013). Linear Static Procedure (LSP) or more specifically known as Equivalent Lateral Force (ELF) method (Valmundsson and Nau, 1997; Das and Nau, 2003) is the simplest and most commonly employed method in seismic design codes (UBC, 1997; EC 8, 2004). In this method, earthquake force is determined from the response spectrum, developed by an ensemble of earthquakes if the fundamental period of the building frame is known. The earthquake force is simply divided by the behaviour factor (response modification coefficient) to take into account the reserve strength of the building thereby allowing pseudo inelastic analysis in a simplified manner. However, the analysis results by ELF method are found to be overly conservative (Wilkinson and Hiley, 2006).

Linear Dynamic Procedure (LDP) can be performed by either using response spectrum method (e.g. De Domenico *et al*., 2018; Moschen *et al*., 2016) or linear time-history analysis method (e.g. Liu *et al*., 2016; Di Cuia *et al*., 2017). The response spectrum method is similar to the ELF method except that it considers more than just the fundamental mode of vibration. In response spectrum method sufficient number of modes of vibrations is considered to account for 90% of the modal mass participation in the analysis (IBC, 2000; EC 8, 2004). Whereas linear time history analysis method (also termed Response-History Analysis) involves a time step-by-

step evaluation of building responses for a given ground acceleration time history using numerical techniques. It has also be mentioned that linear analysis methods are restricted to regular building frame in seismic codes (FEMA-356, 2000; IS 1893, 2016) since the results may not be accurate if applied on highly irregular building frames. It may be noted that both LSP and LDP are limited to linear responses only.

The third method of seismic analysis i.e. Nonlinear Static Procedure (NSP) often known as 'pushover analysis' (e.g. Krawinkler and Seneviratna, 1998; Chopra and Goel, 2002; Kalkan and Kunnath, 2004; Antoniou and Pinho, 2004; *Papanikolaou et al.*, 2005 and Pinho *et al*., 2006) is considered to be the most commonly employed method of nonlinear analysis as it uses simplified nonlinear techniques to estimate seismic responses. In push-over analysis, an inelastic building model is subjected to a static loading and the magnitude of the load is kept increasing until a collapse mechanism is formed. It has been reported that actual inelastic analysis has not been performed in push-over analysis rather it uses the superposition of successive elastic analysis, placing pinned connection at the position of plastic hinges (Krawinkler and Seneviratna, 1998) giving doubts on accuracy of the inelastic analysis. Also, the inelastic capacity of a building depends on the distribution of statically equivalent earthquake forces. These lateral forces are distributed in a fixed pattern proportion to the distribution of the inertia forces in the plane of each floor diaphragm and the fundamental mode shape of the building. Studies have reported that this fixed distribution of lateral loads were not able to predict with sufficient accuracy in the seismic response of tall structures, where higher vibration mode effects other than fundamental mode are considered to account for 90% of modal mass participation in the analysis (Krawinkler and Seneviratna, 1998). Thus inelastic capacity of the tall building may be misrepresented by push-over analysis based only on the fundamental mode. Improved methods in push-over analysis like Modal Pushover Analysis (Chopra and Goel, 2002) and Method of Modal Combinations (Kalkan and Kunnath, 2004) were able to consider the effects of higher modes vibration keeping a fixed distribution of the vertical forces. However, keeping constant lateral load pattern has been observed to ignore the potential redistribution of inertia forces and higher mode effects as yielding and cracking governs the structural behaviour if pushed the

structure beyond elastic limit. The latest approach in this method is the adaptive pushover method (Antoniou and Pinho, 2004) where the vertical distribution of forces is updated at each increment, during the analysis in order to take into account the changes in the structure's stiffness during inelastic deformation. Kalkan and Kunnath, (2006) proposed adaptive modal combination (AMC) technique with the objective of retaining the advantages of both adaptive and modal pushover procedures. Reasonable responses are found to obtain from the new technique with exception at some storey levels. Although adaptive pushover method show apparent enhancement in the assessment of the response at the global level, however it has been reported of having serious deficiencies in the estimation of the structural response at the local level, especially for the intermediate stories (Papanikolaou *et al*., 2005). Also a problem of excessive force concentration has been reported at the locations of the structural damage which may due to modal combination of forces using the SRSS or CQC methodologies where reversals of signs in the load vectors are not included. With a view to overcome the limitations of force-based adaptive push-over analysis, Pinho *et al*., (2006) proposed a paradigm shift in pushover analysis by introducing an innovative Displacement-based Adaptive Pushover (DAP) method which provides improved predictions of results over conventional force-based adaptive push-over analysis throughout the entire range of deformation. Although this method can predict nonlinear behaviours (e.g. inelastic deformation, plastic rotation) of building frames, however, it suffers from a serious shortcoming *viz*., its inability to obtain actual dynamic behaviours, as a function of time.

Among the four aforementioned methods of seismic analysis, NDP or more specifically Nonlinear Time History Analysis (NTHA) is generally considered as the most accurate, robust and detailed method of seismic analysis (e.g. Wilkinson and Hiley, 2006), since it can not only takes care of the nonlinear (material as well as geometric behaviours) but also the dynamic behaviour of building frames. Although, this method (i.e. NTHA) is the preferred choice, for a complete and detailed seismic analysis of frame structures; in practice, the use of this NTHA method is very limited; owing due to the requirement of mainly large computational efforts and convergence issue that may arise in solving non-linear dynamic equations (e.g.

Wilkinson and Hiley, 2006; Mokarram and Banan, 2018). This may be linked to the conventional Finite Element (FE) based solution technique in the Conventional Structural Dynamic Analysis (CSDA) method, wherein the stiffness matrix needs to be updated as the solution progresses, to capture the force reduction beyond attainment of material yielding. However, with the introduction of Force Analogy Method (FAM) by Wong and Yang (1999), the computation workload and convergence issue for Nonlinear Time History Analysis (NTHA) can now be substantially reduced (Li *et al.*, 2014).

Force Analogy Method (FAM) has been found to greatly simplify the overall computational time, due to the consistent use of the initial stiffness matrix (which have been computed only once at the beginning of the solution process), throughout the entire nonlinear analysis. Amongst, many advantages, the FAM algorithm (with its consistent or unchanging stiffness approach) has been considered numerically stable because of its ability to handle not only strain-hardening behaviour, but also elastic-perfectly plastic and strain-softening behaviours, as far as material nonlinearity is concerned. This algorithm has been reported to achieve high degree of accuracy due to the incorporation of state space numerical integration method in structural dynamic analysis. The FAM algorithm is also capable of incorporating geometric nonlinearity using stability functions approach, with better performance in capturing large deformations accurately, than other linearized versions (e.g. P-Δ and geometric stiffness approaches) (see Wong 2014). Although Nonlinear Time History Analysis (NTHA) of moment resisting steel frames using FAM has been reported by Wong and co-workers e.g. Wong and Yang (1999), Zhao and Wong (2006), Wong and Speicher (2015), their study was mostly devoted towards development of FAM techniques and its application in various engineering areas (e.g. performance-based designs, damage, control, etc.) with relatively, less emphasis on analysing in detail the nonlinear behaviour components (e.g. duration and pattern of inelastic displacement formations) of the building floor displacement during the course of earthquake ground motion.

Further, Nonlinear Time History Analysis (NTHA) of both mass regular (e.g. Uang *et al*., 1997; Krishnan *et al*., 2006) and mass irregular (Karavasilis *et al*., 2008; Le-Trung *et al*., 2012) moment resisting steel frames using conventional structural dynamic analysis (CSDA) method (i.e. updated or variable stiffness approach) are available in literature, those studies were mainly directed towards computing maximum responses, say maximum storey drift ratio, plastic rotation, etc. It has also been seen that most studies on mass irregular building frames (Choi, 2004; Pirizadeh and Shakib, 2013) were reported based on limited locations (e.g. bottom, mid and top floors) of the mass irregular floors along the building height, especially looking at maximum story drift ratios. Thus, in this research, an attempt has been made to conduct a detailed systematic investigation to give full range dynamic behaviours (i.e. seismic responses at different scale values of amplitude of earthquake forces until collapse) of mass regular mid-rise (e.g. 6, 8 and 10 storey; FEMA-350, 2000) moment resisting steel frame by performing NTHA considering both material and geometric nonlinearities using FAM methodology, using seven real earthquake ground motion records (*viz*., Kobe, 1995; Northridge, 1994; El_Centro, 1940; Imperial Valley, 1979; Loma Prieta, 1989; Fruili, 1976; and Kocaeli, 1999). The investigation is further extended to 10-storey moment resisting steel frame with single and multi-floor(s) mass irregularity.

1.2 Objectives

The main aim of the thesis is to perform a detailed systematic investigation on seismic behaviours of mass regular and irregular two dimensional mid-rise moment resisting steel frames by performing non-linear time history analysis (NTHA) considering both material and geometric nonlinearities using Force Analogy Method (FAM). The key objectives are then identified as follows:

i. To perform detailed time history analysis of elastic, inelastic and total displacement components of mid-rise moment resisting steel frames.

ii. To study the effects of ground motion and building height on seismic responses of moment resisting steel frames in terms of storey drift ratio and plastic energy dissipation.

iii. To conduct criticality study (investigation of critical scale value of ground acceleration amplitude at which the structure collapses) using Incremental Dynamic Analysis (IDA) under different ground motion records.

iv. To extend the objectives to mass irregular steel frames, considering the effects of a) number of mass irregular floor(s); b) location of mass irregular floor(s); and c) intensity of mass irregularity.

1.3 Thesis Outlines

The thesis has been broadly dived into 6 chapters. The contents of the thesis are briefly summarised below:

Chapter 1 represents a brief introduction on different methods of seismic analysis with their advantages and disadvantages. The importance of non-linear time history analysis (NTHA) along with computational efficiency of Force Analogy Method (FAM), for building frames subjected to earthquake ground accelerations have been highlighted. Thereafter, the research gap has been indicated, followed by enlisting the research objectives.

Chapter 2 shows a detailed literature review pertaining to non-linear time history analysis (NTHA) of building frames (moment resisting steel frames). Literature related to NTHA of mass regular and mass irregular moment resisting steel frames are presented, with a focus on CSDA (i.e. updated or variable stiffness matrix approach) and FAM (i.e. constant initial stiffness matrix approach). Research gap area is then concluded at the end.

Chapter 3 consists of a detail systematic investigation on mass regular mid-rise (6, 8 and 10-storey) moment resisting steel frames by performing NTHA using implemented FAM code in Matlab, considering seven real earthquake acceleration

records (*viz*., Kobe, 1995; Northridge, 1994; El_Centro, 1940; Imperial Valley, 1979; Loma Prieta, 1989; Fruili, 1976; and Kocaeli, 1999) as input ground motions. The results are presented in the form of displacement-based and energy-based responses. Under displacement-based seismic responses, building's responses are presented in the form of elastic, inelastic and total components of floor displacements; and storey drift ratio. Whereas in energy-based seismic responses, building's responses are monitored with the amount of plastic energy dissipated at the plastic hinge locations of the frame members. Incremental Dynamic Analysis (IDA) study has also been performed to investigate the different patterns of collapse of the moment resisting steel frame when subjected to different earthquake ground accelerations.

Chapter 4 presents a parametric study of single-floor mass irregular building frame to investigate the seismic behaviours of the irregular building frame when intensity as well as location of mass irregularity changes along the height of the building frame. Four different intensities of mass irregularities (i.e. 150%, 175%, 200% and 225%) at five different locations (i.e. 20%, 40%, 60%, 80% and 100%) building height have been considered for the investigation. Thus a total of 21 (1 regular + 20 irregular) frames have been analysed for the investigation. The results are presented in the form of storey drift ratios and plastic energy dissipation. The criticality study has also been performed to investigate the single-floor mass irregular frames which are more likely to become un-functional (failure state) early at less earthquake forces. The criticality study has been conducted by finding out the scale values of amplitude of input ground motion at which each single-floor mass irregular frame exceeds allowable storey drift ratio of 4% (i.e. un-functional) as per ASCE 7-16, 2016.

Chapter 5 presents an extension of the single floor mass irregularity (Chapter 4) to multi-floor masses (double and triple floors, with mass irregularity of 150%) irregular building frames, considering two different location patterns *viz*. mass irregularities being located at i) consecutive floors, and ii) non-consecutive floor levels. The performances of multi-floor masses irregular frames have been investigated for various combinations of mass irregular along the building height.

Comparative study of seismic performances between single floor and multi-floor masses irregular frames has also been conducted.

Chapter 6 summarizes the research work and presents overall conclusions along with future research scope.

CHAPTER 2

LITERATURE REVIEW

2.1 Introduction

As mentioned in Chapter 1, among the various methods of seismic analysis *viz*., i) Linear Static Procedure (LSP), ii) Linear Dynamic Procedure (LDP), iii) Nonlinear Static Procedure (NSP) and iv) Nonlinear Dynamic Procedure (NDP); NDP also commonly known as Nonlinear Time History Analysis (NTHA) has been considered as the most robust and accurate method of seismic analysis. In literature, attempts have been made using such NTHA to study the behaviours of both steel (Choi, 2004; Karavasilis *et al*., 2008; Le-Trung *et al*., 2012; Pirizadeh and Shakib, 2013) and reinforced concrete (Das and Nau, 2003; Varadharajan *et al*., 2014) mass regular and irregular frames. However, the present study is mainly focussed on NTHA of mass regular and irregular moment resisting steel building frames, literature on reinforced concrete (RC) building frames are also presented due to similarity in structural behaviours. Review of the literature pertaining to non-linear time history analysis (NTHA) of mass regular and irregular moment resisting steel frames are presented in the following sections, with a focus on Conventional Structural Dynamic Analysis (CSDA) (i.e. updated or variable stiffness matrix approach) and FAM (i.e. constant initial stiffness matrix approach).

2.2 Mass regular moment resisting steel frame:

a) NTHA using CSDA method

In the early days, NTHA was not very feasible due to the requirements of lot of computational efforts. However, with the advancement in computer technology, it became relatively easier to conduct non-linear time history analysis (NTHA). Meyer (1974) performed NTHA on a 60-storey office steel frame building, for the first time

using a conventional Finite Element (FE) (i.e. updated or variable stiffness matrix approach; hereafter refer to as conventional Finite Element/FE) based computer program/software called NLDYN. Thus feasibility of performing NTHA on major structures within reasonable budgets has been demonstrated. To simplify the problem, insignificant degree of freedoms (DOFs) had been omitted by considering rigid diaphragm and lump masses in the analysis. Both material and geometrical (P-Δ effect) were considered in the analysis and responses of the building were investigated in terms of storey displacement, storey shears, plastic hinge formations and energy dissipation. It has been reported that maximum storey displacement and maximum storey shears occurred at top floor and bottom floor levels respectively.

Uang *et al.*, (1997) conducted NTHA on a 13-storey welded steel moment resisting frame as a case study to summarise the building affected by the Northridge earthquake (1994). Conventional Finite Element (FE) based program (DRAIN-2DX) was used in performing NTHA considering material nonlinearity where 2% strain hardening was considered. Two more earthquake records (i.e. El Centro, 1940 and Sylmar, 1994) were also used in the analysis. It has been reported that Sylmar record gave maximum storey drift ratio of 2.2% near 30% height of the building whereas Northridge and El Centro gave maximum storey drift ratio of 1.7% and 1.2% near 46% and 38% building height respectively. It has also been observed that there is a close relationship between storey drift ratio and plastic rotation that with more rotation demand associated with large storey drift ratio.

Ventura and Ding (2000) performed NTHA on a well-instrumented 52-storey steel frame building called FWT located in down-town Los Angeles, California using a conventional FE based computer program CANNY-E. Strain hardening material behaviour has been adopted in bilinear hysteric model in order to maintain numerical convergence in the analysis; however its value has been limited to minimum so as to avoid masking true (physical) instabilities. Three input ground motions (namely Niigata, 1964; Landers, 1992; and Northridge, 1994) earthquakes were used for the analysis. Maximum storey drift ratios of 1.5%, 1.25% and 0.8% have been observed

near 44%, 80% and 84% building height for Niigata, Northridge and Landers earthquakes respectively.

Mulas (2004) conducted NTHA on a 9-storey moment resisting steel frame using conventional FE based computer code called STEFAN (STEel Frame ANalysis). Five simulated ground motions have been used for the analysis of the frame. Material nonlinearity in the form of simple hysteretic model for shear deformation and geometric nonlinearity in the form of P-Δ effect have been considered in the analysis. It has been observed that maximum storey drift ratio of ~0.001% is found to occur near 66% building height.

Kim and Engelhardt (2005) conducted seismic analysis on a 6-storey steel frame by performing NTHA using steel beam with composite slab frame model (CB model) and bare steel frame model using three input ground motion records (namely: Northridge, 1994; Landers, 1992; and Mexico City, 1985). It has been observed that bare steel frame provided more storey drift ratio than CB model. Maximum storey drift ratios of ~ 4.5%, 3.7% and 3.5% have been observed to occur at 43%, 43% and 71% building height of bare steel frame for Mexico City, Landers and Northridge earthquakes respectively.

Wilkinson and Hiley (2006) developed a conventional FE based model to conducted NTHA on a 15-storey idealised building frame considering both material and geometric (P-Δ effects) nonlinearities to study the sequence of plastic hinges formation for predicting the collapse of the building frame. It has been observed that plastic hinge formation started from the base and proceeded towards the top of the building in three different sequences. The first sequence of plastic hinges formation has been observed in lower 40% height of the building, then it has been shifted to upper 40% height of the building and finally it covered the remaining portion of 20% of height of the building.

Krishnan *et al.* (2006) performed NTHA on a 18-story steel moment-frame building considering both material and geometrical nonlinearity (P-Δ effect) using conventional FE based computer program (FRAME3D) as a part of seismic hazard

assessment on the San Andreas Fault. Site specific simulated earthquake ground motions have been used using open-source seismic wave propagation package (SPECFEM3D). The responses of the building frame have been represented by inter-storey drift ratio which becomes the primary structural response parameters to evaluate structural performance. It has been observed that maximum inter-storey drift occurred in bottom-third height of the building. In some location (e.g. San Fernando Valley), maximum inter-storey drift has been reported to exceed 0.10 (i.e. indicative of probable collapse) whereas at other locations (e.g. Los Angeles) maximum inter-storey drifts have been limited to 0.04 to 0.06 only.

Krishnan and Muto (2013) investigated the seismic responses of 18-storey moment resisting steel frames using NTHA method as a part of sensitivity analysis by changing the parameters of input ground motion like frequency content, intensity and duration of ground motion. NTHA has been performed with conventional FE based computer program (FRAME3D) which considers both material and geometric (P-Δ effects) nonlinearities. It has been reported that for long period building frame, only long period ground motion can induce strong responses. It has also been observed that maximum storey drift ratios of ~ 4% and 3.5% have been found to occur at 40% and 80% building height for Imperial Valley and Kobe earthquakes respectively.

Hariri-ardebili *et al.* (2013) performed NTHA on four different heights (i.e. 9, 11, 13 and 15-storey) of steel moment resisting frames using conventional FE based software (PERFORM-3D) considering both material and geometric (P-Δ effect) nonlinearities. Based on the results obtained by NTHA, maximum storey drift ratios of ~ 2.5%, 1.8%, 2.9% and 2.7% have been observed to occur at 44%, 45%, 60% and 74% building height for the 9, 11, 13 and 15-storey building frames respectively.

Mokarram and Banan, (2018) performed NTHA on 5 and 8-storey steel moment resisting frames by using FE based software (OpenSees) as a part of improving optimization techniques on performance-based design of buildings. It has been observed that maximum storey drift ratios of ~ 1.6% and 2.3% are found to occur at 60% and 25% building height for the 5 and 8-storey building frames respectively.

b) Collapse analysis using Incremental Dynamic Analysis (IDA)

Incremental Dynamic Analysis (IDA) (Vamvatsikos and Cornell, 2002) is a parametric analysis method where the structural responses has been determined when subjected to one or more ground motion records, each scaled to multiple levels of intensity. IDA study has been considered as one of the most powerful analysis tool for investigating full range (i.e. responses at different intensities of input ground motion until collapse) dynamic behaviours of the frame structures; however, it involves performing a series of NTHA for each (i.e. different intensities) record of input ground motion which resulted into expensive procedure if conducted by the conventional FE based CSDA method. Two methods of collapse analysis (i.e. Engineering Demand Parameter (EDP) and Intensity Measure (IM)) have been reported in the literatures (Vamvatsikos and Cornell, 2002; Zareian *et al*., 2010). In EDP based method, collapse of the building frame has been measured with building response parameters like maximum storey drift ratio, whereas in IM based method, the building is considered in a state of total collapse at a given intensity of input ground motion if the building experienced infinite floor displacement (i.e. dynamic instability). Dynamic instability is considered equivalent to numerical instability in collapse analysis (Vamvatsikos and Cornell, 2002). Collapse analysis of the building frames using IDA study has also been reported in the literature in connection with sensitivity analysis of collapse capacity of moment resisting frame (Zareian and Krawinkler, 2010); uncertainty associated in estimation of collapse fragility curve (Eads *et al*., 2013); and experimental validation of numerical analysis of collapse of framed structure (Domizio *et al*., 2015).

c) NTHA using FAM method

A simplified method of performing NTHA of building frame known as Force Analogy Method (FAM) has been proposed by Wong and Yang (1999). This algorithm is based on changing the structural displacement field in contrast to the Conventional Structural Dynamic Analysis (CSDA) method of changing stiffness matrix. In this algorithm, all the inelastic behaviours of the structural system are represented by a single equation since each inelastic deformation of the structure is

considered as a degree of freedom in the analysis. The algorithm has been found to be efficient in performing NTHA (Li *et al.* 2014) since it uses only the initial stiffness matrix throughout the entire nonlinear analysis. This algorithm has been reported to achieve high degree of accuracy due to the incorporation of state space numerical integration method in structural dynamic analysis. The algorithm has also been considered numerically stable because of its ability to handle not only strain-hardening behaviour, but also elastic-perfectly plastic and strain-softening behaviours, as far as material nonlinearity is concerned (Wong and Yang, 1999). A brief history for the development of FAM algorithm on performing NTHA is given below.

To demonstrate the applicability of the proposed FAM algorithm, Wong and Yang, (1999) has performed NTHA on a 6 story moment resisting steel frame hospital building, located in Woodland Hills, California. Material nonlinearity in the form of concentrated plastic hinges has been assigned at the ends of the beam to incorporate inelastic behaviours of the members in the analysis, however the column has been considered to behave elastically. Numerical simulations have been found to perform successfully for all the three different cases of material nonlinear behaviours, e.g. strain- hardening, elastic-plastic and strain-softening, thereby confirming the numerical stability of the new algorithm.

Wong and Yang (2002) further extended their previous work in FAM (Wong and Yang, 1999) by deriving a computational method to characterise energy transfer among its various forms during NTHA considering material nonlinearity. The evaluation of plastic energy during inelastic analysis in FAM has become very simple since the accumulation of plastic energy during inelastic deformation is given by simply multiplying the elastic moment with the change in plastic rotations; whereas in CSDA method, plastic energy dissipation is estimated by measuring the enclosed area between moment and plastic rotation (Mahin and Bertero, 1981).

Wong and Wang (2003) modified the classical FAM using static condensation by considering zero rotational mass moment of inertia in mass matrix which resulted in reduction of computational efforts without compromising accuracy of the results. The

modified FAM has been used for conducting performance-based design in terms of energy dissipation during NTHA on the same 6-storey moment-resisting steel frame. The sequence and magnitude of energy flow in the frame has been determined by plastic energy dissipation 'capacity' in each structural member which helps in identifying the critical members to be strengthened to improve the structural performance at the time of major earthquake excitations.

However the modified FAM includes only material nonlinearity, hence in order to predict more accurate nonlinear behaviours of the multi-storey frame structures, Zhao and Wong (2006) has presented a novel approach of seismic analysis which incorporates both material and geometric nonlinearities. P-Δ effect has been incorporated to take into account the effect of geometric nonlinearity in the analysis. FE formulation has been used for the derivation of geometric stiffness matrix. In this formulation there is provision for separating the coupling effects between material and geometric nonlinearities during the NTHA. The robustness of this approach has been verified successfully by implementing on a 5-storey moment-resisting steel frame.

FAM methodology for performing NTHA of steel frame structures has been further improved by Wong and Wang (2007a) by incorporating plastic hinge length (offsets) from the member end; and by Wong and Wang, (2007b) by incorporating deformable panel zones at beam-column connection using rotational springs. It has been observed in general that the responses of the structures with end offsets have been found consistently larger than those from without end offsets. It has also been seen from deformable panel zones model that the capacity of plastic energy dissipation in the beam–column joint has been observed much less than that from the beam and hence it has been desirable to dissipate plastic energy in the beam member only.

The geometric stiffness approach proposed by Zhao and Wong (2006) for the incorporation of geometric nonlinearity in FAM has been found too sensitive. It may be due to the adoption of linearized approximation in geometric stiffness approach where higher-order terms in the strain equation were neglected. Wong (2014) adopted a more rigorous formulation of using stability functions to address geometric

nonlinearity in FAM in a static problem. In stability functions approach, geometric nonlinearity has been addressed by capturing both large P-Δ and small P-Δ effects by solving the fourth-order differential equation in consistent form. This formulation is still based on small displacement theory, however it has been considered better chance of capturing the large displacement response more accurately than other linearized versions of the small displacement approaches like P-Δ and geometric stiffness approaches. Further the author (Wong, 2014) has also commented on the methodologies used by different software developers to address geometric nonlinearity in the analysis. Software packages like Perform-3D and OpenSees used small displacement theory of P-Δ stiffness approach while SAP2000 used geometric stiffness approach to incorporate the effects of geometric nonlinearity which have resulted into inconsistent outputs among different software packages. Wong and Speicher (2015) extended the formulation (Wong, 2014) to solve dynamic problems (NTHA) in steel frame structures by including the state space method in the analysis procedure. This extended formulation has given a provision to perform a more accurate analysis of frame structures where the cost of using large-displacement formulations is not justified.

2.3 Mass irregular moment resisting steel frame using CSDA method

To the best of author's knowledge, the work on the mass irregular building frames was first carried out by Valmundsson and Nau (1997). However NTHA was not used in the analysis, instead LSP (ELF) method was used for the investigation and the results were compared with LDP (linear time history analysis). Das and Nau (2003) conducted NTHA numerically considering both material and geometric (P-Δ effect) nonlinearities on three heights (5, 10 and 20-storey) RC building frames. Single floor mass irregularity has been considered at three different locations along the height of the three different buildings (i.e. at 40%, 80% and 100% building height for 5-storey; 20%, 60% and 100% building height for 10-storey; and 10%, 55% and 100% building height for 20-storey). Mass irregular intensities of 250% and 500% have been considered for the analysis. Marked increased in the storey drift ratio has been observed in the vicinity of mass irregular floor for all the building frames. Storey

drift ratio has been found to increase when the height of the building decreases. Maximum storey drift ratios of 1.02%, 0.91% and 0.87% have been observed when mass irregularity of 250% are located at 40%, 60% and 55% building heights for 5, 10 and 20-storey building frames respectively. Hence in all three frames, maximum storey drift ratios have been observed to occur in middle third height of the building.

Choi (2004) conducted NTHA to investigate the effect of seismic responses in terms of storey drift ratio and plastic hinge rotation due to mass irregularity on 16-storey steel moment-resisting frame buildings using conventional FE based program DRAIN2D+. Single floor mass irregularity of 200% has been located at three different locations (i.e. 12.5%, 50% and 93.75%) building heights. It has been observed that mass irregularity located at bottom (12.5% building height) and top (93.75% building height) are found to be more critical than locating at middle (50% building height). Maximum storey drift ratios of ~3.1%, ~2.8% and 3.2% have been observed to occur near the locations of mass irregularity at 12.5%, 50% and 93.75% building height respectively. Plastic hinges have also been found to concentrate near the areas where mass irregularities are located; however the variation of magnitude of plastic rotation was not significant as compared to storey drift ratio.

Karavasilis *et al.* (2008) conducted parametric studies on the inelastic seismic response on 3, 6, 9, 12 and 15-storey plane steel moment-resisting frames by performing NTHA using conventional FE based program DRAIN-2DX. Single floor mass irregularity located at three different locations (i.e. bottom, middle and top floors) for all the building frames with mass irregularity intensities of 200%, 400% and 600% have been considered. Material nonlinearity in the form of lump plasticity model and geometric nonlinearity in the form of P-Δ effect have been taken into account in the analysis. It has been seen that location of mass irregularity and level of inelastic deformation plays an important role in predicting height-wise deformation demand. Generally, elastic component of deformation has been found to be uniform throughout the building height; whereas inelastic component has been observed to concentrate at the lower storeys (i.e. within 25% to 45% building height). It has been

observed that maximum storey drift ratios (~4%) are found to occur within these lower storey levels.

Le-Trung *et al.* (2012) investigated the seismic behaviour in terms of both seismic demand and seismic capacity of 20-storey mass irregular steel moment resisting frames by performing NTHA using conventional FE based program Drain-2DX. Material nonlinearity in the form of bilinear moment–rotation behaviour with strain hardening ratio of 3% and geometric nonlinearity (P-Δ effect) have been considered in the analysis. Both single floor and multi-floor masses irregularity have been considered in the analysis, with single floor mass irregularity located at two locations (i.e. 5% and 100% building height); and multi-floor masses irregularity being located at two different locations (i.e. from 5% to 25%; and 90% to 100% building height). Mass irregularities of 150% and 200% have been considered in the analysis. It has been observed that when mass irregularities (both single and multi-floor) are located at top floors, larger storey drift ratio have been observed in those storeys and some lower adjacent storeys in comparison to that of regular building. The storey drift ratios for the remaining lower storeys have been found to be lesser than that of regular counterpart. Whereas when mass irregularities (both single and multi-floor) are located at lower storeys, the storey drift ratios for all the above storeys have been observed to be larger than that of the regular counterpart and the maximum storey drift ratios have been seen to confine near the top and bottom storeys of the building frame. Maximum increased in storey drift ratios of ~0.2% and 0.4% than that of reference regular frame have been observed when mass irregularities of 150% and 200% are located at 100% building height respectively.

Pirizadeh and Shakib (2013) investigated the probabilistic seismic performance of mass irregular 10-storey special moment resisting steel frames using conventional FE based software (PERFORM-3D). Incremental Dynamic Analysis (IDA) method has been adopted for the investigation. Material nonlinearity in the form of lumped plasticity and geometric nonlinearity in the form of P–M–M interaction have been considered in the analysis. Both single and multi-floor masses irregularity of 200% have been considered, with the locations of single mass irregular floor at 10% (1st

floor) and 50% (5th floor) building height; and multi-floor masses irregularity at lower half storeys (1st to 5th floors) i.e. 10% to 50% building height, respectively. It has been seen that all the irregular frames attain maximum storey drift ratio near 50% building height at different intensities of input ground motion. Multi-floor masses irregular frame has been found to attain maximum storey drift ratio of ~0.125% at 0.6g of input ground motion; whereas that of single floor mass irregular frames of mass irregularity at 10% and 50% building heights have attained maximum storey drift ratio of ~0.09% and 0.105% respectively at 0.63g of input ground motion.

Varadharajan *et al.* (2014) conducted NTHA on 18-storey mass irregular RC buildings using FE based software (E-Tabs V9.0) to assess the collapse capacity of the irregular buildings. Multi-floor masses irregularities (200% and 300%) located at 1/3rd bottom storeys (5.5 to 33.3)%, 1/3rd middle storeys (38.8 to 66.6)% and 1/3rd top storeys (72.2 to 100)% of building heights have been analysed. Based on the IDA study, it has been observed that the collapse capacity is greatest for mass irregularity at 1/3rd bottom storeys (5.5 to 33.3)% building height while least for mass irregularity at 1/3rd top storeys (72.2 to 100) % building height.

Thus, based on the literature review, some gap areas have been identified in the seismic analysis using NTHA of building frames *viz*., a) most of the research work on seismic analysis using NTHA of both mass regular and irregular moment resisting steel building frames have been found to focus mainly on determining the maximum response parameters (e.g. storey drift ratio and plastic rotations) without considering full range dynamic behaviours; b) for the mass irregular frames, the location of mass irregularity along the building height has been observed to confine at limited locations (e.g. bottom, middle and top floors) for single floor mass irregular frames; whereas at (1/2nd lower storeys, 1/3rd lower storeys, 1/3rd middle storeys and 1/3rd top storeys) for multi-floor masses irregular frames; and c) criticality study (investigation of critical scale value of ground acceleration amplitude corresponding to codal allowable storey drift ratio), among various mass irregular frames located at different floor levels has not been performed. To the best of author's knowledge, seismic analysis (or NTHA) of mass irregular moment resisting steel frames using Force

Analogy Method (FAM) has not reported in the literature. Thus, a detailed systematic Nonlinear Time History Analysis (NTHA) of both mass regular and irregular moment resisting steel frames needs to be addressed by considering both material and geometric nonlinearities using FAM methodology, to assess full range dynamic behaviours ensuring maximum coverage of mass irregular floor/floors throughout the building height, thereby seeking more insights. The sequence of criticality of mass irregular frames due to various locations of mass irregular floor/floors along the building height will also be addressed by critical analysis using IDA study.

2.4 Conclusion

In this chapter a brief literature review on NTHA for both mass regular and irregular moment resisting steel frames is presented. Literature review under mass regular moment resisting steel frame has further been reported based on different methods of analyses i.e. using CSDA (i.e. updated or variable stiffness matrix approach) method and FAM (i.e. constant initial stiffness matrix approach) method. It has been reported that maximum storey drift ratio occurred within 40% to 75% building height using CSDA method. However, in FAM method, the main focus was devoted in improvising the NTHA techniques. From the literatures of mass irregular frames using CSDA method, it has been observed that maximum storey drift ratio occurs near the vicinity of mass irregular floors. Literatures on mass irregular floors using FAM have not been reported as per author's knowledge. Finally, gap areas have been identified and objectives of the thesis are presented.

CHAPTER 3

NONLINEAR TIME HISTORY ANALYSIS OF MASS REGULAR MOMENT RESISTING STEEL FRAME USING FAM

3.1 Introduction

It has been observed from the literature review in Chapter 2 that among the different methods of seismic analysis (i.e. Linear static procedure, LSP; Linear dynamic procedure, LDP; Nonlinear static procedure, NSP; and Nonlinear dynamic procedure, NDP); NDP (more specifically known as Nonlinear Time History Analysis, NTHA) is generally considered as the most accurate, robust and detailed method of seismic analysis (e.g. Wilkinson and Hiley, 2006), since it can not only takes care of the nonlinear behaviours (material as well as geometric) but also the dynamic behaviour of building frames. Although, this method (i.e. NTHA) is the preferred choice, for a complete and detailed seismic analysis of frame structures; in practice, the use of this NTHA method is very limited; owing due to the requirement of large computational efforts that may arise in solving non-linear dynamic equations (see e.g. Wilkinson and Hiley, 2006; Mokarram and Banan, 2018). This may be linked to the use of conventional Finite Element (FE) based solution technique in the Conventional Structural Dynamic Analysis (CSDA) method, wherein the stiffness matrix needs to be updated as the solution progresses, to capture the force reduction beyond attainment of material yielding. However, with the introduction of Force Analogy Method (FAM) by Wong and Yang (1999), the computation workload for Nonlinear Time History Analysis (NTHA) can now be substantially reduced (see e.g. Li *et al*., 2014).

In the early days, NTHA was not widely adopted due to the requirements of lot of computational efforts. However, with the advancement in computer technology, it became relatively easier to conduct Nonlinear Time History Analysis (NTHA). Meyer (1974) performed NTHA on a frame structure, for the first time to best of

author's knowledge using a conventional Finite Element (FE) based computer program/software called NLDYN. Subsequently, in a similar line, researchers like, Uang *et al*., (1997); Ventura and Ding (2000); Mulas (2004); Krishnan and Muto (2013); Hariri-ardebili *et al*. (2013) and Mokarram and Banan, (2018) used conventional FE based programs/softwares like DRAIN-2DX; CANNY-E; STEFAN; FRAME3D; PERFORM-3D and OpenSees respectively, to perform NTHA of moment resisting steel frames. It has been observed that most of the works were mainly aimed at determining the maximum responses (e.g. storey drift ratios and plastic rotations) of building frames without considering full range dynamic behaviours (i.e. responses at different scale values of amplitude of input ground motion). Thus in this chapter, an attempt has been made to undergo a detailed systematic investigation to assess full range dynamic behaviours of mass regular mid-rise (6, 8 and 10-storey) (FEMA-350, 2000) moment resisting steel frames by performing NTHA considering both material and geometric nonlinearities using FAM methodology considering seven real earthquake ground motion records (*viz*., Kobe, 1995; Northridge, 1994; El_Centro, 1940; Imperial Valley, 1979; Loma Prieta, 1989; Fruili, 1976; and Kocaeli, 1999).

In this chapter, first part represents the introduction of Force Analogy Method (FAM), and then the validation of the implemented FAM code in Matlab (R2012b) will be presented. A detailed systematic investigation is then presented for a typical 10-storey steel frame subjected with Kobe earthquakes. Collapse analysis of the 10-storey steel frame using Incremental Dynamic Analysis (IDA) study has also been shown. Additionally, the effect of earthquake ground motions on mid-rise moment resisting steel frames of different heights (e.g. 6, 8 and 10-storeys) has been presented followed by the assessment of the effect of building heights on seismic responses.

3.2 Force Analogy Method (FAM)

FAM is an algorithm to study the inelastic behaviour of structural system using only the initial stiffness matrix. It was proposed by Wong and Yang (1999). The algorithm

is based on inelastic displacement concept proposed by Lin (1968) where inelastic behaviour of structural member is determined by changing the structural displacement field which is different from CSDA method of changing stiffness. Lin (1968) used this inelastic displacement concept for the application of stress and strain in continuum mechanics where the inelastic behaviour was defined by plastic strain. In FAM, all the inelastic behaviours of the structural system have been represented by a single equation since each inelastic deformation of the structure is considered as a degree of freedom in the formulation. This new algorithm has been reported to be efficient in computational time since only the initial stiffness matrix is used throughout the entire nonlinear analysis. In a case study, Li *et al*., (2014) reported the computational time efficiency of FAM by as much as 70% reduction as compared to that of the solution by SAP2000 (2011) which employs the CSDM. The algorithm has also been found to achieve a high degree of accuracy due to the incorporation of state space numerical integration method in structural dynamic analysis. The FAM algorithm has also been considered to be numerically stable since it can analyse not only strain-hardening problems, but also elastic-perfectly plastic and strain-softening problems, as far as material nonlinear behaviour is concerned. In the literature, FAM has been used for the structural analysis of reinforced concrete members/structures (see e.g. Chao and Loh, 2007; *Li et al*., 2013; Li *et al*., 2014a; Li, *et al*., 2014b and Li *et al*., 2015), structural control study (see e.g. Wong, 2005 and Pang and Wong, 2006), energy based seismic analysis (see e.g. Wong, 2008; Wong and Johnson, 2009; Wong, 2011 and Li and Li, 2011).

The basic concept of FAM is briefly described here (see Figure 3.1). When lateral force $f_S(t)$ excites a Single Degree of Freedom (SDOF) system, lateral deformation $x(t)$ and support moment $m_S(t)$ are formed (see Figure 3.1a). The plastic hinge located at the support of SDOF system will measure the plastic rotation $\theta''(t)$ caused by the moment demand exceeding the yield moment capacity of the member. Force-deformation curve is shown in Figure 3.1b; where, $K_e(t)$ and $K_t(t)$ denote the initial elastic stiffness and the varying post-yield stiffness respectively. The lateral deformation $x(t)$ of SDOF system is represented by point C (see Figure 3.1b). The basic concept of FAM is to extend the initial stiffness line OA until it reaches the

force $f_S(t)$ level at point B (see Figure 3.1b). The displacement corresponding to point B is defined as elastic displacement $x'(t)$ and the difference between the total displacement $x(t)$ and elastic displacement $x'(t)$ is defined as the inelastic or plastic displacement $x''(t)$. Figure 3.1c represents moment-plastic rotation relationship.

For a moment-resisting frame with n Degree Of Freedoms (DOFs) and p Plastic Hinge Locations (PHLs), the total displacement $x(t)$ at each DOF is given by the summation of elastic displacement $x'(t)$ and inelastic displacement $x''(t)$

$$x(t) = x'(t) + x''(t) \tag{3.1}$$

Similarly, the total moment, $m_S(t)$ at plastic hinge location (PHL) is given by the summation of elastic moment $m_S'(t)$ due to elastic displacement $x'(t)$ and inelastic (residual) moment $m_S''(t)$ due to inelastic displacement $x''(t)$.

$$m_S(t) = m_S'(t) + m_S''(t) \tag{3.2}$$

The displacements in Equation (3.1) and moments in Equation (3.2) are inter-related by the following expressions (Wong and Speicher, 2015):

$$m_S'(t) = K'(t)^T x'(t) \tag{3.3}$$

$$m_S''(t) = -[K''(t) - K'(t)^T K(t)^{-1} K'(t)]\theta''(t) \tag{3.4}$$

where, $K(t)$ is $n \times n$ global stiffness matrix, $K'(t)$ is $n \times p$ stiffness matrix formed by relating plastic rotations at the PHLs with the restoring forces at the DOFs, $K''(t)$ is the $p \times p$ stiffness matrix formed by relating plastic rotations with corresponding residual moments at the PHLs and $\theta''(t)$ is the plastic rotation at each PHL (refer Wong and Yang, 1999).

Putting Equations (3.3) and (3.4) into Equation (3.2) and rearranging the terms gives the first governing of FAM for dynamic analysis as:

$$m_S(t) = K'(t)^T x(t) - K''(t)\theta''(t) \tag{3.5}$$

The second governing equation of FAM relates the inelastic displacements $x''(t)$ with the plastic rotation $\theta''(t)$ as (see Wong and Speicher, 2015):

$$x''(t) = K(t)^{-1} K'(t)\theta''(t) \tag{3.6}$$

Dynamic equation of motion $M\ddot{x}(t)+C\dot{x}(t)+K(t)x'(t)=-M\ddot{g}(t)-F_a(t)$ is solved by using state space numerical integration method. Thus,

$$z_{k+1} = \begin{Bmatrix} x(t) \\ \dot{x}(t) \end{Bmatrix} = F_d z_k + J_d a_k + G_d x''_{d,k} \tag{3.7}$$

Where, F_d, J_d and G_d are constants (refere Appendix A), and z_k, a_k and $x''_{d,k}$ are displacement cum velocity vector, ground acceleration and inelastic displacement vector respectively.

In FAM, plastic energy (PE) dissipation is determined by multiplying elastic moment (m') with change in plastic rotation (θ'') (see Wong and Zhao, 2007).

$$PE = \int_0^t x'_d(t)\bar{K}_L dx''_d = \int_0^t x'_d(t)K_p d\theta'' = \int_0^t m'(t)d\theta'' = \sum_{k=1}^{t_k} m_{i,k}(\theta''_{i,k} - \theta''_{i,k-1}) \tag{3.8}$$

The aforementioned FAM formulation has been coded in Matlab (R2012b). Detail dynamic analysis in FAM incorporating both material and geometric nonlinearities using state space numerical integration method has been presented in Appendix A.

3.3. Validation of implemented FAM code

A 10-storey mass regular moment resisting steel frame (see Figure 3.2) reported in the literature for seismic analysis studies, (e.g. Zhang *et al.*, 2007; Wong and Johnson, 2009; and Li and Wong, 2014) has been considered for validation of the implemented FAM code in Matlab. The 10-storey steel frame has equal storey height of 4.27 m and 3 bays of equal width 7.62 m (see Figure 3.2). All the frame members have been considered axially rigid, resulting into 50 Degree Of Freedoms (DOFs) (i.e. from x_1 to x_{50}) as shown in Figure 3.3. Plastic hinges have been assigned at both the ends of each structural member, thus there are a total of 140 Plastic Hinge

Locations (PHLs) (see Figure 3.4). Mass moment of inertias at the rotational DOFs (i.e. from x_{11} to x_{50}) have been ignored to condense the size of the matrices by static condensation method where all the 40 rotational DOFs (i.e. from x_{11} to x_{50}) have been eliminated reducing to only 10 translational DOFs (i.e. from x_1 to x_{10}). It is worth mentioning that, apart from reducing the size of the problem; most importantly, static condensation of mass matrix provides an avenue to invert it; otherwise, it would be undefined with a singular mass matrix. Members' section properties have been provided as per (ASTM A6/A6M-07 (2007) and section details are represented in Table 3.1. The stiffness matrices have been formulated based on the section properties given in Table 3.1. A 50×50 K matrix, 50×140 K' matrix, and 140×140 K'' matrix have been developed by assembling the individual stiffness matrices for each member (refer Appendix A for details). After the application of static condensation, K matrix reduces to 10×10 $\bar{K}$ matrix, K' matrix reduces to 10×140 $\bar{K}'$ matrix, and K'' matrix reduces to 140×140 $\bar{K}''$ matrix. The resulting condensed elastic stiffness matrix $\bar{K}_e$ of the whole steel frame becomes of the form,

$$\bar{K}_e = \begin{bmatrix} 7.34 & -3.93 & 0.59 & -0.06 & 0.01 & 0.00 & 0.00 & 0.00 & 0.00 & 0.00 \\ -3.93 & 6.19 & -3.42 & 0.55 & -0.05 & 0.01 & 0.00 & 0.00 & 0.00 & 0.00 \\ 0.59 & -3.42 & 5.74 & -3.27 & 0.47 & -0.05 & 0.00 & 0.00 & 0.00 & 0.00 \\ -0.06 & 0.55 & -3.27 & 5.15 & -2.77 & 0.43 & -0.04 & 0.00 & 0.00 & 0.00 \\ 0.01 & -0.05 & 0.47 & -2.77 & 4.68 & -2.68 & 0.39 & -0.04 & 0.00 & 0.00 \\ 0.00 & 0.01 & -0.05 & 0.43 & -2.68 & 4.43 & -2.49 & 0.39 & -0.04 & 0.00 \\ 0.00 & 0.00 & 0.00 & -0.04 & 0.39 & -2.49 & 4.18 & -2.36 & 0.35 & -0.03 \\ 0.00 & 0.00 & 0.00 & 0.00 & -0.04 & 0.39 & -2.36 & 3.63 & -1.86 & 0.24 \\ 0.00 & 0.00 & 0.00 & 0.00 & 0.00 & -0.04 & 0.35 & -1.86 & 2.78 & -1.23 \\ 0.00 & 0.00 & 0.00 & 0.00 & 0.00 & 0.00 & -0.03 & 0.24 & -1.23 & 1.02 \end{bmatrix} kN/m$$

Storey mass of 218.9 Mega-gram (Mg) as reported in (Li and Wong, 2014) has been considered for each floor giving a total mass of 2189 Mg for the entire building frame. Thus, the condensed mass matrix, M_{dd} for the entire building frame becomes

$$M_{dd} = \begin{bmatrix} 218.9 & 0 & 0 & 0 & 0 & 0 & 0 & 0 & 0 & 0 \\ 0 & 218.9 & 0 & 0 & 0 & 0 & 0 & 0 & 0 & 0 \\ 0 & 0 & 218.9 & 0 & 0 & 0 & 0 & 0 & 0 & 0 \\ 0 & 0 & 0 & 218.9 & 0 & 0 & 0 & 0 & 0 & 0 \\ 0 & 0 & 0 & 0 & 218.9 & 0 & 0 & 0 & 0 & 0 \\ 0 & 0 & 0 & 0 & 0 & 218.9 & 0 & 0 & 0 & 0 \\ 0 & 0 & 0 & 0 & 0 & 0 & 218.9 & 0 & 0 & 0 \\ 0 & 0 & 0 & 0 & 0 & 0 & 0 & 218.9 & 0 & 0 \\ 0 & 0 & 0 & 0 & 0 & 0 & 0 & 0 & 218.9 & 0 \\ 0 & 0 & 0 & 0 & 0 & 0 & 0 & 0 & 0 & 218.9 \end{bmatrix} Mg$$

Using stiffness matrix ($\bar{K}_e$) and mass matrix (M_{dd}), the 10 frequencies of vibration are calculated as shown in Table 3.2. Damping of 3% has been considered for all the ten modes of vibrations. Considering mass proportional Rayleigh damping, condensed damping matrix, C_{dd} has been obtained as,

$$C_{dd} = \begin{bmatrix} 7.24 & -2.32 & -0.06 & -0.07 & -0.03 & -0.02 & -0.01 & -0.01 & -0.01 & 0.00 \\ -2.32 & 6.19 & -2.26 & -0.10 & -0.09 & -0.04 & -0.03 & -0.02 & -0.01 & -0.01 \\ -0.06 & -2.26 & 5.90 & -2.29 & -0.13 & -0.10 & -0.05 & -0.03 & -0.02 & -0.02 \\ -0.07 & -0.10 & -2.29 & 5.57 & -2.07 & -0.13 & -0.11 & -0.06 & -0.04 & -0.03 \\ -0.03 & -0.09 & -0.13 & -2.07 & 5.31 & -2.07 & -0.15 & -0.11 & -0.06 & -0.04 \\ -0.02 & -0.04 & -0.10 & -0.13 & -2.07 & 5.15 & -2.00 & -0.14 & -0.11 & -0.07 \\ -0.01 & -0.03 & -0.05 & -0.11 & -0.15 & -2.00 & 4.99 & -1.99 & -0.13 & -0.12 \\ -0.01 & -0.02 & -0.03 & -0.06 & -0.11 & -0.14 & -1.99 & 4.64 & -1.75 & -0.16 \\ -0.01 & -0.01 & -0.02 & -0.04 & -0.06 & -0.11 & -0.13 & -1.75 & 4.04 & -1.57 \\ 0.00 & -0.01 & -0.02 & -0.03 & -0.04 & -0.07 & -0.12 & -0.16 & -1.57 & 2.35 \end{bmatrix} kNs/m$$

Considering all the 140 plastic hinges exhibit elastic perfectly plastic material nonlinear behaviour with moment capacity $m_{c,i}$ of the i^{th} plastic hinges as

$$m_{c,i} = f_y \times Z_i \qquad i = 1,\ldots,140$$

where, f_y =250 MPa (yield stress) and Z_i is the plastic section modulus of the i^{th} plastic hinge. Thus,

$$if \begin{cases} m_i(t) \le m_{c,i} \\ m_i(t) > m_{c,i} \end{cases}, \qquad then, \begin{cases} \Delta\theta_i''(t) = 0 \\ m_i(t) = m_{c,i} \end{cases} \qquad i = 1,...,140$$

A uniformly distributed load (u.d.l) of 21.89 kN/m (Li and Wong, 2014) has been applied on all the beams to give the axial compressive forces in the columns. A storey gravity load of Q (5978 KN) (Li and Wong, 2014) has been applied on each floor to take into account the geometric nonlinearity (mainly P-Δ effect) of the gravity columns. Kobe earthquake (see Figure 3.5) used by (Li and Wong, 2014) has considered as the input ground motion.

For validating the implemented FAM Matlab code, two building responses (i.e. roof displacement, x_{10}; and moment at PHL#1, m_1) of Li and Wong, (2014) have been selected. The comparison of the roof displacement, x_{10}; and moment at PHL#1, m_1, of the present work and those obtained from Li and Wong, (2014) are shown in Figures 3.6a and 3.6b. It has been observed that the results of implemented FAM code are in good agreement with that of Li and Wong, (2014). Hence the implemented FAM Matlab code is then used to conduct the Nonlinear Time History Analysis (NTHA) of steel building frame, under various earthquakes (presented in the subsequent sections).

3.4. Typical systematic analysis of mid-rise moment resisting steel frame

A typical detailed systematic NTHA using FAM of a mid-rise moment resisting steel frames has been performed considering the same 10-storey steel frame (Li and Wong, 2014) (see Figure 3.2), using the same Kobe (1995) earthquake record (see Figure 3.5) as the input ground motion. The responses of the building frame are presented in terms of displacement-based (e.g. floor displacement; storey drift ratio) and energy-based (e.g. plastic energy) responses.

a) Displacement-based seismic responses

Building floor displacements, i.e. total *x(t)* (consisting of both elastic *x'(t)* and inelastic *x''(t)* displacements), inelastic *x''(t)* and elastic *x'(t)* time histories have been shown in Figure 3.7a, 3.7b and 3.7c respectively. It has been seen that total

displacement time history has similar pattern with that of input ground motion (see Figure 3.5a) in having rise, strong motion and decay portions. Large deformation with permanent shifting of axis of vibration (or mean vibration location) of different floor time history responses has been observed after 7.30 sec of input ground motion (see Figure 3.7a). Such large deformation with permanent shifting of axis of vibration may be due to the occurrence of inelastic deformation since Kobe earthquake has highest PGA (0.82g), highest PGV (79.3 cm/sec), dominant period of ground excitation (0.9 sec) and longer strong motion duration (~6 sec) (see Figure 3.5). Variation of inelastic displacement components with time is shown in Figure 3.7b. It has been seen that inelastic displacement components occurs only during a specific period (i.e. from 3.01 sec to 7.30 sec) of input ground motion time history. For example, first inelastic displacement component occurs at 3.01 sec (see Figure3.7b) at the onset of strong motion due to the formation of first six plastic hinges (4.3% of all PHLs, see Figure 3.8a) with plastic energy dissipation of 2.15 KJ (see Table 3.3) at the beam members of 8^{th} floor level of 10-storey steel frame. As the strong motion proceeds, the occurrence of inelastic displacement component has also been found progressing with the new formation of plastic hinges across the building frame as well as increasing in magnitudes of the existing plastic hinges. For example, at 4.10 sec (during strong motion period), formation of plastic hinges has covered 38.6% of all PHLs (see Figure 3.8b) with 647.25 KJ (see Table 3.3) of plastic energy dissipation. Whereas at 7.30 sec of input ground motion, formation of plastic hinges has covered 72.8% of all PHLs (see Figure 3.8c) with 3698.49 KJ (see Table 3.3) of plastic energy dissipation. It has been observed that formation of plastic hinges ended at 7.30 sec since then there is neither formation of new plastic hinges nor increase in magnitudes of existing plastic hinges till the end of time history. Inelastic floor displacements after 7.30 sec have been observed to have permanent shift from the axis of building. The amount of shifting is observed to be different for different floor levels (see Figure 3.7b), and this may resulted into the permanent shifting of axis of vibration of total floor time history after 7.30 sec of input ground motion (see Figure 3.7a). It has also been observed that elastic component time history (see Figure 3.7c) has similar pattern with that of input ground motion (e.g. rise, strong motion and

decay portions); however, permanent shifting of axis of vibration has not been seen in case of elastic component time history.

For investigating the variation of elastic, inelastic and total displacement components at various floor levels along the building height, three instants (i.e. 3.01 sec, 4.10 sec and 7.30 sec) of the time history have been considered (see Figure 3.9). The three instants are selected in order to indicate onset, progress and end of inelastic displacement component formation respectively. It has been seen that elastic displacement component of all the floors exhibit linear variation along the height of the building (see Figure 3.9a); however non-uniform variation of inelastic component has been observed, wherein it increases sharply from base till 40% building height, with slight decrease around 60% building height, and then finally increases till top of the building height. The slight decrease in inelastic component from around 60% building height may be due to the formation of comparatively large inelastic floor deformations towards opposite (negative) side of the building at these floor levels in earlier instances (e.g. 5.20 sec) (see Figure 3.10) of time history which may resulted into less deformation towards the positive side of the building in the subsequent cycles of vibration. Variation of relative floor displacements along the building height can better be explained by storey drift ratio which is defined as,

$$\text{Storey drift ratio} = \frac{\text{Difference in floors' displacement of two consecutive floors}}{\text{storey height}} \text{x}100\%$$

Maximum storey drift ratio of ~2.05% has been observed at ~40% building height (see Figure 3.11a). Such observation of maximum storey drift ratio below mid-height of the building is in agreement with the findings of previous researchers (e.g. Ventura and Ding, 2000; Kim and Engelhardt, 2005; Hariri-ardebili *et al.*, 2013; and Krishnan and Muto 2013). It has also been observed that there appears to have a close relationship between maximum storey drift ratio and storey-wise plastic energy dissipation. Large amount of plastic energy has been observed to dissipate at the location where there is maximum storey drift ratio, as also reported by Uang *et al.*, (1997).

b) Energy-based seismic responses

The seismic responses of the building frame has been found to monitor from the amount of energy (e.g. plastic energy) dissipated at each member of the building frame, using conventional FE based CSDA method (e.g. Akbas *et al*., 2001; Chou and Uang, 2003; and Uang *et al*., 1997). However to the best of author's knowledge, investigation of detailed energy distribution across the frame structure using conventional FE based CSDA method has not been reported. In CSDA method, plastic energy dissipation has been approximated by calculating the area enclosed between the force and displacement responses (e.g. Mahin and Bertero, 1981). However in FAM, plastic energy dissipation can be estimated simply by multiplying elastic moment with change in plastic rotation (Wong and Zhao, 2007) as given in Equation 3.8.

Energy-based seismic analysis may be used to identify the structural members of the building frames which suffered major damages during earthquakes since large amount of energy (plastic energy) is dissipated at these damaged members of the structure; wherein displacement-based seismic analysis has found to be difficult in identifying such damaged members in the structure (Wong and Wang, 2003). Structural health monitoring can be performed by using energy-based seismic analysis since it can identify the sick (damaged) members in the structure. For example, the beam members at 3rd, 4th, 5th and 8th floor levels; and two inner ground floor columns are found to be critical (see Figure 3.8c) since maximum plastic energies are dissipated first at these members. Thus, probable future failure of the building frame structure may be prevented by strengthening or retrofitting the damaged members of the structure in advance.

c) Collapse analysis of moment resisting steel frame

A typical collapse analysis has been conducted on 10-storey steel frame using IDA study by increasing the intensity of amplitude of input ground motion (Kobe earthquake, 1995) gradually from 0.3 to 1.8. Time history responses of the steel

frame at scales values of 0.3, 0.6, 0.9, 1.2, 1.5 and 1.8 have been shown in Figure 3.12. As per EDP based method of collapse analysis (Vamvatsikos and Cornell, 2002; Zareian *et al*., 2010) the building functionality condition has been measured in terms of maximum storey drift ratio. The allowable maximum storey drift ratio of moment resisting frame has been considered as 4%, considering risk category I and II in case of NTHA (ASCE 7-16, 2016). Thus, a building frame is considered un-functional if the maximum storey drift ratio exceeds 4%. It has been found that 10-storey steel frame becomes un-functional (maximum storey drift ratio > 4%) at scale value of 1.21 (see Figure 3.13) near 8^{th} floor level (i.e. 80% building height). Results of the collapse analysis performed by using the IM based method (Vamvatsikos and Cornell, 2002; Zareian *et al*., 2010) has been shown in Figure 3.14. It has been seen that at lower scale values of amplitudes of input ground motion (i.e. less than 1.0); IDA curve of 4^{th} storey is found critical since 4^{th} storey experiences maximum storey drift ratio than the remaining storeys in the frame. However, at higher scale value (i.e. greater than 1.0), IDA curve of 8^{th} storey is found to be critical since extreme softening (more storey drift ratio at infinitesimal increase of scale value) occurs as soon as the scale value crosses 1.0, and thereby gradually becoming to attain dynamic instability at scale value of 1.8. The remaining storeys are seen to attain dynamic instability at scale value of 2.1. 'Weaving patter' (successive segments of softening and hardening) of IDA curve has been found in the IDA curve of 6^{th} storey (see Figure 3.14) which indicates 'self-stabilizing' nature of frame storey with increase in intensity of earthquake forces (Vamvatsikos and Cornell, 2002). This weaving pattern of IDA curve indicates that dynamic behaviours of frame structure is non-monotonic to intensity of input ground motion; rather it depends on the pattern as well as the timing of the motion rather than just the intensity of forcing function.

3.5 Effect of earthquake ground motions on mid-rise moment resisting steel frames

For investigating the effect of ground motion records on seismic responses of the mid-rise moment resisting steel frames; three moment resisting steel frames of different heights (i.e. 6, 8 and 10-storeys) (see Figures 3.2 and 3.15) and seven real

earthquake ground motion records having different earthquake characteristics (*viz*., Kobe, 1995; Northridge, 1994; El_Centro, 1940; Imperial Valley, 1979; Loma Prieta, 1989; Friuli, 1976; and Kocaeli, 1999) (see Figures 3.16-3.22) have been considered. 8-storey steel frame has been constructed from 10-storey steel frame (see Figures 3.2) by eliminating the bottom two storeys; similarly 6-storey steel frame has also been constructed from 8-storey steel frame by eliminating the bottom two storeys (see Figures 3.15). Time periods and frequencies of different modes of 10, 8 and 6-storey steel frames are shown in Tables 3.2, 3.4 and 3.5 respectively. Fundamental time periods of 10, 8 and 6-storey steel frame are computed to be 1.54, 1.32 and 1.05 sec respectively. Also, details of the seven earthquakes ground motion records (i.e. PGA, PGV and dominant time periods,) are shown in Table 3.6. Effects of earthquake ground motions on 10-storey, 8-storey and 6-storey steel frames are presented in subsequent sections.

a) Effect of earthquake ground motions on 10-storey steel frame

The story drift ratio and plastic energy dissipation of the reference 10-storey steel frame for the seven earthquakes are shown in Figure 3.23. It has been observed that among the seven earthquakes, three earthquakes (i.e. El_Centro, 1940; Imperial Valley, 1979; and Friuli, 1976) resulted in linear responses of the reference 10-storey steel frame as indicated by the absence of plastic energy dissipation for these three earthquakes (see Figure 3.23b, Table 3.7); whereas the remaining four earthquakes (i.e. Kobe, 1995; Northridge, 1994; Loma Prieta, 1989; and Kocaeli, 1999) resulted in nonlinear responses as indicated by plastic energy dissipation (see Figure 3.23b, Table 3.7). The non-linear responses may be related to the critical characteristics of these four earthquakes (i.e. peak ground acceleration (PGA) and peak ground velocity to acceleration ratio (V/A) (Sucuoğlu and Nurtuğ, 1995), peak ground velocity (PGV) (Krishnan and Muto, 2013), dominant period of ground motion and effective response duration (Sucuoğlu and Nurtuğ, 1995; Krishnan and Muto, 2013)). Among the seven earthquakes, Kobe earthquake has been found to give the maximum seismic responses since Kobe earthquake has highest PGA (0.82g) (refer Table 3.6), highest PGV (79.3 m/sec) (refer Table 3.6), dominant period of ground

excitation (0.9 sec) (refer Table 3.6) close to 10-storey fundamental period (1.54 sec) (refer Table 3.2), and effective longer duration of strong motion (0.6 sec) (see Figure 3.16a). It has also been observed that Kocaeli earthquake has found to give higher seismic response than Northridge earthquake for 10-storey steel frame (see Figure 3.23) although PGA of Northridge (i.e. 0.57 g) is more than that of Kocaeli (i.e. 0.35 g) (refer Table 3.6). It may relate with the findings of (Krishnan *et al*., 2006) that PGA which is dominated by the higher frequencies has been found to have little effect on the seismic behaviour of long period (e.g. 10-storey steel frame) building since the amplitudes of high frequency ground acceleration are likely to have had attenuated significantly due to long propagation distance. Hence seismic behaviours of long period building frame has been found to have better correlation with PGV rather than PGA. Further long period building frames have been generally observed to be more responsive with long period seismic excitation (Krishnan and Muto, 2013). Thus, the observed higher seismic responses of relatively longer period (1.54 sec) 10-storey steel frame due to Kocaeli earthquake may be associated with larger PGV (62 m/sec) and longer period (2.2 sec) of seismic excitation as compared to that of Northridge earthquake (PGV 51.8 m/sec and period of seismic excitation 0.5 sec). It has also been observed that PGV and period of ground motion of Loma Prieta earthquake are found to be 44.5 cm/sec and ~1.5 sec respectively (see Table 3.6). Thus, the sequence of earthquakes (giving nonlinear responses) in order of decreasing criticality for 10-storey steel frames is found to be as Kobe, Kocaeli, Northridge and Loma Prieta (see Figures 3.23, Table 3.7). It has also been seen that maximum storey drift ratio and maximum plastic energy dissipation are found to occur within 30% to 40% building height for 10-storey steel frame for all seven earthquakes (see Figure 3.23).

b) Effect of earthquake ground motions on 8-storey steel frame

Similar observations as that of 10-storey steel frame have also been seen in case of 8-storey steel frame. The sequence of earthquakes (giving nonlinear responses) in order of decreasing criticality (maximum storey drift ratio, plastic energy dissipation) for 8-storey steel frames is found to be as Kobe, Kocaeli, Northridge and Loma Prieta (see

Figures 3.24, Table 3.8). However, maximum storey drift ratio and maximum plastic energy dissipation occur within 30% to 50% building height for 8-storey steel frame for all seven earthquakes (see Figure 3.24).

c) Effect of earthquake ground motions on 6-storey steel frame

For 6-storey steel frame, it has been observed that among seven earthquakes, two earthquakes (i.e. Imperial Valley, 1979 and Friuli, 1976) resulted in linear responses as there is no plastic energy dissipation for these two earthquakes (see Figure 3.25b, Table 3.9); whereas remaining earthquakes (i.e. Kobe, 1995; Northridge, 1994; El_Centro, 1940; Loma Prieta, 1989; and Kocaeli, 1999) resulted in nonlinear responses as indicated by plastic energy dissipation (see Figure 3.29b, Table 3.9). Among seven earthquakes, Kobe earthquake has been found to give the maximum responses since Kobe earthquake has maximum PGA of 0.82g, PGV of 79.3 m/sec with dominant period of ground motion T of ~0.9 sec (see Table 3.6) which is close fundamental time period of 6-storey steel frame (i.e. 1.05 sec, refer Table 3.5). In case of 6-storey steel frame, Kocaeli earthquake has been found to give lesser seismic response than Northridge earthquake (see Figure 3.25); it may be due to the reason that dominant period of ground motion of Northridge earthquake (i.e. 0.5 sec, refer Table 3.6) is much closer to the fundamental period of 6-storey steel frame (i.e. 1.05 sec, refer Table 3.5) than that of Kocaeli earthquake (i.e. 2.2 sec, refer Table 3.6). Thus, it has been observed that long period ground excitation has been seen to have less effect on short period building frame. The sequence of earthquakes (giving nonlinear responses) in order of decreasing criticality for 6-storey steel frames is found to be as Kobe, Northridge, El_Centro, Kocaeli and Loma Prieta (see Figures 3.25, Table 3.9). Unlike 8 and 10-storey steel frames, it has also been observed that maximum storey drift ratio occurs at 20% building height whereas maximum plastic energy dissipation occur within 0% to 20% building height for 6-storey steel frame for all seven earthquakes (see Figure 3.25).

3.6 Effect of building height on seismic responses of mid-rise moment resisting steel frames

The effect of storey height on seismic responses of mid-rise moment resisting steel frames is presented in the form of variation of storey drift ratio and plastic energy dissipation as shown in Figures 3.26-3.32, for all seven earthquakes. It has been observed that seismic responses (i.e. storey drift ratio, plastic energy dissipation) increases as the height of the building frame decreases (i.e. from 10-storey to 6-storey) when subjected to Kobe earthquake (see Figure 3.26). It is because Kobe earthquake has shorter period of ground excitation (~0.9 sec) and hence shorter periods building frames (e.g. 6-storey (1.05 sec) and 8-storey (1.32 sec)) are likely to respond more than the longer period 10-storey (1.54 sec) steel frame. Thus it has been seen that seismic responses increases as the height of building frame decreases for short period ground excitations (i.e. Kobe (T ~0.9 sec), Figure 3.26; Northridge (T ~0.5 sec), Figure 3.27; El_Centro (T ~0.6 sec), Figure 3.28; Imperial Valley (T ~0.9 sec), Figure 3.29; and Friuli (T ~0.8 sec), Figure 3.31); whereas seismic responses decreases as the height of building frame decreases for long period ground excitations (i.e. Loma Prieta (T ~1.5 sec), Figure 3.30; and Kocaeli (T ~2.2 sec), Figure 3.32).

3.7 Collapse analysis of moment resisting steel frame under different earthquake ground motions

Collapse analysis has been conducted for 10-storey steel frame considering those earthquake ground motions (i.e. Kobe, Northridge, Loma Prieta and Kocaeli) which give nonlinear seismic responses. 10-storey steel frame has been considered since collapse behaviour is more reflected in taller building frames. It has been observed in general that IDA curves of 4^{th} storey is found to be critical at lower scale values (i.e. lower than 1.0) of amplitude of ground motions, since 4^{th} storey experience greater maximum storey drift ratio than other storeys (see Figure 3.33); however at higher scale values (i.e. greater than 1.0), any storey may become critical. For example, 8^{th}, 2^{nd}, 4^{th} and 2^{nd} storeys become critical at higher scale values for Kobe, Northridge,

Loma Prieta and Kocaeli earthquakes respectively (see Figure 3.33). Thus, collapse of the building frame can be initiated from any storey level at higher scale values depending on the natures of earthquake ground motion and building frame. It has also been observed that 10-storey steel frame collapses early at lowest scale of 2.1 when subjected by Kobe earthquake, thus becoming the most critical among the seven earthquakes. The sequence of criticality of earthquakes in collapse analysis of 10-storey steel frame is found to be as Kobe, Northridge, Kocaeli and LomaPrieta (see figure 3.33).

3.8 Conclusion

This chapter presents a detailed systematic investigation on mass regular mid-rise (6, 8 and 10-storey) moment resisting steel frames by performing NTHA using implemented FAM code in Matlab considering both material and geometric nonlinearities. Seven real earthquake ground acceleration records have been considered in the analysis. The results are presented in the form of displacement-based responses (e.g. floor displacement (elastic, inelastic and total) and storey drift ratio); and energy-based responses (e.g. plastic hinge formation; plastic energy dissipation). The following conclusions are drawn from the above analysis.

1. Elastic component of floors' displacement has been observed to exhibit uniform (linear) variation along the building height.
2. Inelastic component of floors' displacement has been observed to exhibit non-uniform variation along the building height. It has been observed that maximum amount of inelastic component is found to concentrate near lower storeys (i.e. 20% to 40% building height) of building frames.
3. Maximum amount of plastic energy has been found to dissipate at the location where there is maximum storey drift ratio along the building height.
4. The seismic response of the building frame is found to be maximum when the input ground motion has critical characteristics like maximum PGA and PGV values, periods of ground excitation close to building fundamental period and large duration of strong motion.

5. Seismic response of the building frame has been found to increase when the height of the building frame decreases for short period ground excitation; on the other hand, the seismic response has been found to decrease when the height of the building frame decreases for long period ground excitation.
6. Based on the IDA study it has been observed in general that lower storey (e.g. 4th storey of 10-storey steel frame) becomes critical at lower scale values (i.e. less than 1.0) of amplitude of ground motion; however the same lower storey may or may not become critical at upper scale values of amplitudes of ground motion.

Table 3.1: Section properties used in 6, 8 and 10-storey moment resisting steel frames

Type	Sections	Moment of Inertia, (I) × 10^{-3} m^4	Plastic Section Modulus, (Z) × 10^{-3} m^3	Yield Moment, (M_y) KN-m
A	W14 × 370	2.26	12.06	3015.21
B	W14 × 311	1.80	9.88	2470.34
C	W14 × 283	1.59	8.88	2220.44
D	W14 × 257	1.41	7.98	1995.12
E	W14 × 193	0.99	5.81	1454.35
F	W14 × 605	4.49	21.63	5407.73
G	W14 × 550	3.92	19.33	4834.18
H	W14 × 455	2.99	15.33	3834.57
I	W14 × 426	2.74	14.24	3560.08
J	W14 × 342	2.03	11.01	2753.02
K	W36 × 260	7.20	17.43	4358.95
L	W36 × 230	6.24	15.25	3814.08
M	W36 × 210	5.49	13.65	3412.60
N	W36 × 182	4.70	11.76	2941.47
O	W36 × 150	3.76	9.52	2380.22
P	W36 × 135	3.24	8.34	2085.25
Q	W27 × 94	1.36	4.55	1138.90

Table 3.2: Building periods, frequencies and damping for different modes of 10-storey steel frame

Modes	Periods (Sec)	Frequency (H_Z)	Damping (%)
1	1.54	0.64	3
2	0.55	1.78	3
3	0.33	2.95	3
4	0.23	4.22	3
5	0.18	5.52	3
6	0.14	6.76	3
7	0.12	8.15	3
8	0.10	9.48	3
9	0.09	10.58	3
10	0.08	12.12	3

Table 3.3: Plastic energy dissipated in Kilo-Joules (KJ) by 10-storey steel frame for Kobe Earthquake

Floors	3.01 sec	4.60 sec	7.30 sec
0	0.00	0.00	169.20
1	0.00	0.00	234.92
2	0.00	0.00	352.94
3	0.00	15.68	519.78
4	0.00	56.79	642.82
5	0.00	73.84	479.85
6	0.00	64.74	266.39
7	0.00	154.75	344.84
8	2.15	162.57	449.11
9	0.00	118.88	234.97
10	0.00	0.00	3.67
Total	**2.15**	**647.25**	**3698.49**

Table 3.4: Building periods, frequencies and damping for different modes of 8-storey steel frame

Modes	Periods (sec)	Frequency (H_Z)	Damping (%)
1	1.32	0.76	3
2	0.47	2.11	3
3	0.28	3.55	3
4	0.19	5.07	3
5	0.15	6.58	3
6	0.21	8.19	3
7	0.10	9.73	3
8	0.09	11.06	3

Table 3.5: Building periods, frequencies and damping for different modes of 6-storey steel frame

Modes	Periods (sec)	Frequency (H_Z)	Damping (%)
1	1.05	0.95	3
2	0.38	2.61	3
3	0.22	4.43	3
4	0.15	6.37	3
5	0.11	8.48	3
6	0.09	10.5	3

Table 3.6: Earthquakes record data (Courtesy: Strong-motion virtual data center, VDC, 2012)

	Earthquakes	Recording station:	PGA (g)	PGV (m/sec)	Dominant periods T (sec)
1	The Kobe (Japan) January 16, 1995.	KJMA, Japan Meteorological Agency	+0.6, -0.82	+79.2, -79.3	0.9
2	The Northridge (USA) January 17, 1994.	090 CDMG STATION 24278	+0.57, -0.35	+42, -51.8	0.5
3	El_Centro (USA) May 19, 1940.	USGS STATION 0117	+0.35, -0.27	+38.5, -20	0.6
4	The Imperial Valley (USA) October 15, 1979.	USGS STATION 5115	+0.29, -0.32	+31.5, -23	0.9
5	The Loma Prieta (USA) October 18, 1989.	090 CDMG STATION 47381	+0.37, -0.28	+44.5, -35	1.5
6	The Friuli (Italy) May 06, 1976.	TOLMEZZO(000)	+0.35, -0.26	+20, -22	0.8
7	The Kocaeli (Turkey) August 17, 1999.	YARIMCA(KOERI330)	+0.20, -0.35	+58, -62	2.2

Table 3.7: Plastic Energy (PE) dissipated in Kilo-Joules (KJ) for 10-storey steel frame

	Kobe	Northridge	El-Centro	Imperial Valley	Loma Prieta	Friuli	Kocaeli
Gr Floor	169.66	49.94	0.00	0.00	16.90	0.00	21.36
1st Floor	237.71	56.36	0.00	0.00	3.85	0.00	30.15
2nd Floor	314.88	64.53	0.00	0.00	66.71	0.00	316.01
3rd Floor	526.41	269.22	0.00	0.00	166.06	0.00	511.38
4th Floor	631.79	142.86	0.00	0.00	66.34	0.00	380.99
5th Floor	542.74	47.45	0.00	0.00	8.58	0.00	162.05
6th Floor	357.79	0.00	0.00	0.00	0.00	0.00	0.21
7th Floor	445.01	0.12	0.00	0.00	0.00	0.00	0.00
8th Floor	474.80	10.16	0.00	0.00	0.00	0.00	0.00
9th Floor	258.19	0.00	0.00	0.00	0.00	0.00	0.00
10th Floor	1.86	0.00	0.00	0.00	0.00	0.00	0.00
Total	**3960.86**	**640.63**	**0.00**	**0.00**	**328.44**	**0.00**	**1422.14**

Table 3.8: Plastic Energy (PE) dissipated in Kilo-Joules (KJ) for 8-storey steel frame

	Kobe	Northridge	El-Centro	Imperial Valley	Loma Prieta	Friuli	Kocaeli
Gr Floor	304.74	11.11	0.00	0.00	20.79	0.00	121.49
1st Floor	522.36	37.74	0.00	0.00	20.73	0.00	203.96
2nd Floor	1063.81	112.69	0.00	0.00	28.62	0.00	434.72
3rd Floor	880.79	88.23	0.00	0.00	17.93	0.00	387.00
4th Floor	615.99	9.23	0.00	0.00	0.00	0.00	44.25
5th Floor	283.81	0.00	0.00	0.00	0.00	0.00	25.02
6th Floor	352.95	0.00	0.00	0.00	8.12	0.00	8.69
7th Floor	248.58	0.00	0.00	0.00	0.00	0.00	0.00
8th Floor	6.88	0.00	0.00	0.00	0.00	0.00	0.00
Total	**4279.91**	**258.99**	**0.00**	**0.00**	**96.20**	**0.00**	**1225.12**

Table 3.9: Plastic Energy (PE) dissipated in Kilo-Joules (KJ) for 6-storey steel frame

	Kobe	Northridge	El-Centro	Imperial Valley	Loma Prieta	Friuli	Kocaeli
Gr Floor	1265.32	159.46	108.50	0.00	22.41	0.00	42.77
1st Floor	2248.15	107.57	47.92	0.00	0.00	0.00	0.00
2nd Floor	404.55	0.00	0.00	0.00	0.00	0.00	0.00
3rd Floor	503.01	0.00	5.70	0.00	0.00	0.00	4.94
4th Floor	333.86	13.38	14.06	0.00	0.00	0.00	0.00
5th Floor	245.30	3.23	0.00	0.00	0.00	0.00	0.00
6th Floor	0.00	0.00	0.00	0.00	0.00	0.00	0.00
Total	**5000.18**	**283.64**	**176.18**	**0.00**	**22.41**	**0.00**	**47.71**

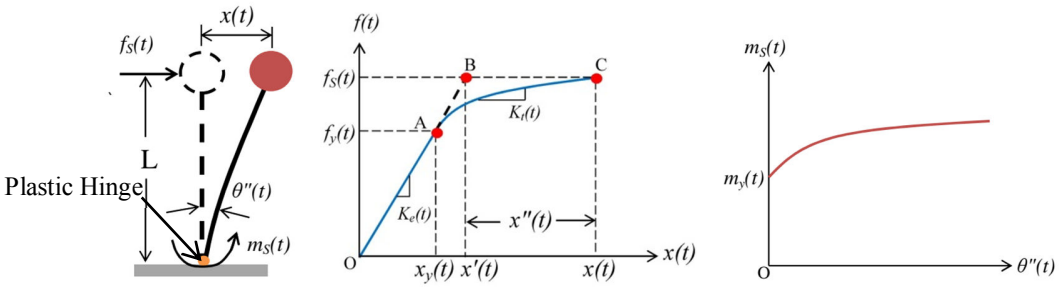

Figure 3.1: Framework of the FAM: (a) SDOF system, (b) force-displacement relationship and (c) moment-plastic rotation relationship

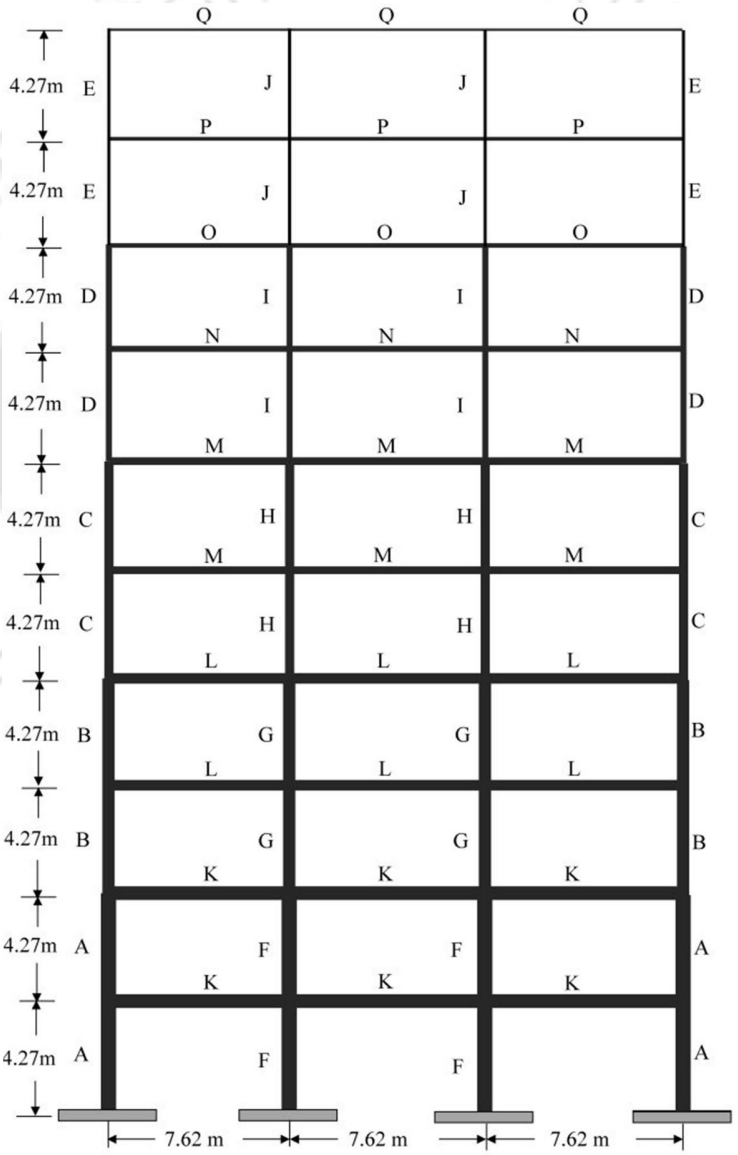

Figure 3.2: 10-storey moment resisting steel frame (Li and Wong, 2014)

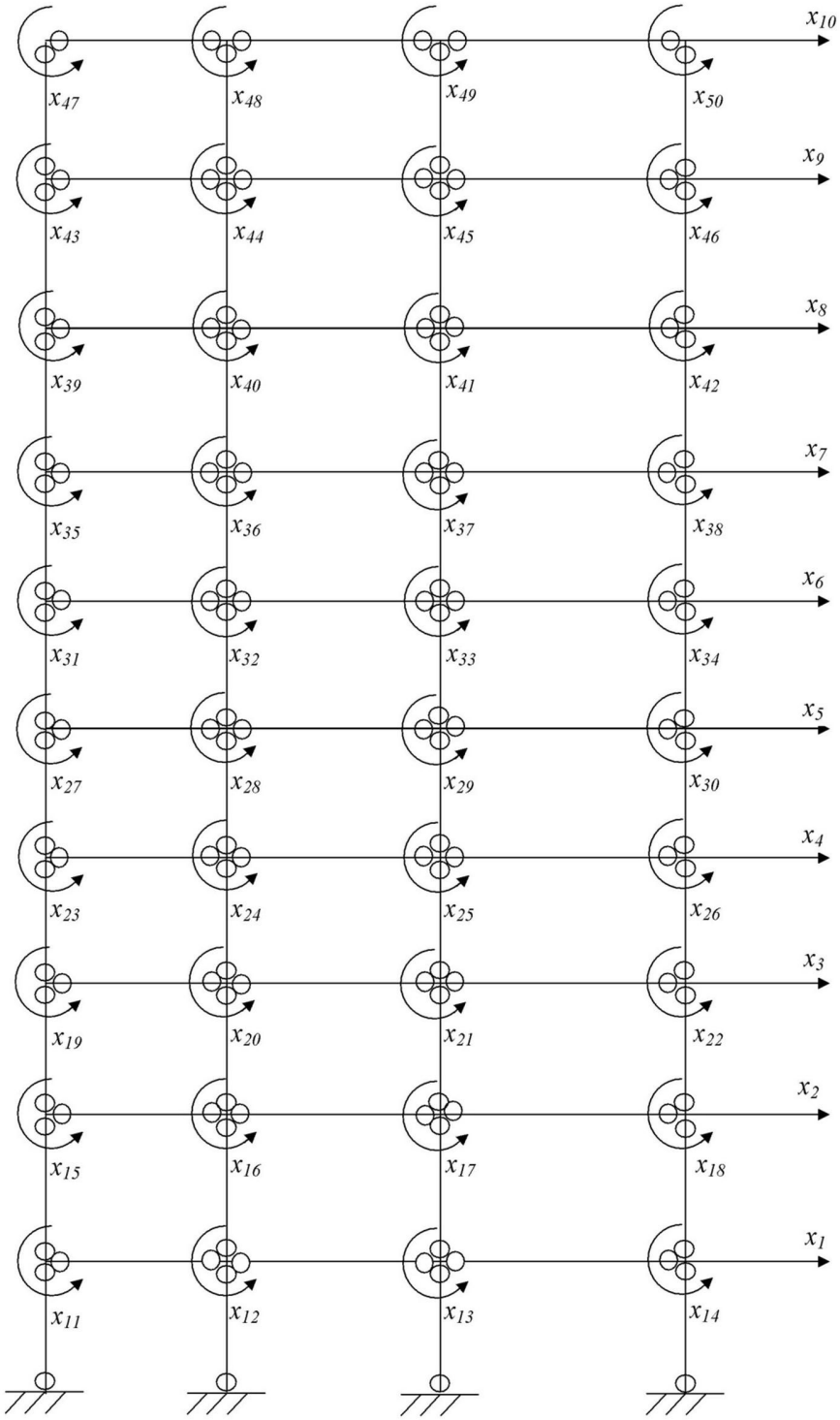

Figure 3.3: 10-storey steel frame showing Degree Of Freedoms (DOFs)

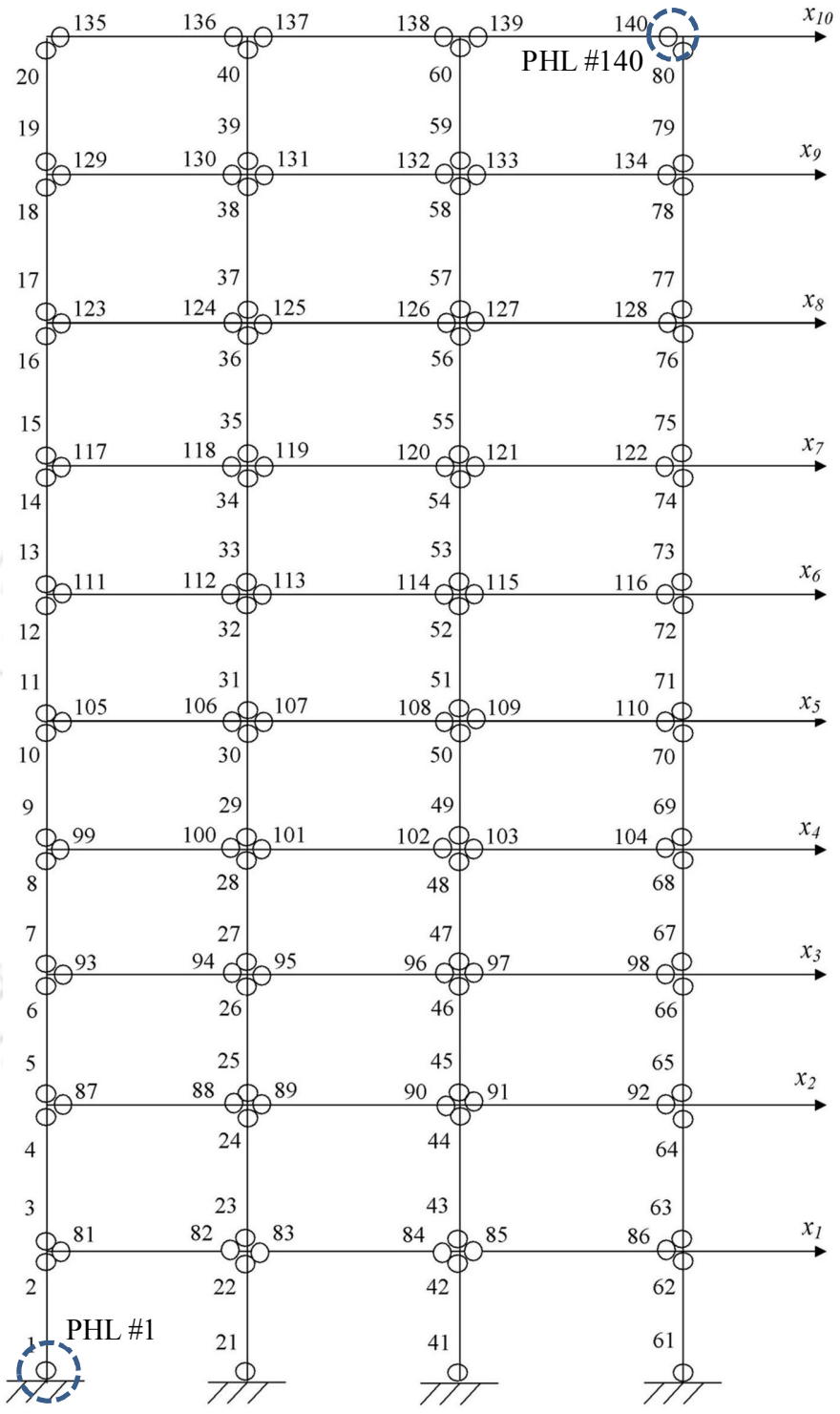

Figure 3.4: 10-storey steel frame showing Plastic Hinge Locations (PHLs)

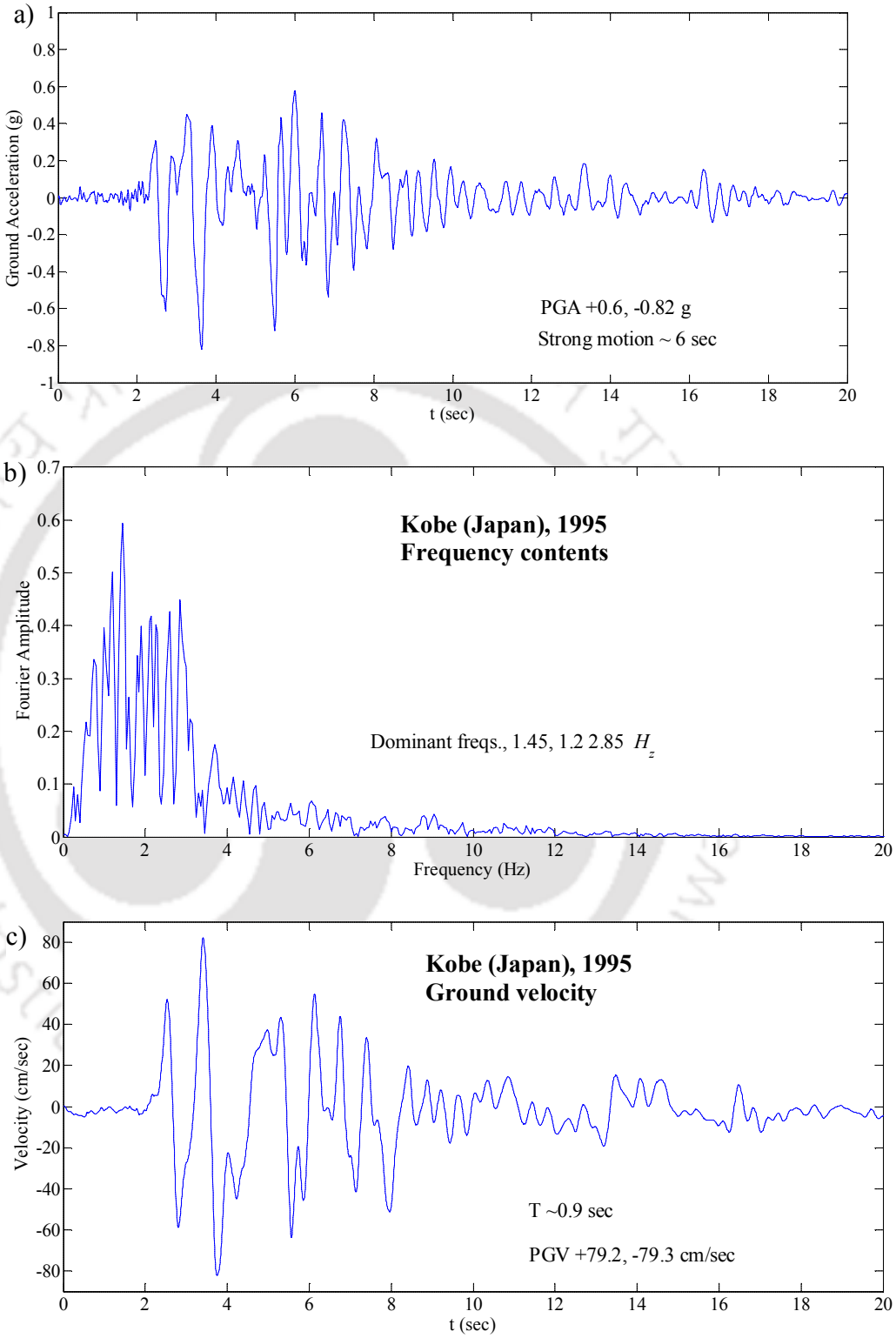

Figure 3.5: Kobe earthquakes (1995) a) ground acceleration, b) frequency and c) ground velocity

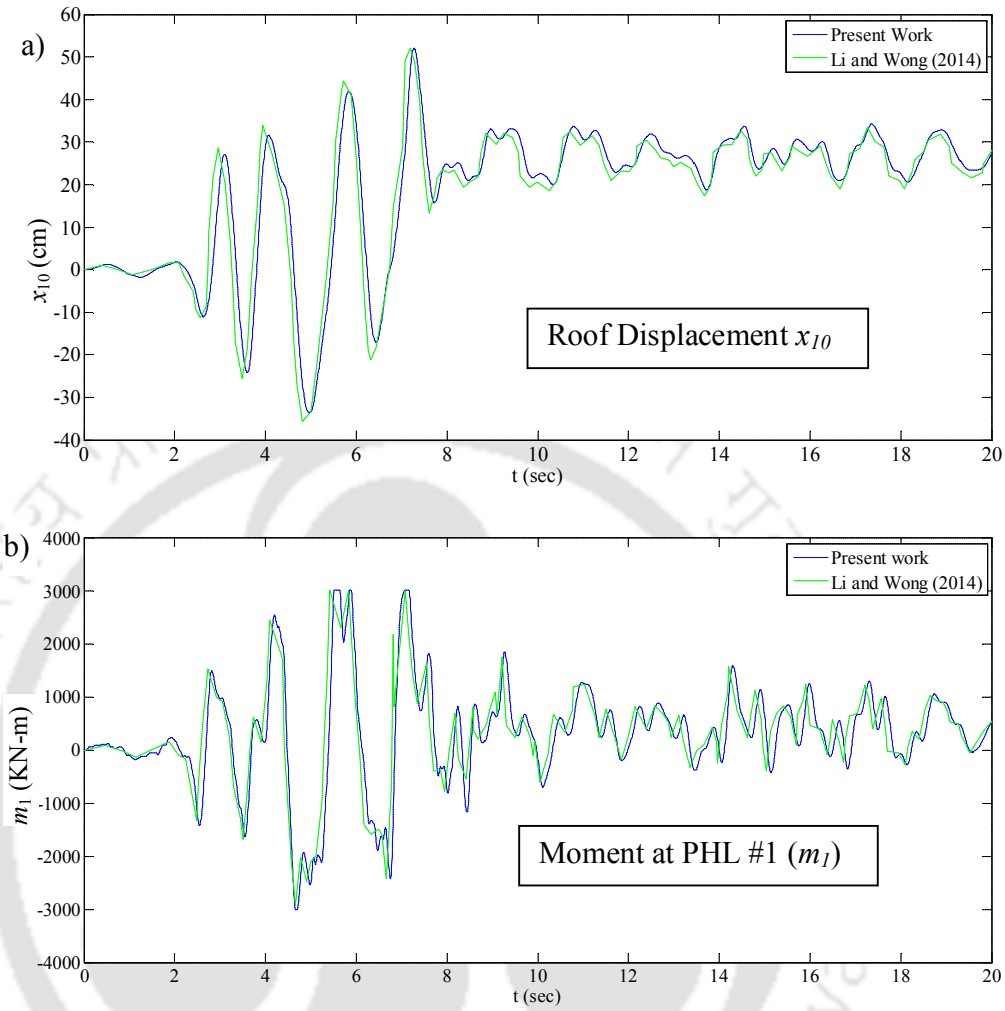

Figure 3.6: Validation of implemented Matlab code with Li and Wong, 2014.

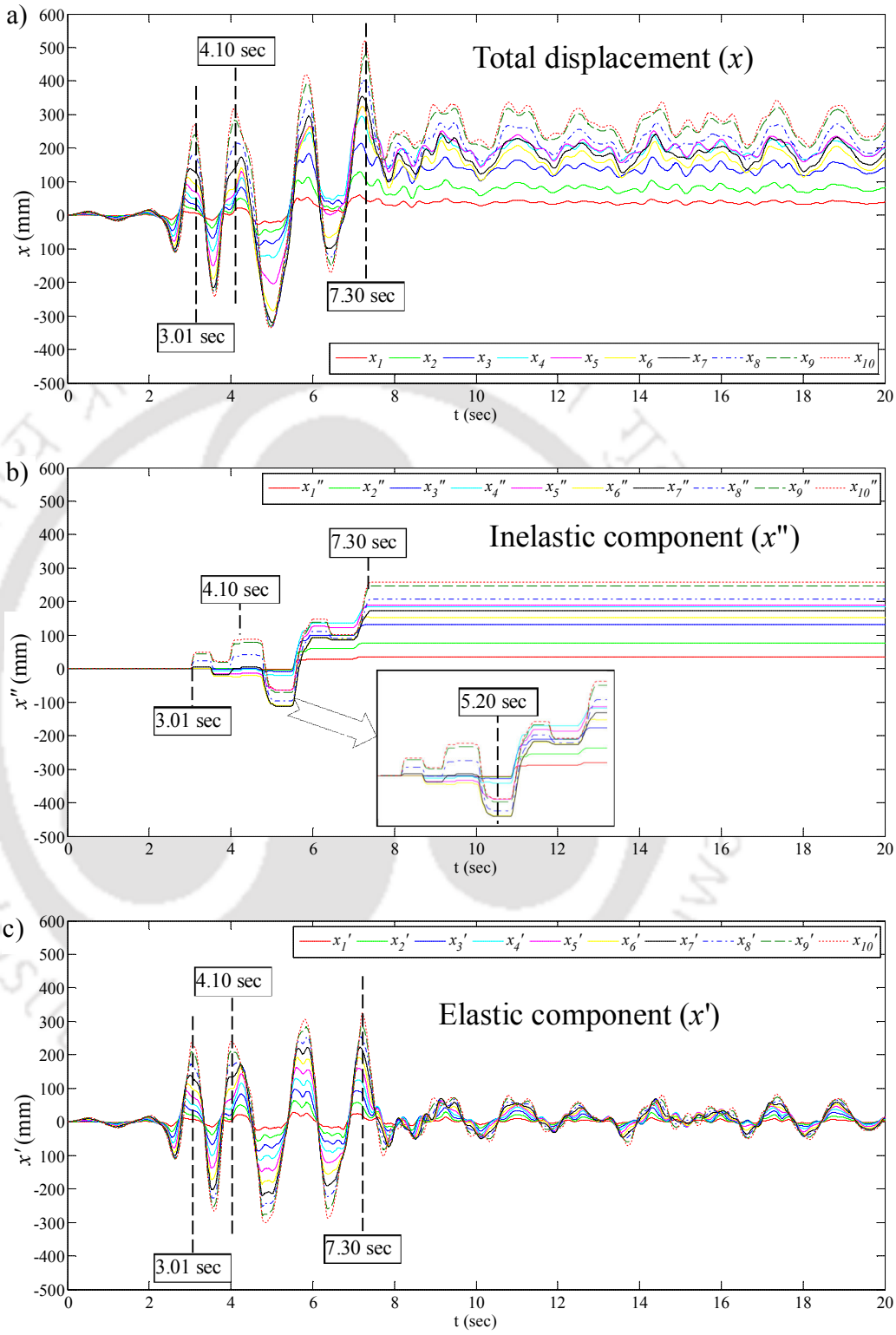

Figure 3.7: Time history responses of 10-storey steel frame for Kobe earthquake: a) Total displacement, b) Inelastic component and c) Elastic component.

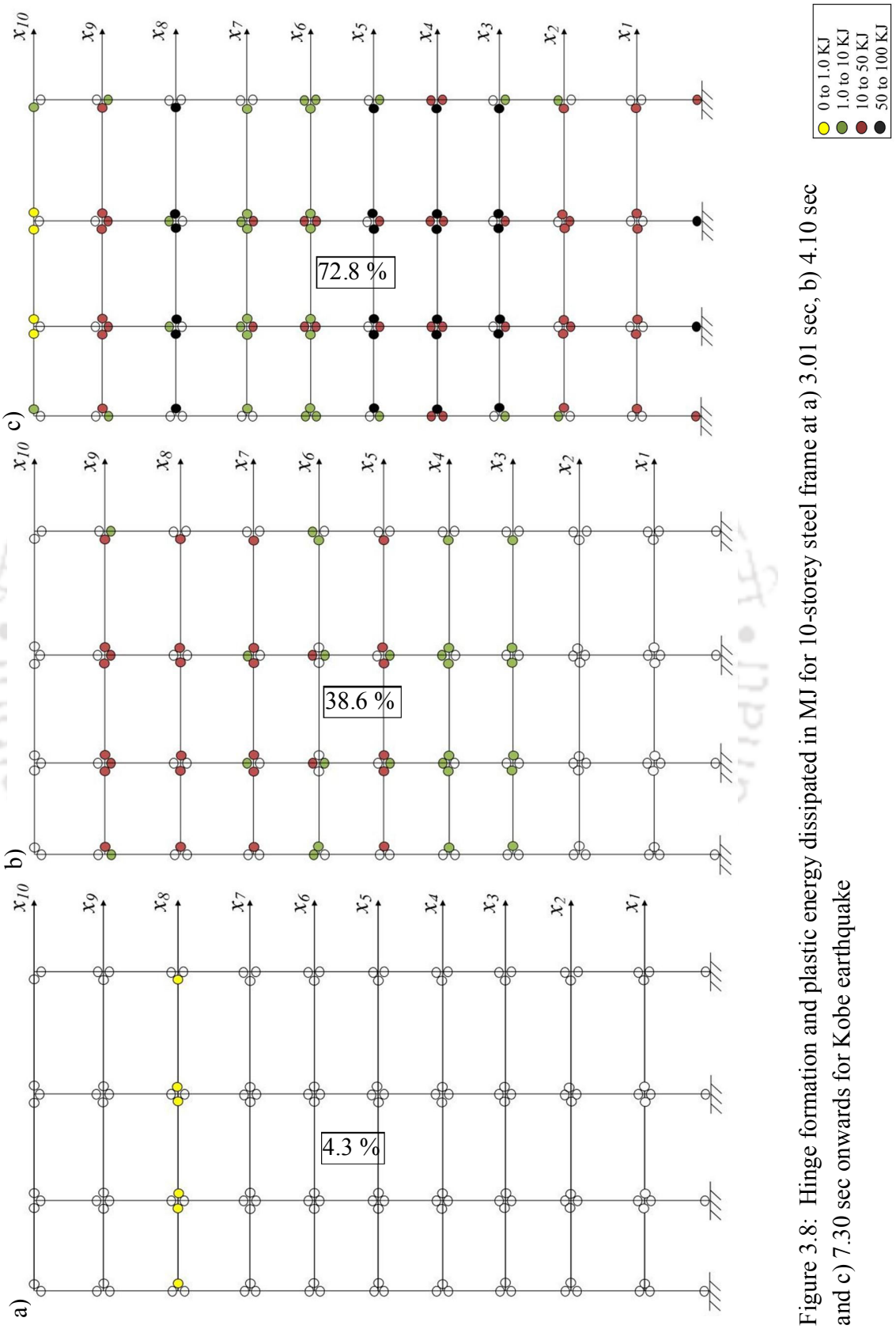

Figure 3.8: Hinge formation and plastic energy dissipated in MJ for 10-storey steel frame at a) 3.01 sec, b) 4.10 sec and c) 7.30 sec onwards for Kobe earthquake

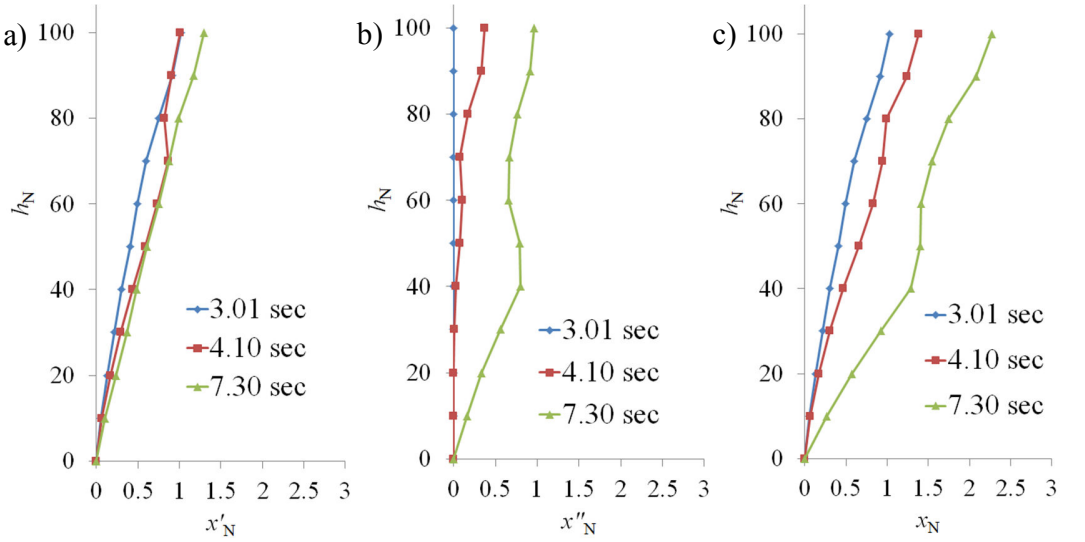

Figure 3.9: Floor displacements components a) Elastic b) Inelastic and c) Total displacement for 10-storey steel frame for Kobe earthquake

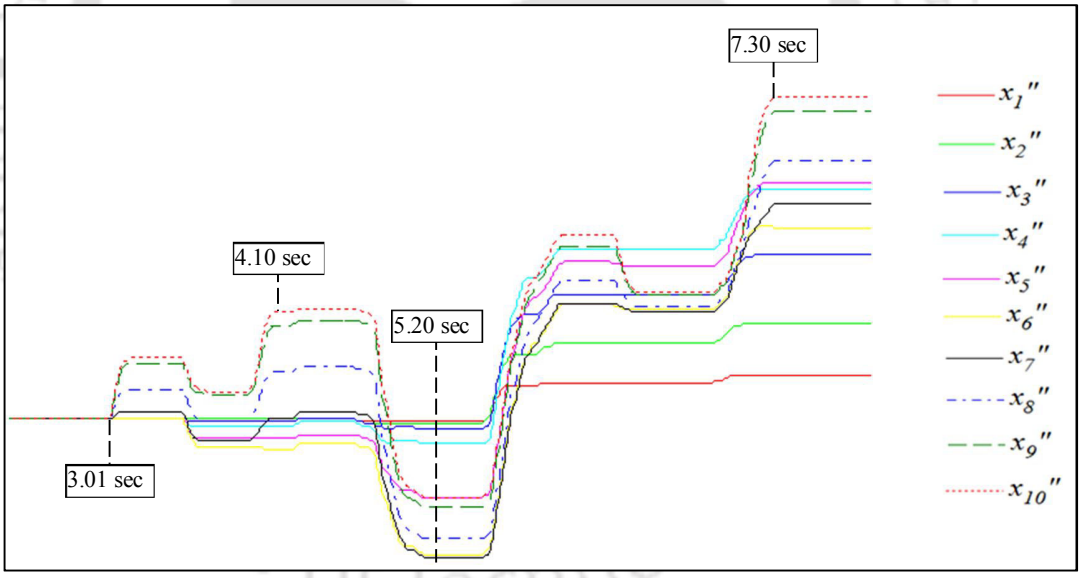

Figure 3.10: Inelastic component time history during strong motion periods of ground motion (refer Figure 3.7b)

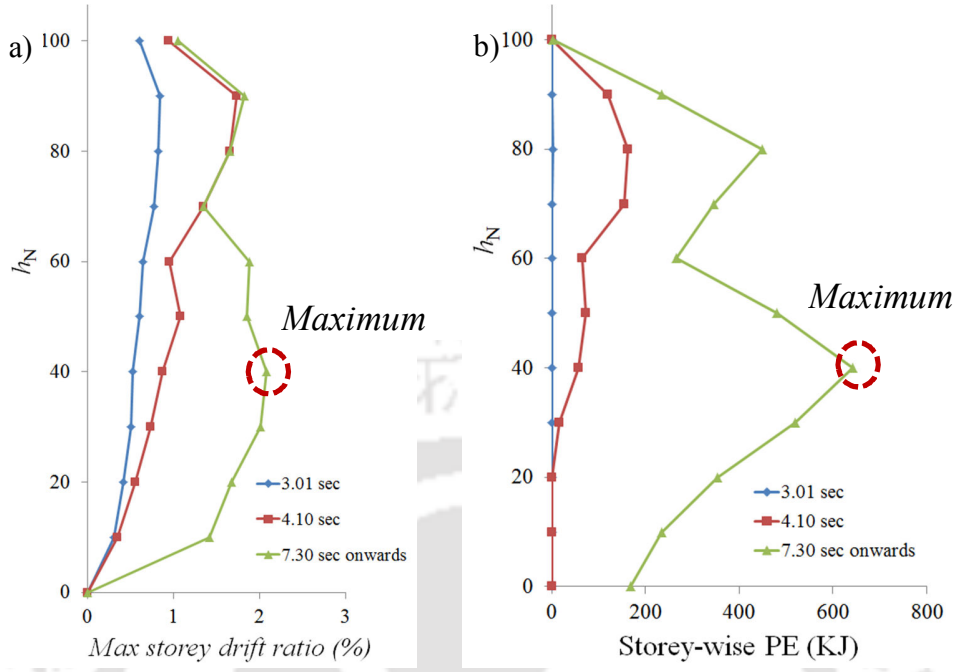

Figure 3.11: a) Storey drift ratio and b) storey-wise plastic energy dissipation for10-storey steel frame at different instants of Kobe earthquake

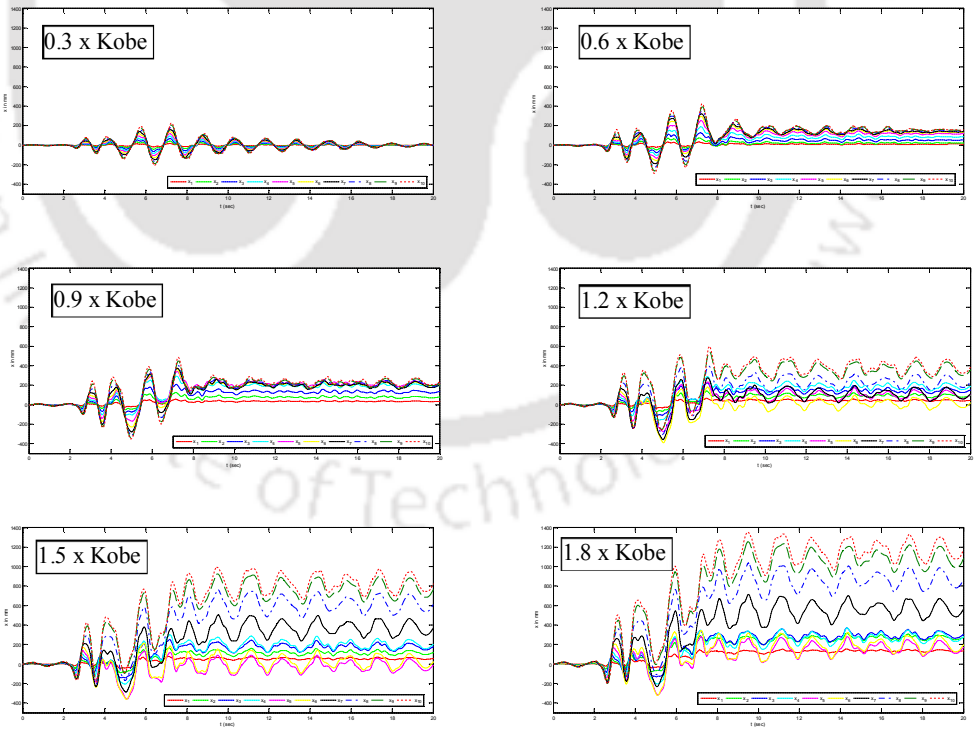

Figure 3.12: Total floor displacements for 10-storey steel frame at different scale values of Kobe earthquake

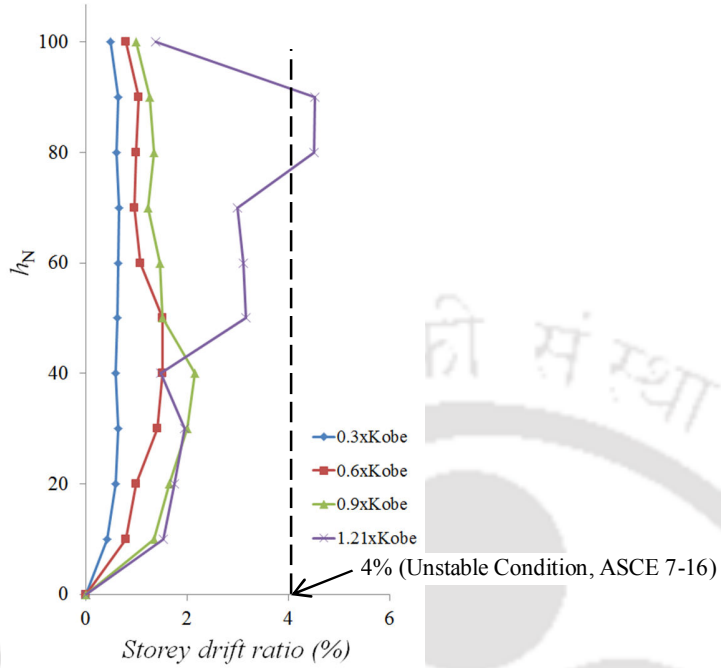

Figure 3.13: Storey drift ratio for 10-storey steel frame at different scale values of Kobe earthquake

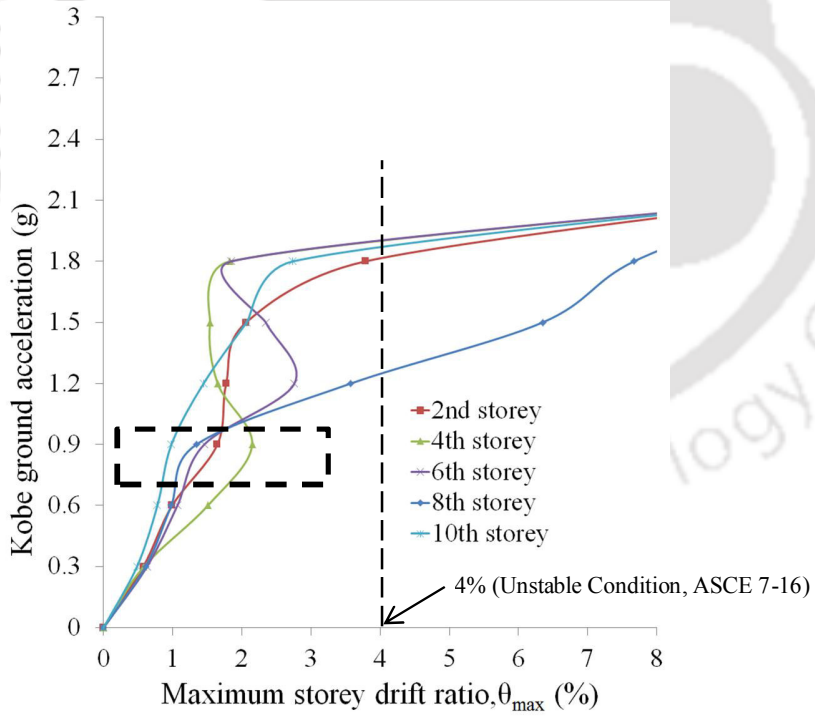

Figure 3.14: Storey-wise IDA curves of maximum storey drifts of 10-storey steel frame for Kobe earthquake

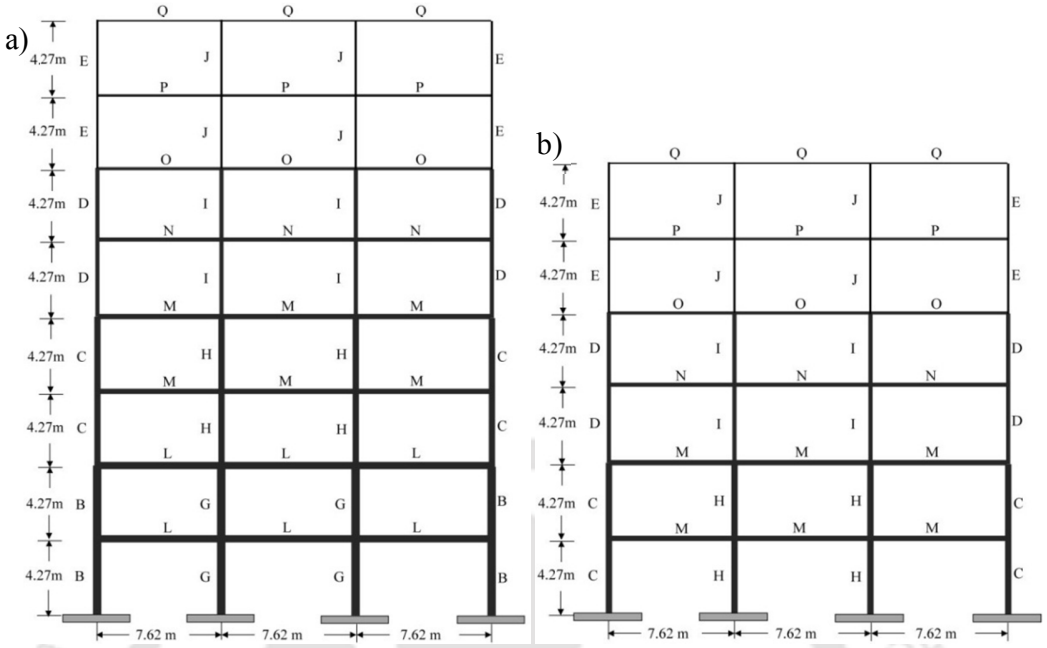

Figure 3.15: a) 8-storey and b) 6-storey moment resisting steel frames

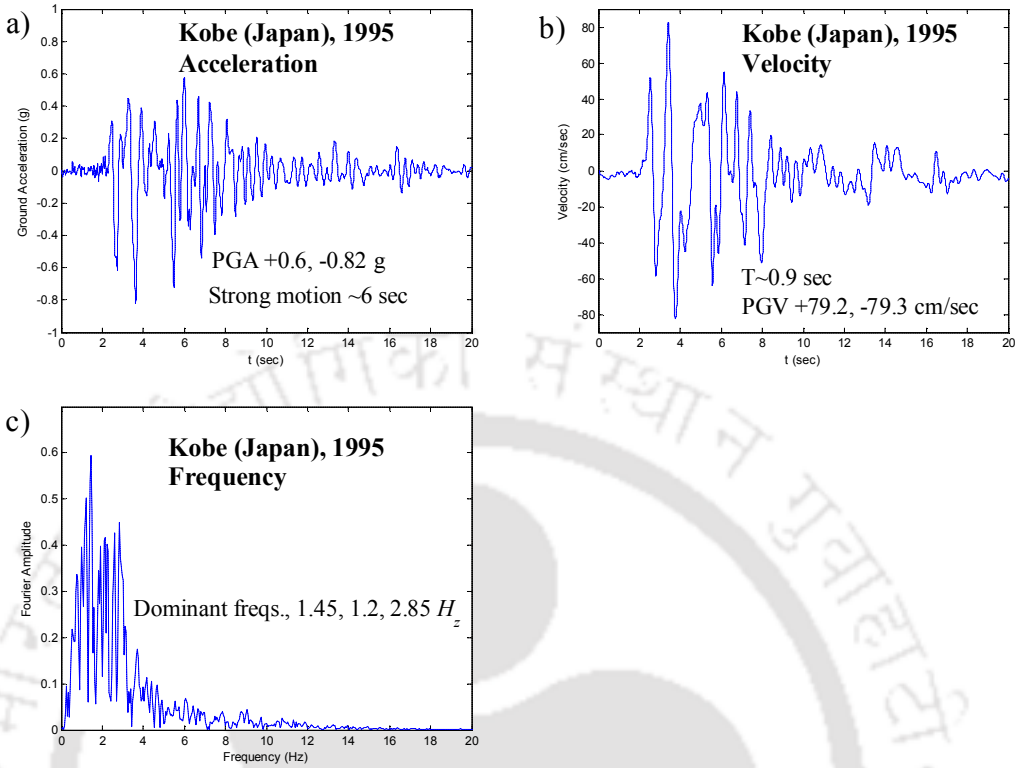

Figure 3.16: Kobe earthquake a) acceleration, b) velocity and b) frequency

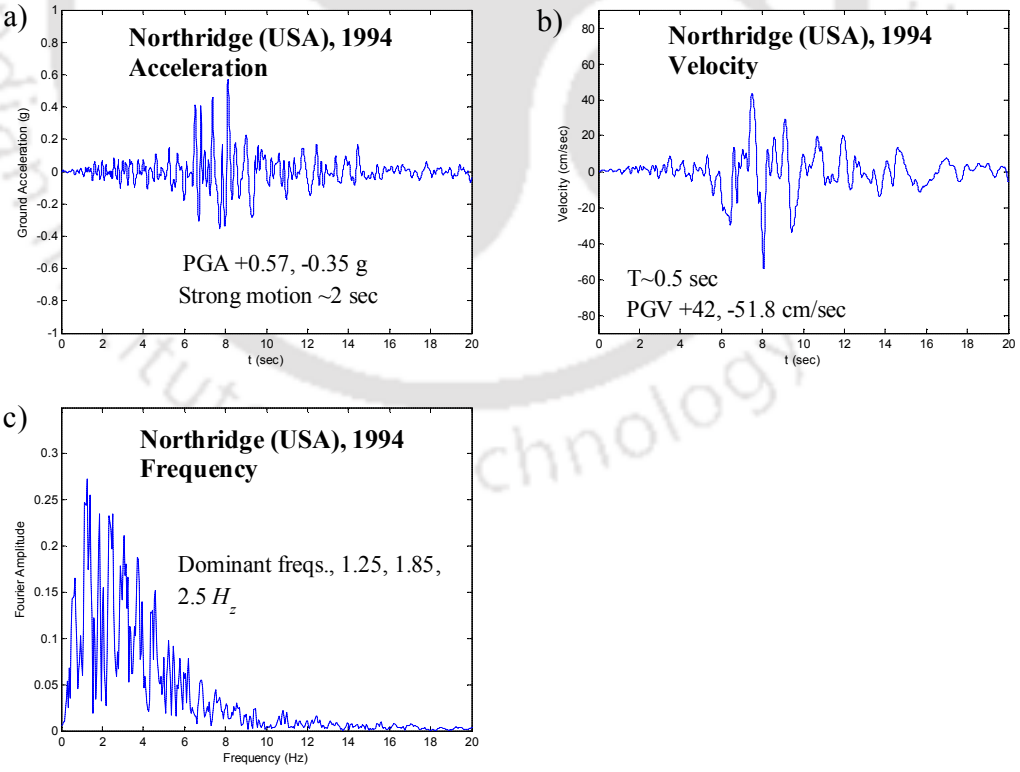

Figure 3.17: Northridge earthquake a) acceleration, b) velocity and b) frequency

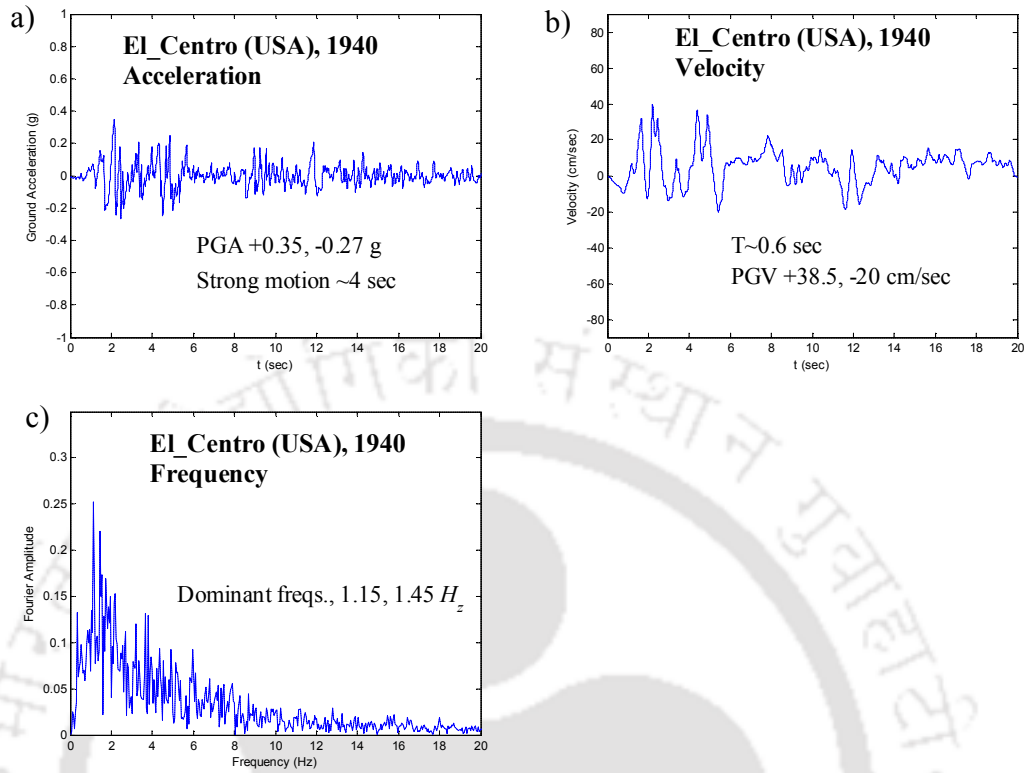

Figure 3.18: El_Centro earthquake a) acceleration, b) velocity and b) frequency

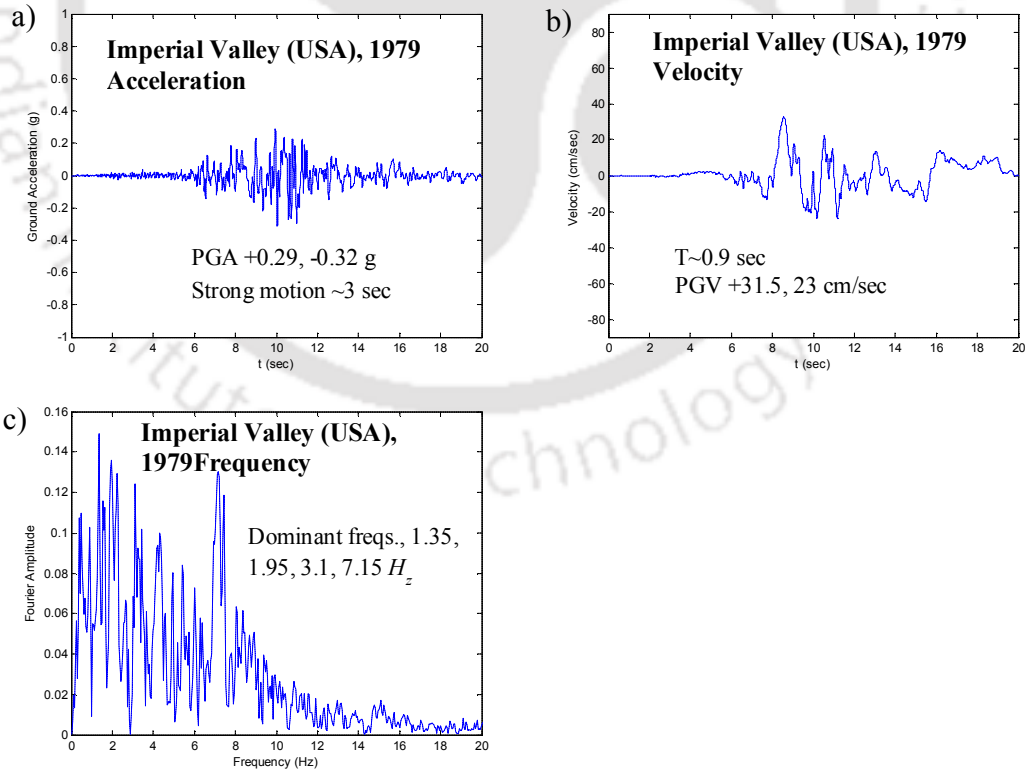

Figure 3.19: Imperial Valley earthquake a) acceleration, b) velocity and b) frequency

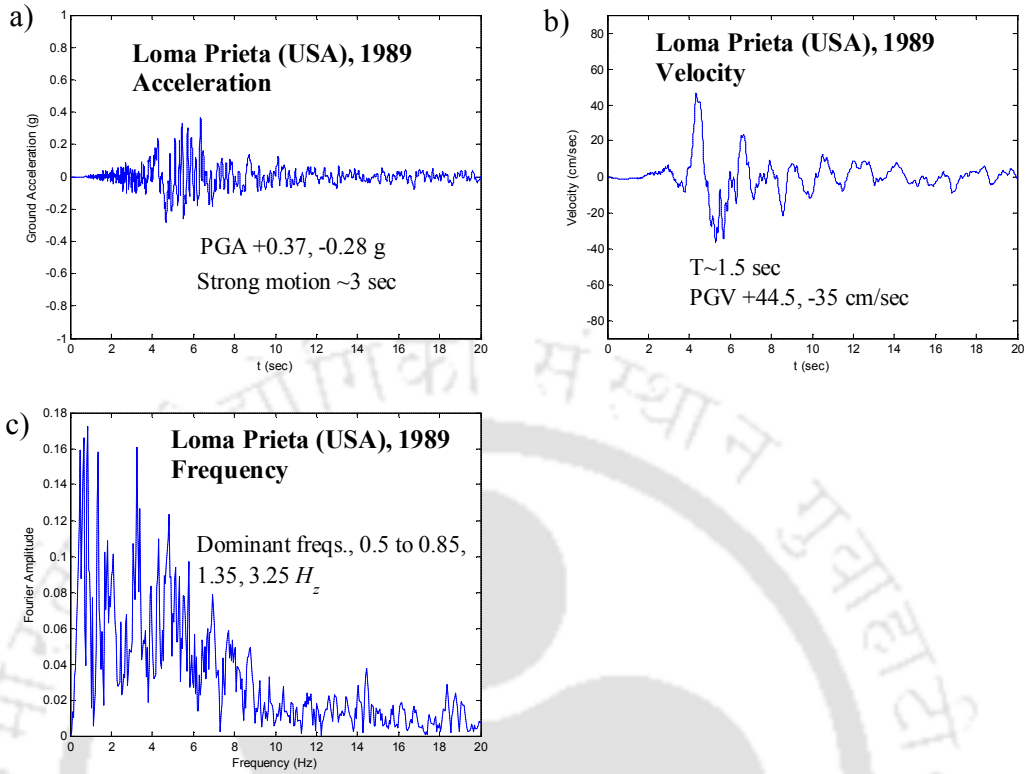

Figure 3.20: Loma Prieta earthquake a) acceleration, b) velocity and b) frequency

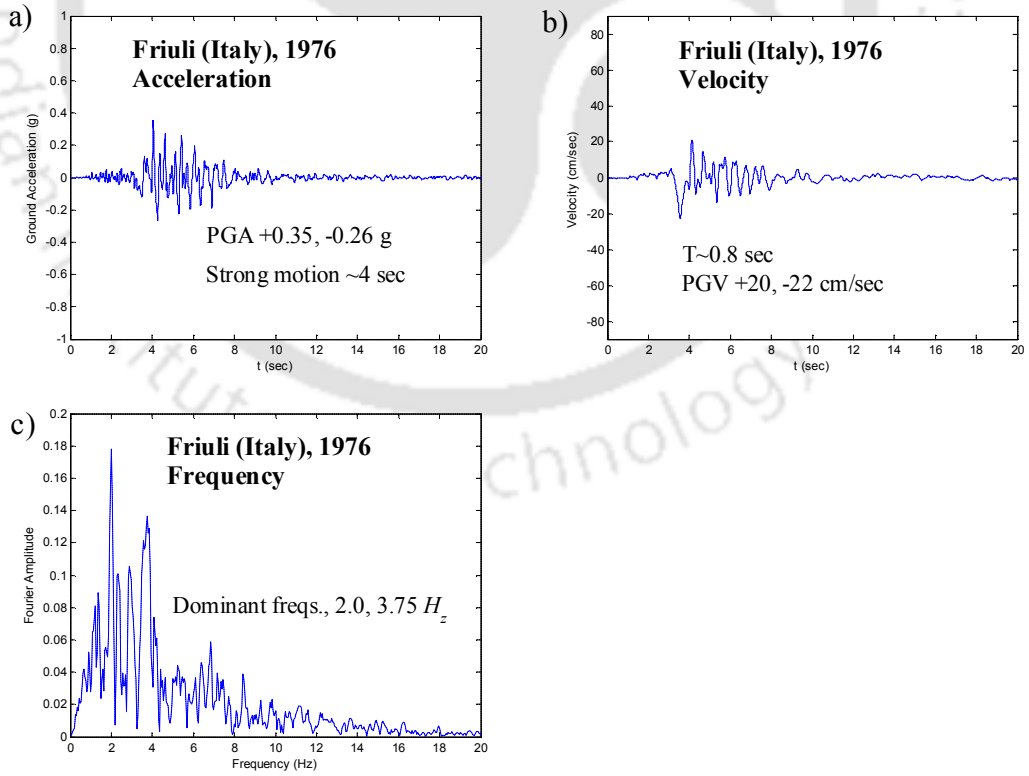

Figure 3.21: Friuli earthquake a) acceleration, b) velocity and b) frequency

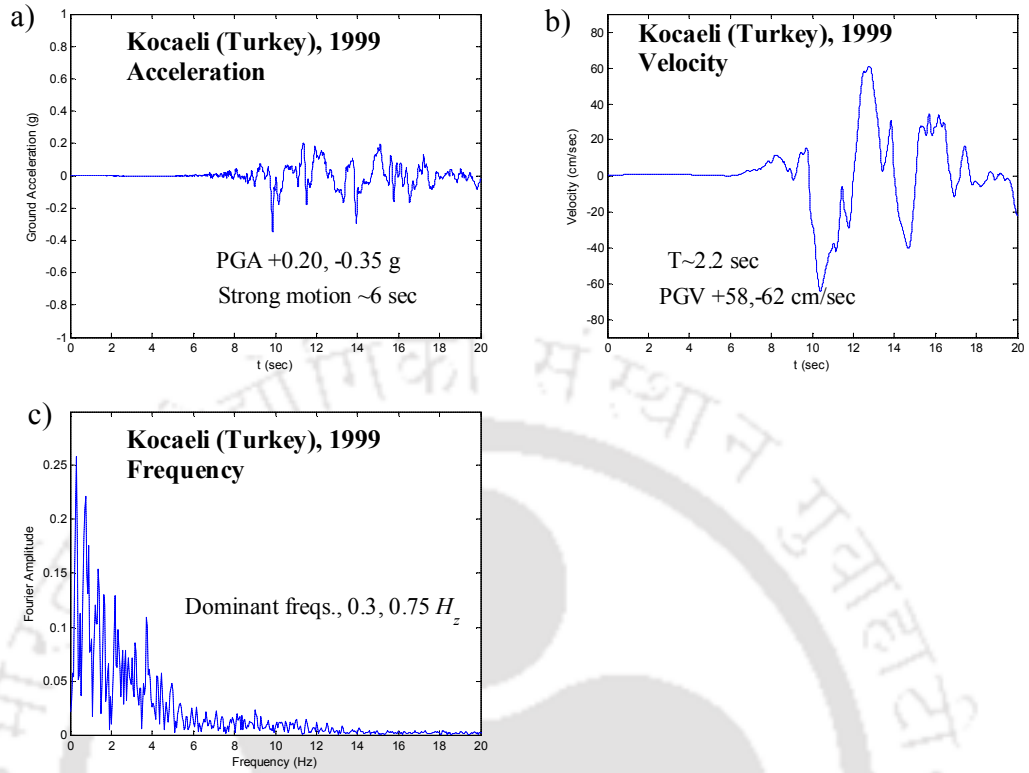

Figure 3.22: Kocaeli earthquake a) acceleration, b) velocity and b) frequency

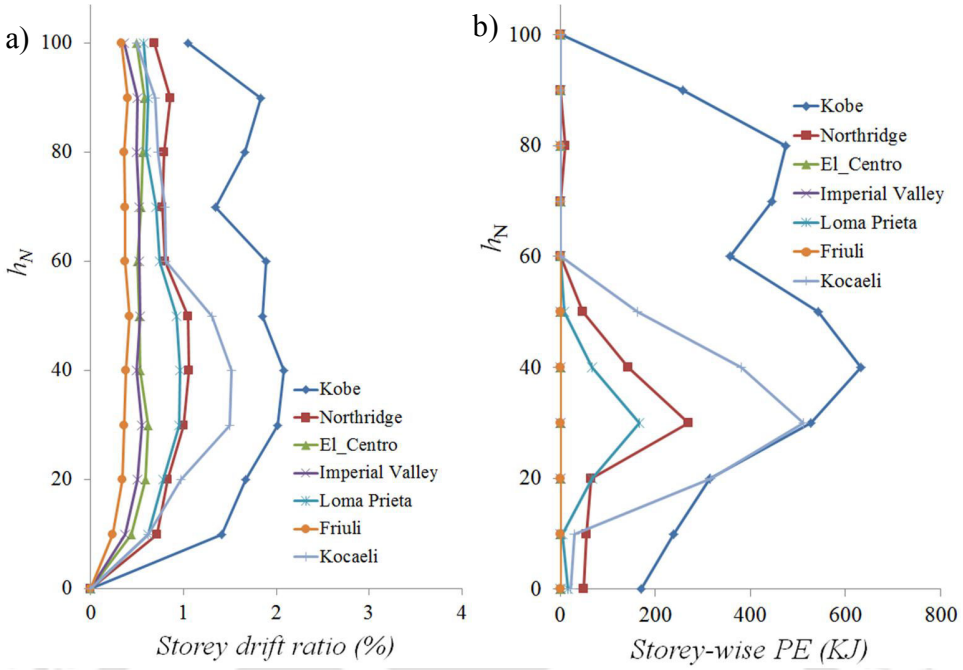

Figure 3.23: a) Storey drift ratio and b) plastic energy dissipation for 10-storey steel frame

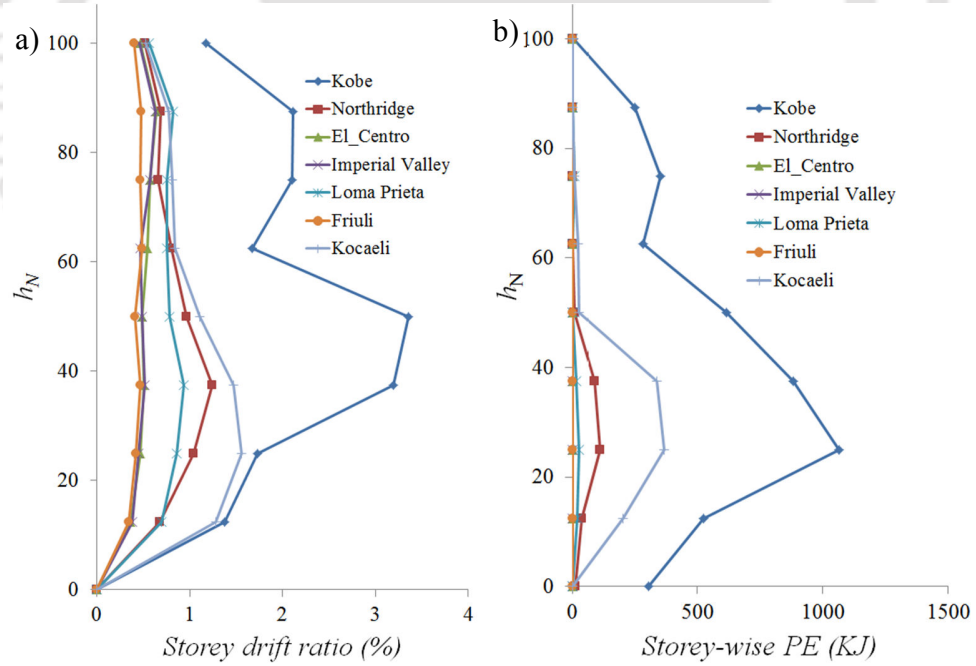

Figure 3.24: a) Storey drift ratio and b) plastic energy dissipation for 8-storey steel frame

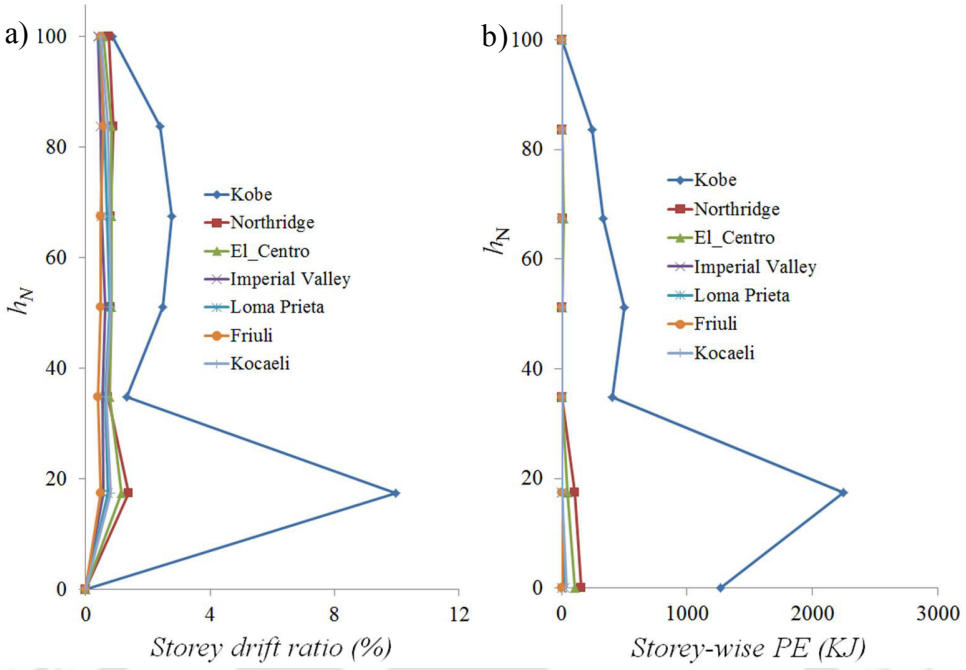

Figure 3.25: a) Storey drift ratio and b) plastic energy dissipation for 6-storey steel frame

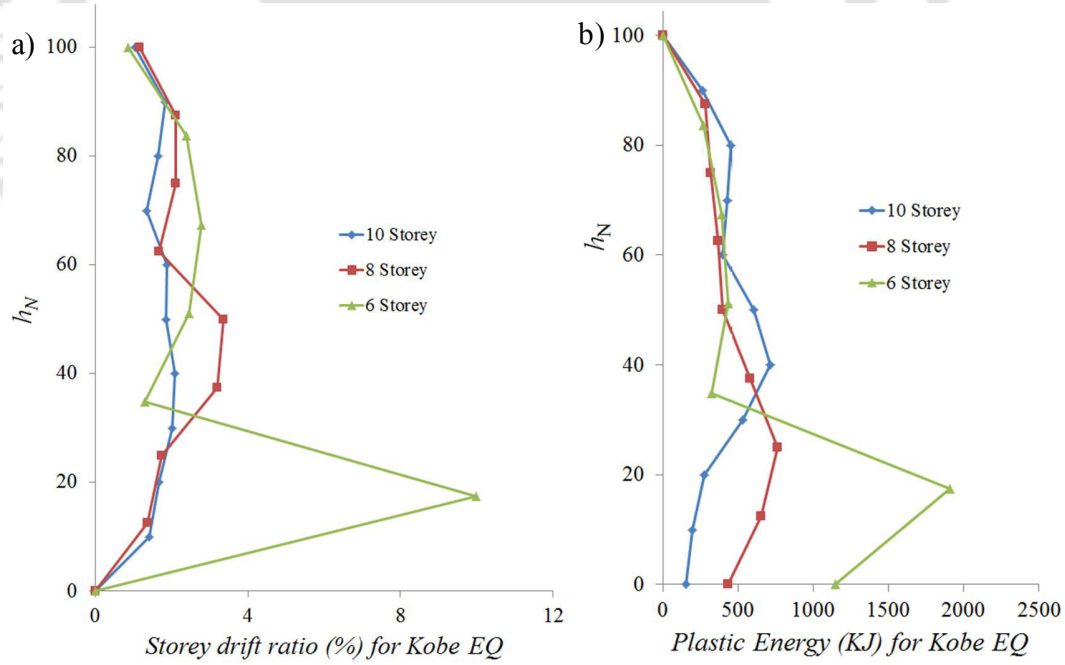

Figure 3.26: a) Storey drift ratio and b) plastic energy dissipation for Kobe earthquake

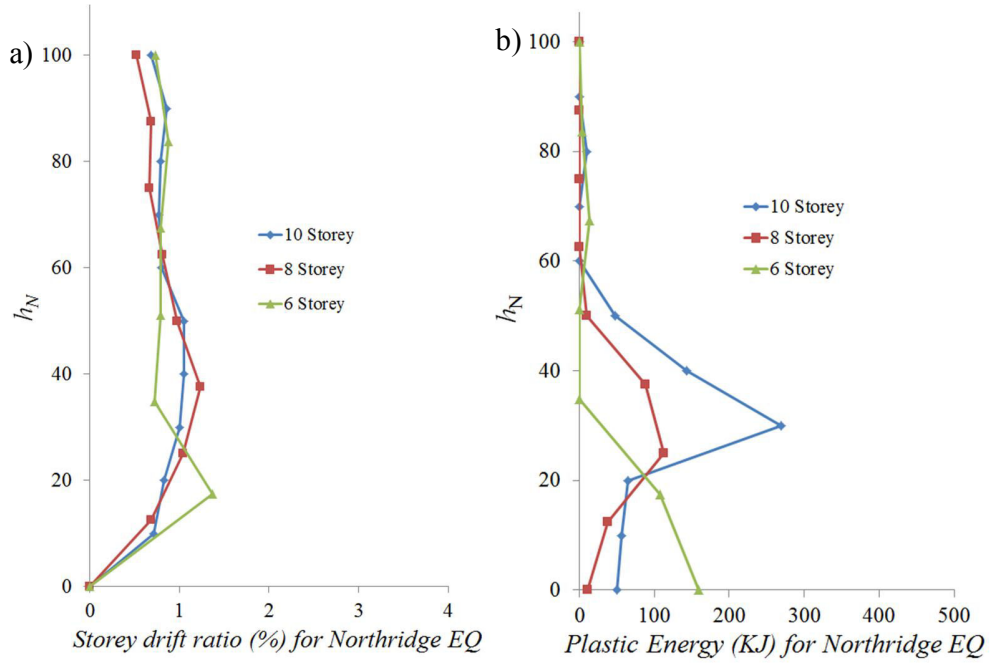

Figure 3.27: a) Storey drift ratio and b) plastic energy dissipation for Northridge earthquake

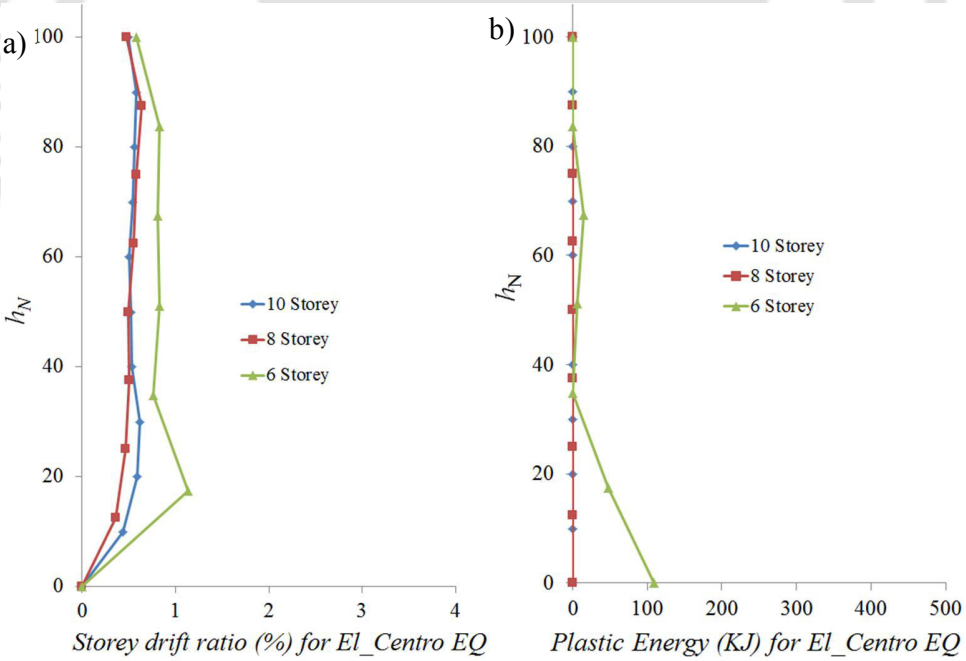

Figure 3.28: a) Storey drift ratio and b) plastic energy dissipation for El-Centro earthquake

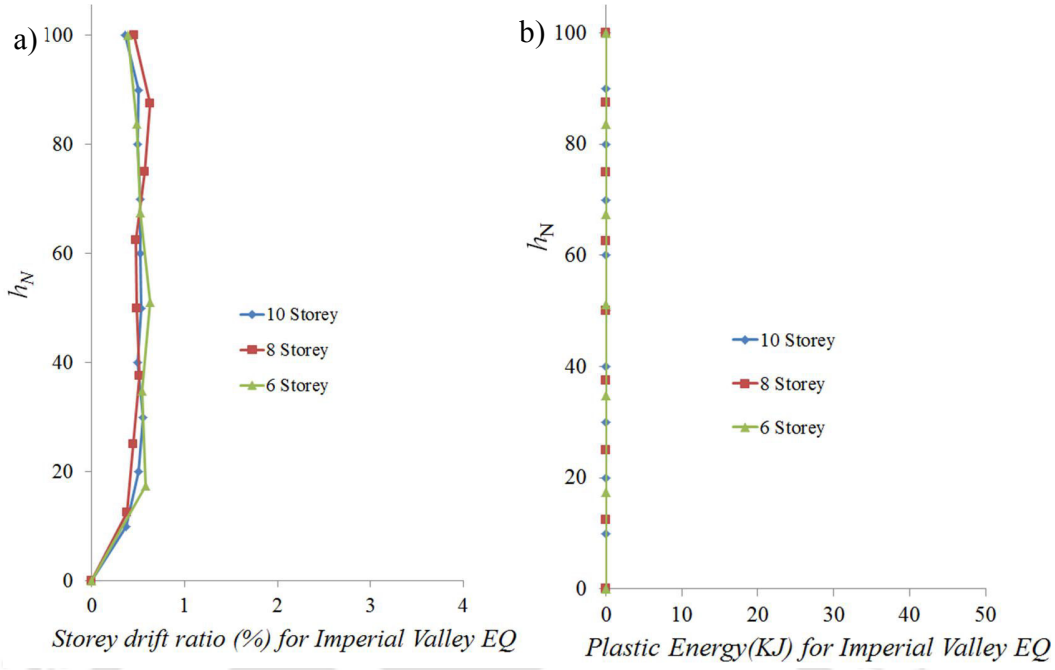

Figure 3.29: a) Storey drift ratio and b) plastic energy dissipation for Imperial Valley earthquake

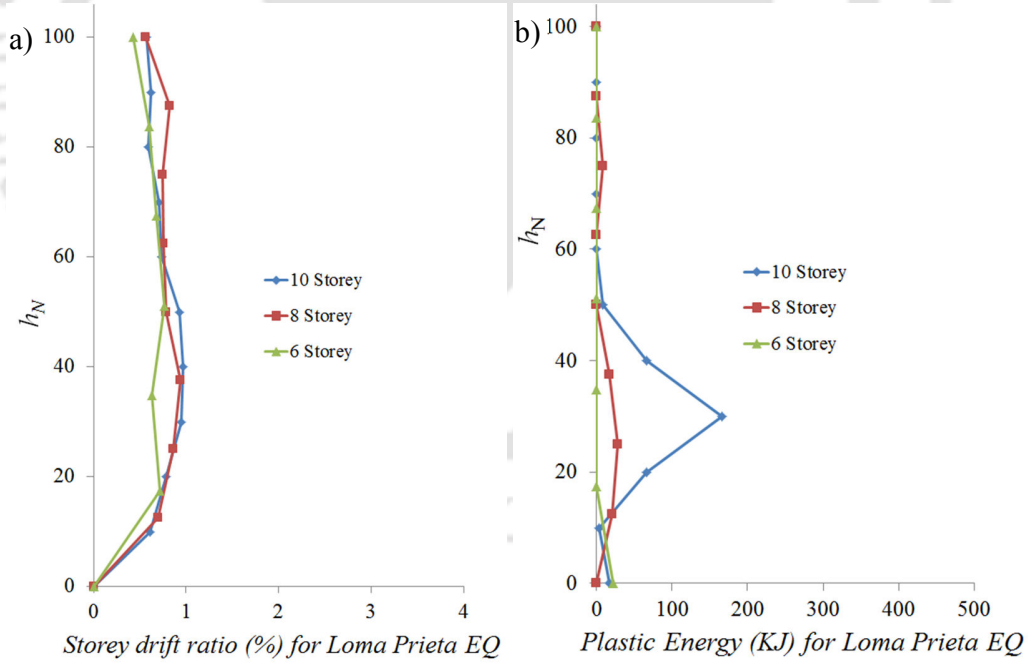

Figure 3.30: a) Storey drift ratio and b) plastic energy dissipation for Loma Prieta earthquake

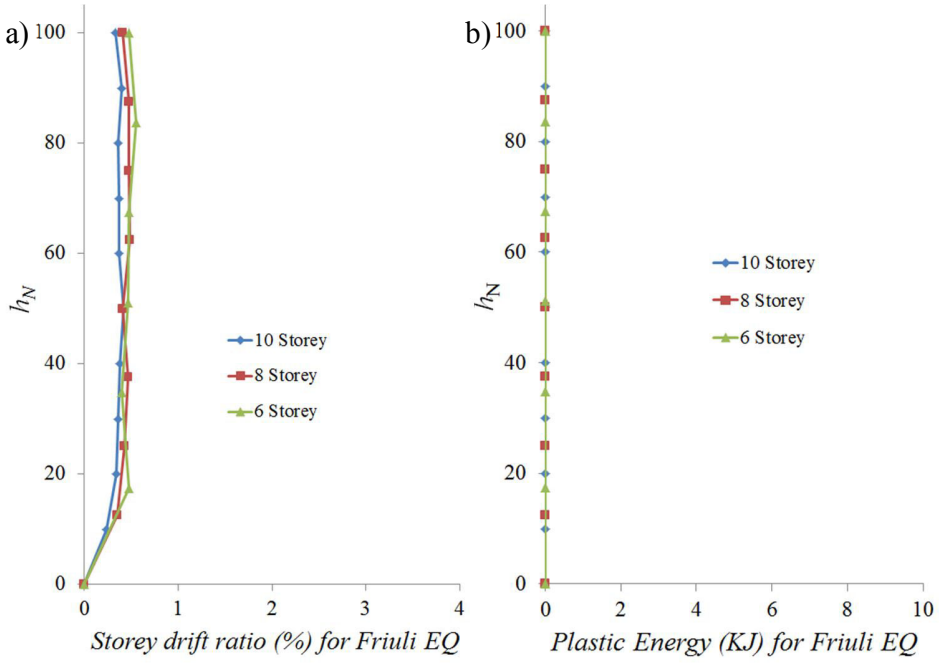

Figure 3.31: a) Storey drift ratio and b) plastic energy dissipation for Friuli earthquake

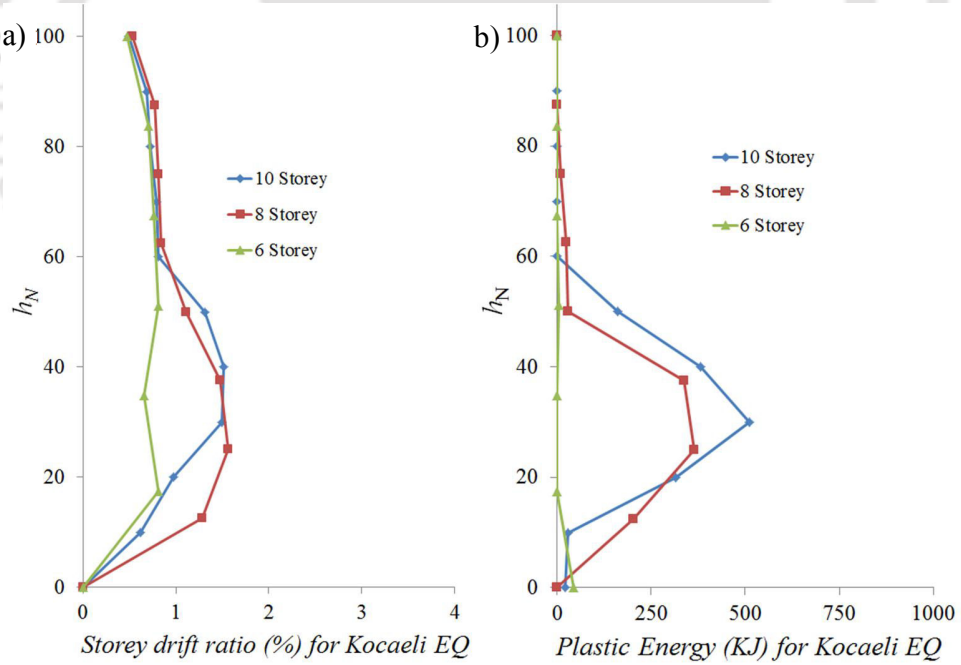

Figure 3.32: a) Storey drift ratio and b) plastic energy dissipation for Kocaeli earthquake

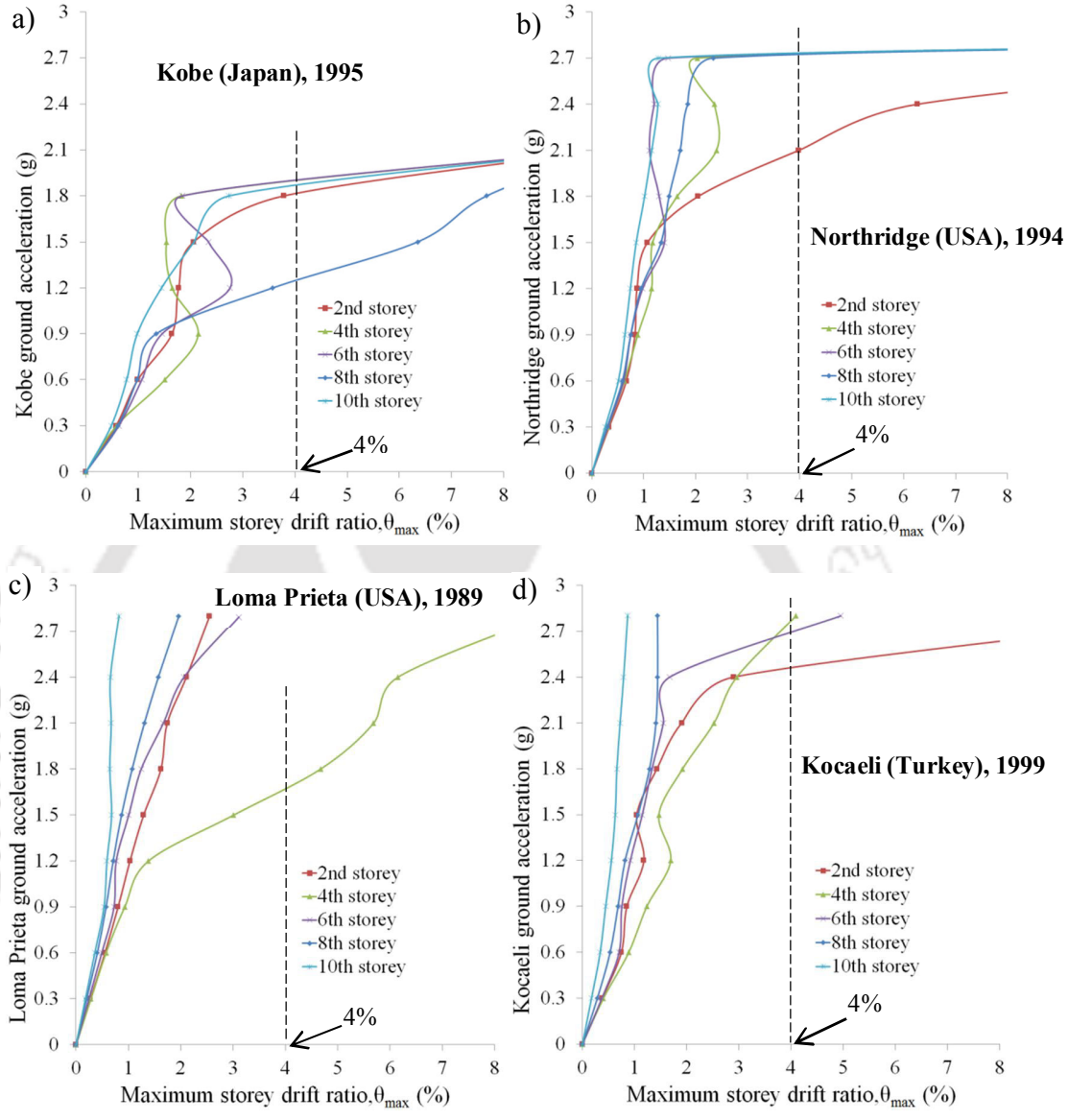

Figure 3.33: IDA curves of 10-storey moment resisting steel frame for different earthquakes

CHAPTER 4

NONLINEAR TIME HISTORY ANALYSIS OF SINGLE FLOOR MASS IRREGULAR MOMENT RESISTING STEEL FRAME USING FAM

4.1 Introduction

In Chapter 3, NTHA of mass regular (uniform distribution of floor masses along the building height) steel moment resisting frames have been presented. In this chapter, the previous study has been extended, to assess the effects of single floor mass irregularity (i.e. non-uniform distribution of floor mass along the building height) (Das and Nau, 2003; Choi, 2004) on moment resisting steel frame, using NTHA. As per Uniform Building Code (UBC)-1997, a building is considered to be irregular in mass if the effective mass of a storey or storeys are more than 150% of the effective mass of the neighbouring adjacent storeys. Mass irregular building frames have been reported to have resulted into greater seismic responses (and hence critical) as compared to regular counterparts, when excited by the same earthquake force (see e.g. Choi, 2004; Le-Trung *et al.*, 2012). Irregularity in storey mass may arise due to variation in floor use patterns e.g. residential, parking, commercial/shopping, heavy machinery floors etc. (e.g. multi-storied residential-cum-shopping complex building structures (see e.g. Figures 1.1 of chapter 1), where lower storeys are used for shopping complex); or due to conversion of existing floor(s) use, for similar requirements. Thus it becomes imperative and pertinent, to conduct detailed seismic analysis of such irregular buildings, before certifying them suitable for use.

From the literature review (Chapter 2), it has been seen that most studies on mass irregular building frames (e.g. Choi, 2004; Pirizadeh and Shakib, 2013) have been reported based on limited mass irregular floor locations (e.g. bottom, mid and top floors) of the mass irregular floors along the building height, especially looking at maximum seismic responses in terms of story drift ratios, without considering full

range dynamic behaviours. Thus, in this chapter, an attempt has been made to conduct a detailed systematic Nonlinear Time History Analysis (NTHA) of single floor mass irregular moment resisting steel frames considering both material and geometric nonlinearities using FAM methodology, to assess full range dynamic behaviours ensuring maximum coverage of single mass irregular floor throughout the building height. Effect of mass irregularity intensity on seismic behaviours of the steel building frame will also be investigated. The sequence of criticality of single floor mass irregular frames due to various locations of mass irregular floor along the building height will also be addressed by collapse analysis using IDA study.

The 10-storey moment resisting steel frame of Chapter 3 (see Figure 3.2) has been considered as the reference regular frame in this chapter; for comparison with the case of mass regular frame. For investigating the effect of location of mass irregularity on seismic behaviours of building frame; the reference regular frame has been converted into a number of single floor mass irregular frames by locating single mass irregular floor at different floor levels (i.e. 2^{nd}, 4^{th}, 6^{th}, 8^{th} and 10^{th} floor levels) along the building height; thus ensuring that the location of mass irregular floor covers most locations of building height. Also, for investigating the effect of intensities of mass irregularity on seismic behaviours of building frame; four different intensities (i.e. 150%, 175%, 200% and 225%) of mass irregularities have been considered in the analysis. Further, it has been observed in Chapter 3 that Kobe earthquake (1995) has been found to give the maximum seismic responses to the 10-storey steel reference frame; and thus Kobe earthquake (1995) has been considered as a typical strong input ground motion for the analysis of single floor mass irregular 10-storey moment resisting steel frame in this chapter. In this chapter, first, a typical detail analysis of single floor mass irregular frame will be presented using mass irregularity intensity of 150%., followed by investigations with increasing mass irregular intensities to 175%, 200% and 225%. The results would be presented in the form of storey drift ratio, floor displacements, plastic energy dissipation and IDA curves.

4.2. Analysis of single floor mass irregular frames

A single floor mass irregular frame has been shown in Figure 4.1 where red colour at 2nd floor level indicates mass irregularity located at 2nd floor level. The nomenclature used in the present study follows the pattern XMY, where X indicates the intensity of mass irregularity, M indicates regular floor mass and Y indicates the floor level at which mass irregularity is located. Thus in irregular frame 1.50M2, 1.50 indicates 150% mass irregularity; M indicates regular floor mass and 2 indicates that mass irregularity is located at 2nd floor level. In order to cover all ranges of building height, single floor mass irregular frames are formed by locating mass irregular floor at different floor levels (i.e. 2nd, 4th, 6th, 8th and 10th floors) of the building frame. Only alternate floor levels are considered in order to bring clarity presenting results. Since four intensities of mass irregularity (i.e. 150%, 175%, 200% and 225%) located at different five floor levels (i.e. 2nd, 4th, 6th, 8th and 10th floor levels) have been considered in the analysis, and hence a total of twenty mass irregular frames have been analysed, as listed in Table 4.1. 1n order to have a common input ground motion, for each of the combination of irregular floor mass and its location along the building height, Kobe earthquake (1995) amplitude has been scaled by trial method, to arrive a suitable scale value such that, it is possible to analyse all the frames, without causing un-functional state (exceeding allowable storey drift ratio of 4%, ASCE 7, 2016) or dynamic instability (total collapse) in any of the combinations mentioned above. It may be mentioned that such approach of scaling amplitudes of input ground motion for conducting seismic performance investigations have also been adopted in the literature (e.g. Pirizadeh and Shakib, (2013); Tremblay and Poncet, (2005); Wong and Speicher, (2015); etc.)

4.2.1 Single floor mass irregular frames (150% mass irregularity)

The results of the single floor mass irregular frames (150% mass irregularity) have been presented in the form of storey drift ratio (see Figures 4.2a and 4.4a), floor displacements (see Figures 4.2b and 4.3), plastic energy dissipation (see Figure 4.8) and IDA curves (see Figure 4.9). As per EDP based method of collapse analysis

(Vamvatsikos and Cornell, 2002; Wong and Zhao, 2007), it has been observed from Figure 4.2a that the irregular frame 1.50M4 becomes un-functional (exceeding allowable storey drift ratio of 4%, ASCE 7, 2016) early at the lowest scale value (0.783) of amplitudes of Kobe earthquake. Thus, irregular frame 1.50M4 is found to be the most critical frame among the group. Floor displacements are found to be maximum for the irregular frame 1.50M4 as compared to those of other irregular frames, at 0.783 scale value as shown in Figure 4.2b. At this scale value (0.783), the remaining irregular frames are found to be still in working condition i.e. still within the specified allowable range of 4% storey drift ratio. From Figure 4.3b, it can be seen that inelastic displacement component of mass irregular frame 1.50M4 keeps increasing beyond 6 sec of time history (which may be related to new formation of plastic hinges as well as increase in magnitudes of existing plastic hinges) making the irregular frame the most critical. Elastic and total floors' displacement component response histories of irregular frame 1.50M4 are also shown in Figures 4.3a and 4.3c. The most critical nature of the irregular frame (1.50M4) may be related to the critical behaviour of 4^{th} storey of the reference regular frame (Figure 3.2) in Chapter 3 (see earlier Figure 3.14). It has been seen from storey-wise IDA curves (see Figure 3.14) of the reference regular frame that IDA curve of 4^{th} storey has been found to obtain maximum storey drift ratios than those of other storeys as indicated inside the marked rectangular (see Figure 3.14). Thus, it is seen that when the mass irregular floor is located at this critical storey (i.e. 4^{th} storey) floor level of the reference regular frame, the irregular frame is found to be most critical among other irregular frames (i.e. mass irregularity at 2^{nd}, 6^{th}, 8^{th} and 10^{th} floor levels). Hence it may be observed that, mass irregular frame is most critical when mass irregular floor is located at ~40% building height. Similar occurrence of the criticality of mass irregularity location near 40% building height have been reported by pervious researchers (*viz*., Das and Nau, 2003; Karavasilis *et al.*, 2008). Similarly the scale values of amplitudes of Kobe earthquake at which other irregular frames (i.e. mass irregularity at 2^{nd}, 6^{th}, 8^{th} and 10^{th} floor levels) become un-functional are found to be 0.817, 0.943, 0.996 and 1.086 respectively (see Figure 4.4a), which are of lesser values in comparison to the corresponding scale value (i.e. 1.21) of the reference regular. Maximum floor

displacements of all the irregular frames at their corresponding scale values of un-functional states have been shown in Figure 4.4b. It has been seen that floor displacements of each single floor mass irregular frame are found to increase from base until the floor level where mass irregular floor is located, however no further increase in floor displacements have been observed at upper floor levels above mass the irregular floor (see Figure 4.4b). Also, total floor displacement time histories of all irregular frames at their corresponding un-functional states have been shown in Figure 4.5. Large inter-floor displacements have been observed between the floors levels located below the mass irregular floor (see Figure 4.5). The sequence of mass irregular frames in decreasing order of criticality are found to be as 1.50M4, 1.50M2, 1.50M6, 1.50M8 and 1.50M10 (see Figure 4.6); i.e. single floor mass irregularity located above mid-height are found to be more safer than that located below mid-height of the building frame. The sequence of criticality of single floor mass irregular frames (see Figure 4.6) has been found to depend on the sequence of criticality of storeys (i.e. 4^{th}, 2^{nd}, 6^{th}, 8^{th} and 10^{th} storeys) of the reference regular frame as indicated in storey-wise IDA curves of reference regular frame (see Figure 3.14).

Further, it has also been observed that maximum storey drift ratio (see Figures 4.4a and 4.7) and maximum floor displacement (see Figure 4.4b) have been found to occur at the storey level just below the storey where mass irregular floor is located. Such observations of occurrence of maximum storey drift ratio near the location of mass irregular floor has been reported in the literature (e.g. Choi, 2004 and Le-Trung *et al.*, 2012). This may be due to increased plastic energy dissipation below the mass irregular floor (see Figure 4.8). It has also been observed that storey drift ratio of each irregular frame is found to increase by ~2% from reference regular frame at location just below the location of mass irregular floor (see Figure 4.7); however it has been seen that at other locations of the building height, storey drift ratios of mass irregular frames are found to be lesser than that of the reference regular frame. This may be associated with the localisation of the distribution of plastic energy dissipation just below the location of mass irregular floor (see Figure 4.8).

For assessing collapse capacities and full range dynamic behaviours of 150% mass irregular frames, IM based method of collapse analysis (Vamvatsikos and Cornell, 2002; Wong and Zhao, 2007) has been performed using IDA study. The intensity of the input ground motion is made to increase at the rate of 0.2 scale value. Floor wise IDA curves of 150% single floor mass irregular frames have been shown in Figure 4.9. It has been observed in general that softening (more storey drift ratio at infinitesimal increase of scale value) is found to occur either in the IDA curves of the storey where mass irregularity is located or at immediate lower storey, before becoming collapse/dynamic instability (see Figures 4.9). Irregular frame 1.50M4 has been found to become collapse/dynamic instability early at the lowest amplitude scale value of 0.8 indicating the most critical frame among the group. Based on the IDA curve, extreme softening is found to be associated with 2^{nd} storey of the irregular frame 1.50M4 before becoming dynamically unstable (Figure 4.9b). Thus, suggesting that collapse state (dynamic instability) may be first initiated by 2^{nd} storey of irregular frame 1.50M4 which is then followed by the rest of storeys of the frame. Similar observations have also been found in the irregular frame 1.50M2 but at a higher amplitude scale value of 0.817 (Figure 4.9a). Irregular frame 1.50M6 has been seen to experience dynamic instability at a amplitude scale value of 0.943 (Figure 4.9c); whereas that of mass irregularity at upper storey levels (i.e.1.50M8 and 1.50M10) have been found to become dynamic instability near scale value of 1.2 (Figures 4.9d-e). Thus, in general, the sequence of criticality to attain dynamic instability decreases as the location of mass irregular floor moves away from the base towards the top of the building. Extreme softening just before becoming dynamic instability has been observed to occur in IDA curves of 8^{th} storey for irregular frames 1.50M8 and 1.50M10 (Figures 4.9d-e). Thus, for mass irregularity at upper storeys (i.e. 1.50M8 and 1.50M10), dynamic instability has been initiated first at 8^{th} storey level which is then followed by the rest of the storeys. 'Weaving patter' of IDA curve has been found in the IDA curve of 6^{th} storey of irregular frame of 1.50M8 (Figure 4.9d) which indicates 'self-stabilizing' behaviour of frame structure with increase in intensity of earthquake forces (Vamvatsikos and Cornell, 2002). This weaving pattern of IDA curve indicates that dynamic behaviours of frame structure is non-

monotonic to intensity of input ground motion; rather it depends on the pattern as well as the timing of the motion than just the intensity of forcing function.

4.2.2 Effect of intensity of mass irregularity

The effect of mass irregular intensity on seismic behaviours of single floor mass irregular frames has been carried out by considering three more mass irregular intensities (i.e. 175%, 200% and 225%). It has been observed that similar to that of 150% mass irregular frames, mass irregular floor located at 40% building height (i.e. 4th storey) is found to be the most critical for other intensities of mass irregularity (i.e. 175%, 200% and 225%) (see Figures 4.10b-d); however the scale value at which each critical irregular frame becomes un-functional is found to decrease (i.e. more critical) as the intensity of mass irregularity increases. The corresponding scale values at which the irregular frames 1.75M4, 2.00M4 and 2.25M4 become un-functional (exceeding allowable storey drift ratio of 4%, ASCE 7, 2016) are found to be 0.586, 0.501 and 0.453 respectively (see Figures 4.10b-d). Maximum floor displacements for all the irregular frames for all four intensities of mass irregularity (150%, 175%, 200% and 225%) at their corresponding scale values of un-functional states have been shown in Figure 4.11; wherein, maximum floor displacements are found when mass irregular floor is located at 40% building height (4th storey). The scale values to attain un-functional state for the remaining irregular frames of mass irregularity (i.e. 175%, 200% and 225%) are also found to decrease as the intensity of mass irregularity increases. It has been observed that 175% mass irregular frames i.e. 1.75M2, 1.75M6, 1.75M8 and 1.75M10 are found to become un-functional at scale values 0.615, 0.741, 1.0 and 0.973 respectively (see Figure 4.12b); 200% mass irregular frames i.e. 2.00M2, 2.00M6, 2.00M8 and 2.00M10 are found to become un-functional at scale values 0.527, 0.535, 0.828 and 0.850 respectively (see Figure 4.12c); and 225% mass irregular frames i.e. 2.25M2, 2.25M6, 2.25M8 and 2.25M10 are found to become un-functional at scale values 0.817, 0.586, 0.501 and 0.453 respectively (see Figure 4.12d). The sequences of criticality for all the irregular frames for all four intensities of mass irregularity (150%, 175%, 200% and 225%) are shown in Figure 4.13. It has been observed that single mass irregular floor located

above mid-height of the building is found to be more safer (i.e. un-functional state at higher scale values) than that located below the mid-height of the building (i.e. un-functional state at lower scale values) for all four intensities of mass irregularity (see Figure 4.13). The irregular frame 2.25M4 has been found to the most critical frame among all the single floor mass irregular frames for all four intensities of mass irregularity since it becomes un-functional at lowest scale value of 0.453 (see Figure 4.14). It has been observed that irregular frames 1.50M4, 1.75M4, 2.00M4 and 2.25M4 are found to be more critical than the reference regular frame by 35.2%, 51.5%, 58.5% and 62.5% respectively (see Figure 4.13).

Collapse analysis of single floor mass irregular frames of mass irregularity (175%, 200% and 225%) have been performed by considering IM based method of collapse analysis using IDA study. It has been observed that similar to that of 150% mass irregular frames, collapse state (dynamic instability) may be first initiated at the storey level where mass irregularity is located or at immediate lower storey level, which is then followed by the rest of storeys of the frame (see Figures 4.15-4.17). However, the scale value at which the irregular frames become dynamic instability is found to decrease (i.e. more critical) as the intensity of mass irregularity increases. It has been observed that irregular frames 1.75M4, 2.00M4 and 2.25M4 are found to become dynamic instability early at the lowest scale values of 0.6, 0.51 and 0.46 respectively (see Figures 4.15-4.17) indicating the most critical frame among the respective group of mass irregularity. It has also been observed that for irregular frames of higher intensity of mass irregularity at lower storey levels (e.g. 2.25M2, 2.25M4), immediate dynamic instability has been observed at lowest scale values (e.g. 0.51 and 0.46) (see Figures 4.17a-b) i.e. at the onset of nonlinear behaviour thus expressing only linear seismic response followed by immediate collapse of the frame.

4.3 Conclusion

This chapter presents a parametric study of single-floor mass irregular building frame to investigate the seismic behaviours of the irregular building frame when intensity as well as location of mass irregularity changes along the height of the building frame.

Four different intensities of mass irregularities (i.e. 150%, 175%, 200% and 225%) at five different locations (i.e. 20%, 40%, 60%, 80% and 100% building height) have been examined. The results are presented in the form of total floors' displacements; storey drift ratios and plastic energy dissipation. Criticality analysis of all the single floor mass irregular frames has been performed using IDA study. The following conclusions are drawn from the above analysis.

1. The criticality (i.e. becoming un-functional by exceeding allowable storey drift ratio of 4% (ASCE 7, 2016) or dynamic instability/collapse) of single floor mass irregular frames may be related to the criticality of the storey levels in the reference regular frame. It has been seen from the storey-wise IDA curves of reference regular frame that the storey located at 40% building height is found to be the most critical. The criticality decreases as the storey moves away from 40% building height.
2. It has been observed that single floor mass irregular frame is found to be the most critical when mass irregular floor is located at 40% building height.
3. The criticality of single floor mass irregular frames has generally been found to decrease as the location of mass irregular floor moves away from the base towards the top of the building frame.
4. It has also been observed that maximum storey drift ratio or maximum floor displacement has been found to occur at the storey level just below the storey where mass irregular floor is located.
5. Storey drift ratio of single floor mass irregular frame at un-functional state has been found to increase by ~2% than that of reference regular frame near the location of mass irregular floor; wherein, the storey drift ratio are found to be less than that of the reference regular frame at other locations along the building height.
6. Plastic energy dissipation has been found to concentrate only near the location of mass irregular floor.
7. The criticality of single floor mass irregular frames increases as the intensity of mass irregularity increases.

8. Irregular frames of higher intensity of mass irregularity at lower storey levels (e.g. 2.25M2, 2.2.5M4) are found to be highly critical since they attained dynamic instability immediately at the onset of nonlinear behaviour thus showing only linear seismic responses followed by immediate collapse of the frames.

Table 4.1: Nomenclature of single floor mass irregular frames

Groups	**Single floor mass**
1.	1.50M2, 1.50M4, 1.50M6, 1.50M8 and 1.50M10
2.	1.75M2, 1.75M4, 1.75M6, 1.75M8 and 1.75M10
3.	2.00M2, 2.00M4, 2.00M6, 2.00M8 and 2.00M10
4.	2.25M2, 2.25M4, 2.25M6, 2.25M8 and 2.25M10

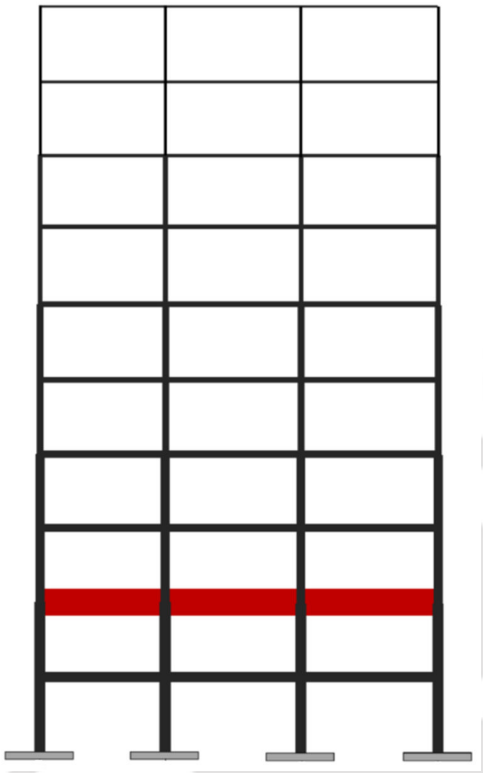

Figure 4.1: Nomenclature of single floor mass irregular frame

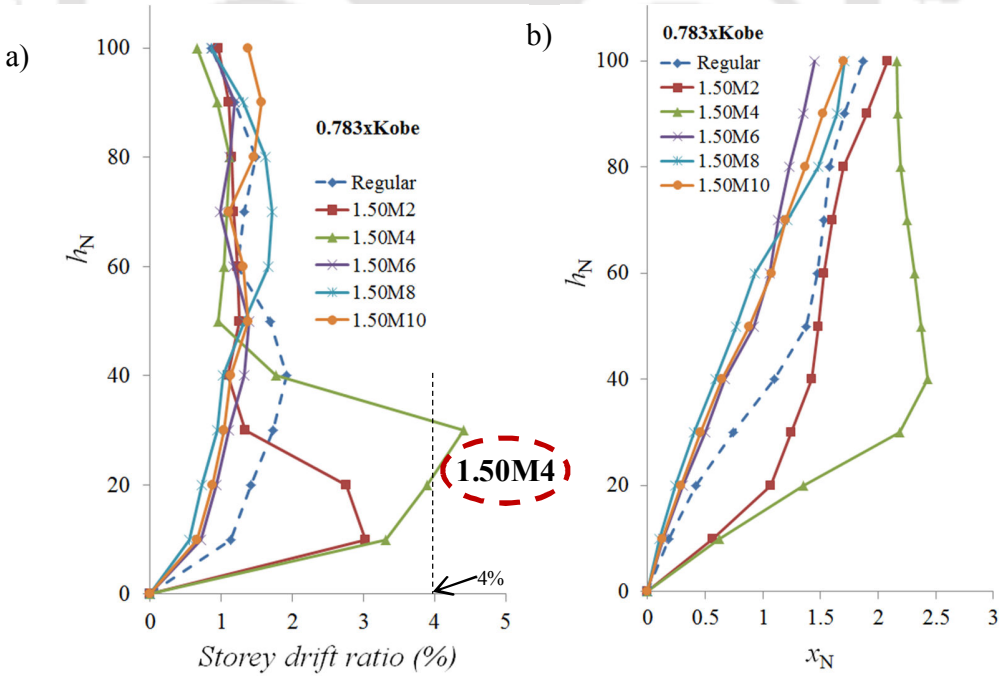

Figure 4.2: a) Storey drifts ratio and b) Maximum floor displacement for 150% single floor mass irregular frames at 0.783xKobe

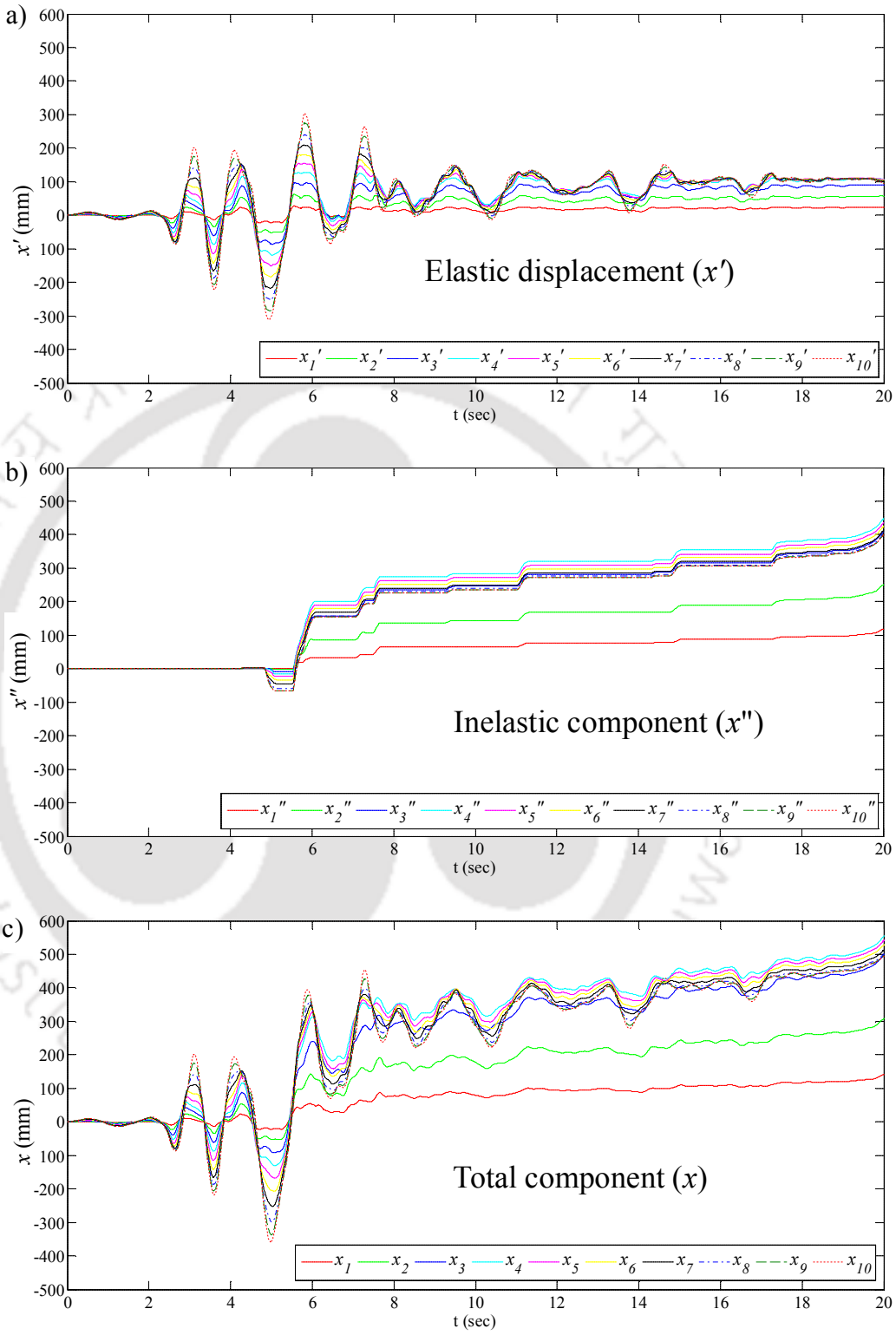

Figure 4.3: Time history responses of 1.50M4 frame: a) Elastic component, b) Inelastic component and c) Total displacement at 0.873xKobe earthquake

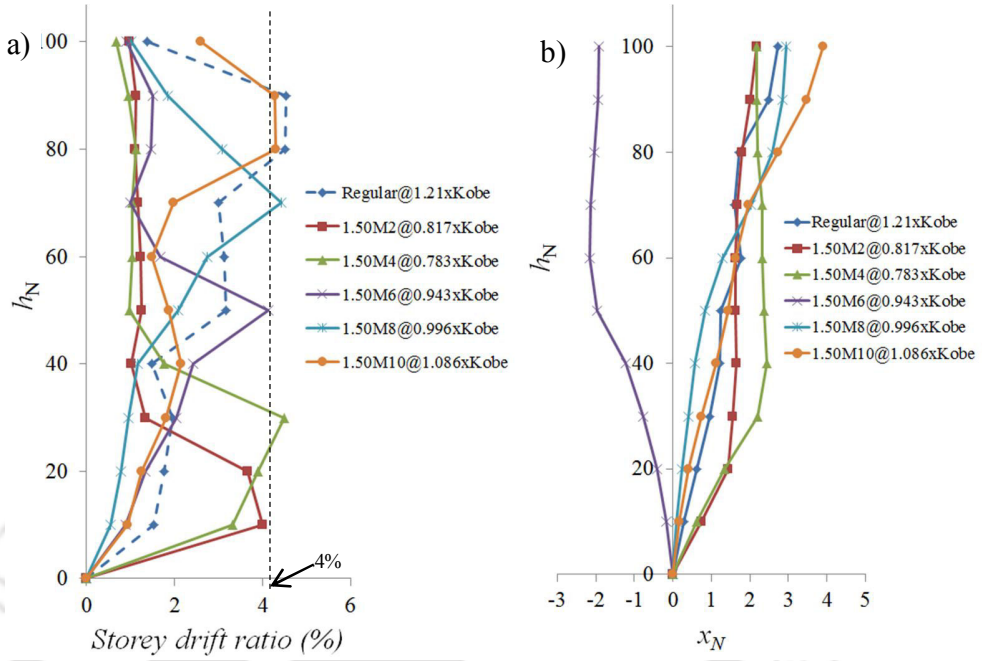

Figure 4.4: a) Storey drift ratio at collapse states and b) Total floor displacements for 150% mass irregular frames

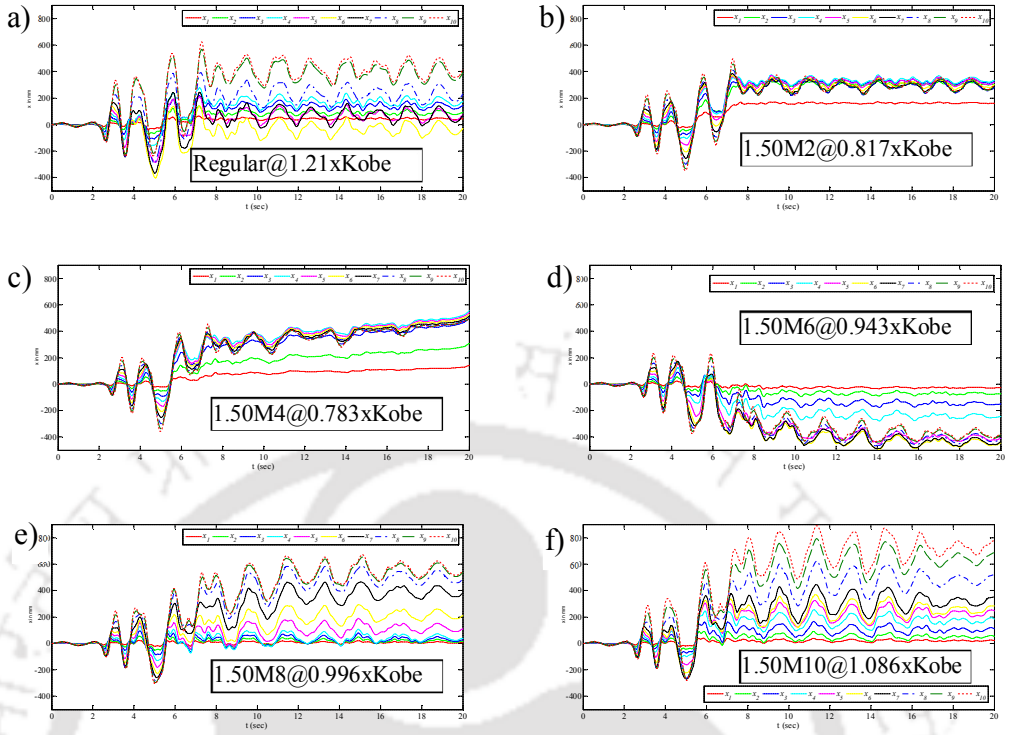

Figure 4.5: Total floor time histories at collapse state for a) Regular b) 1.50M2 and c) 1.50M4 d) 1.50M6 e) 1.50M8 and f) 1.50M10

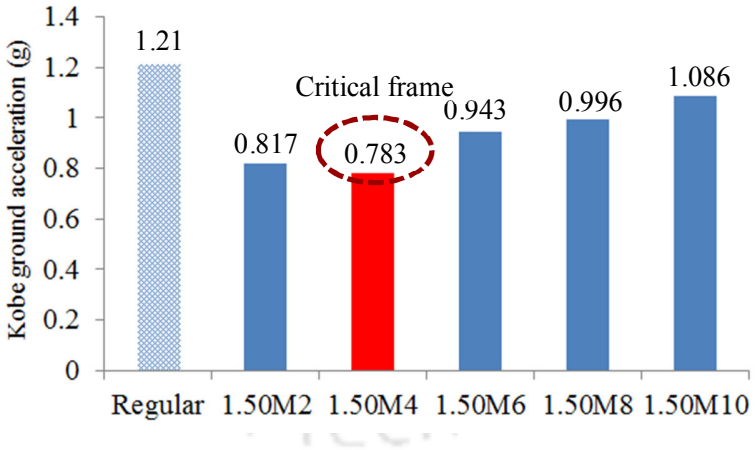

Figure 4.6: Bar chart of scale values at collapse state for 150% mass irregular frames

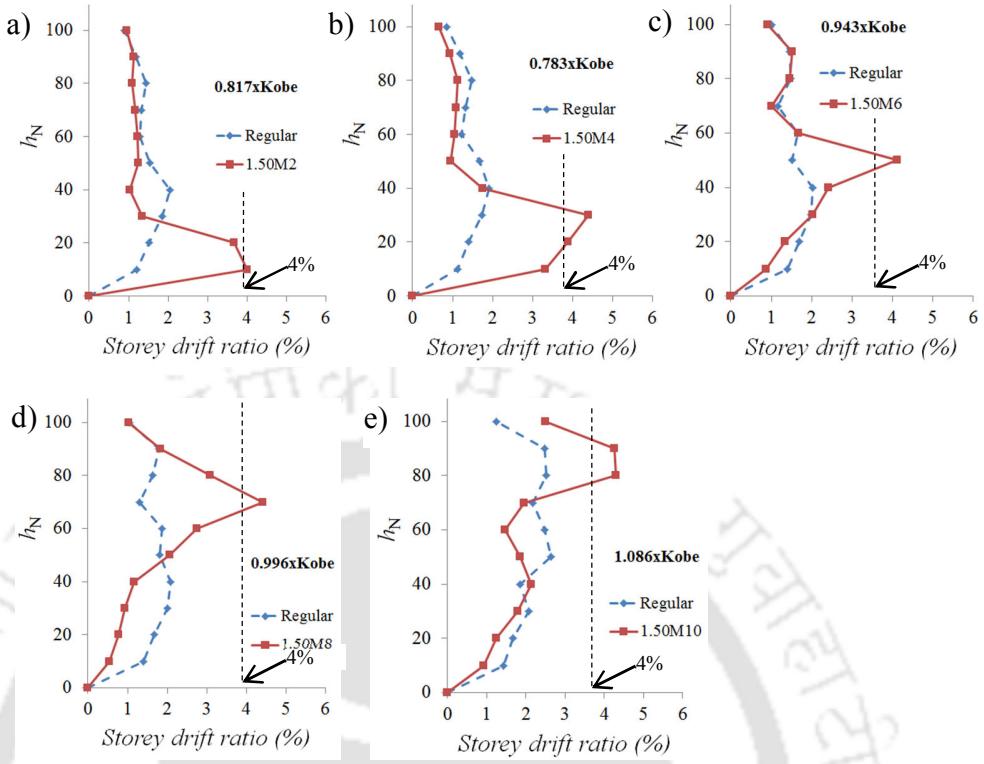

Figure 4.7: Storey drift ratios of 150% mass irregular frames in comparison with corresponding regular frame

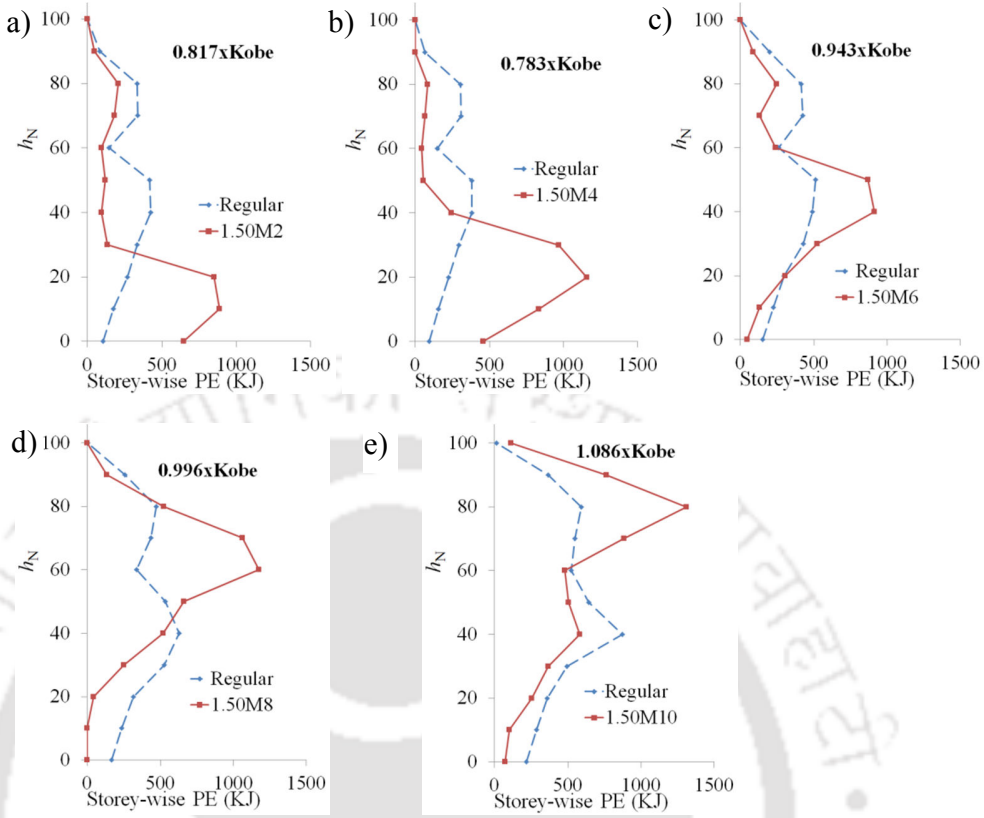

Figure 4.8: Comparison of plastic energy dissipation for 150% mass irregular frames with reference regular frame

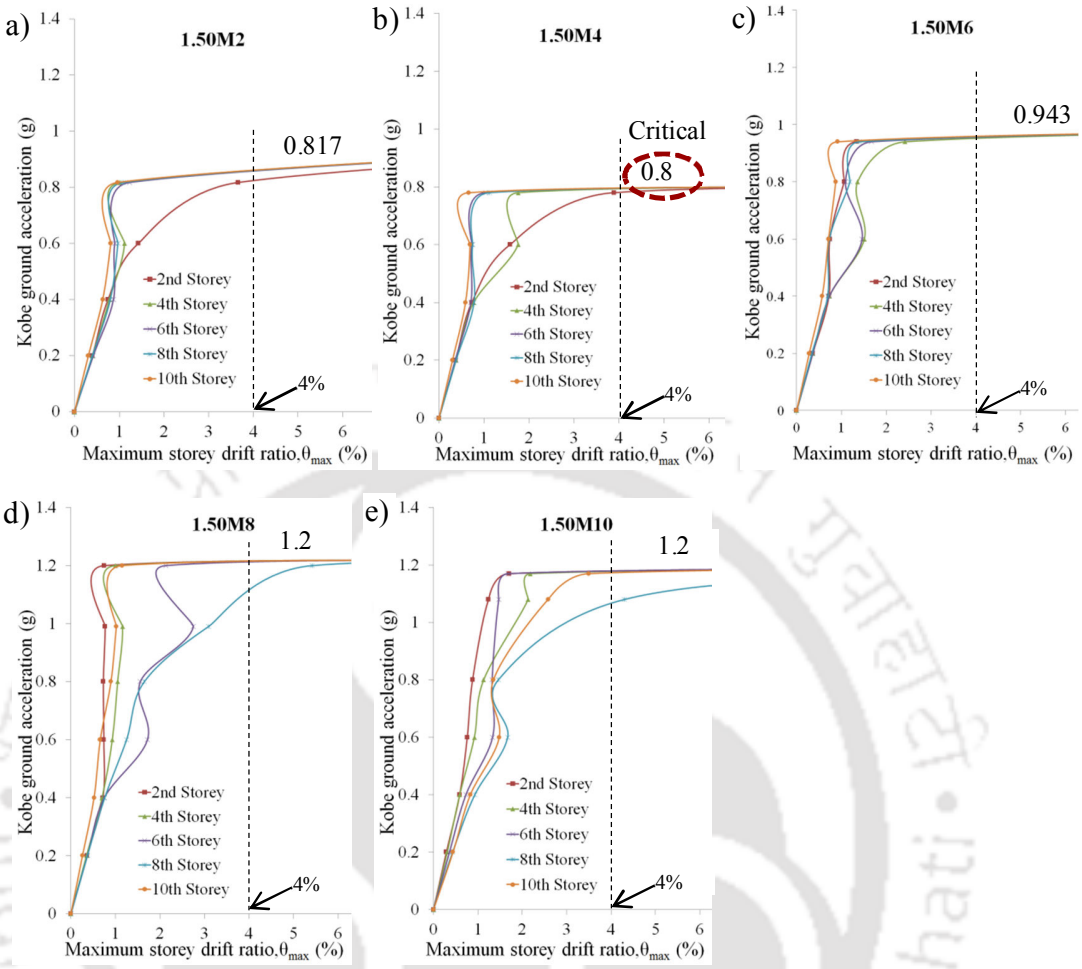

Figure 4.9: Storey-wise IDA curves for 150% mass irregular frames

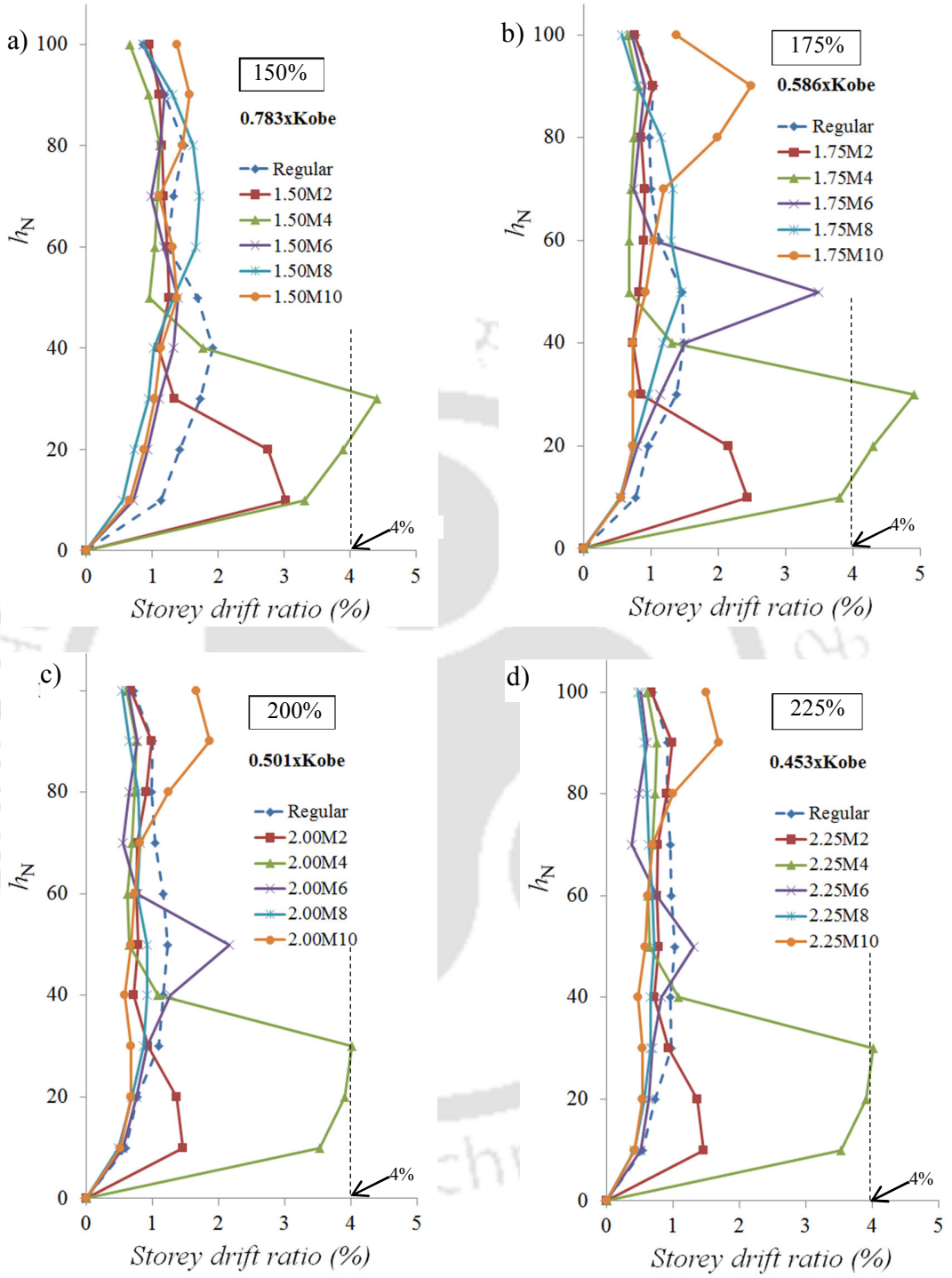

Figure 4.10: Storey drift ratio at un-functional state for a) 150% b) 175% c) 200% and d) 225% single floor mass irregular frames.

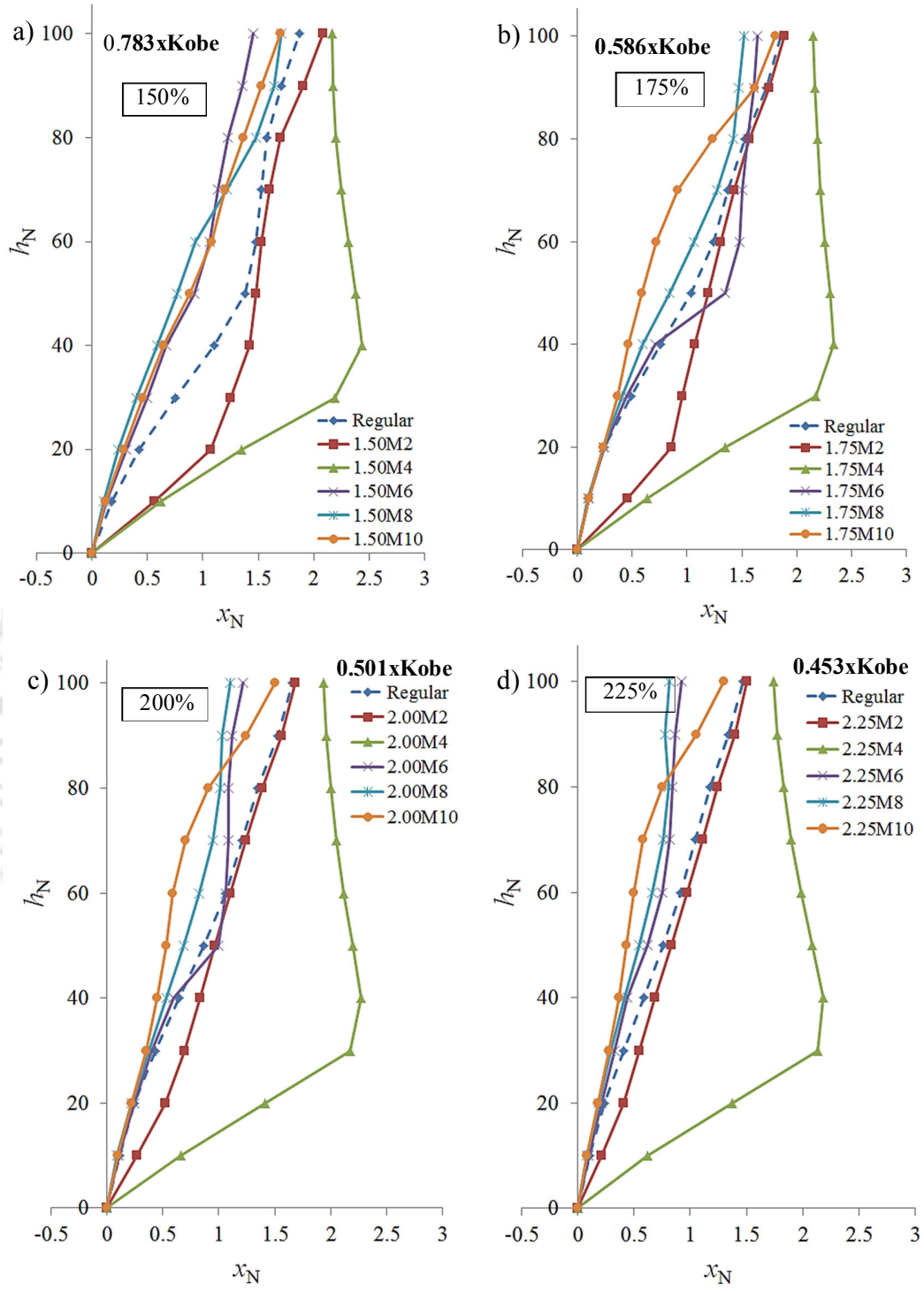

Figure 4.11: Maximum floor displacements for a) 150% b) 175% c) 200% and d) 225% single floor mass irregular frames.

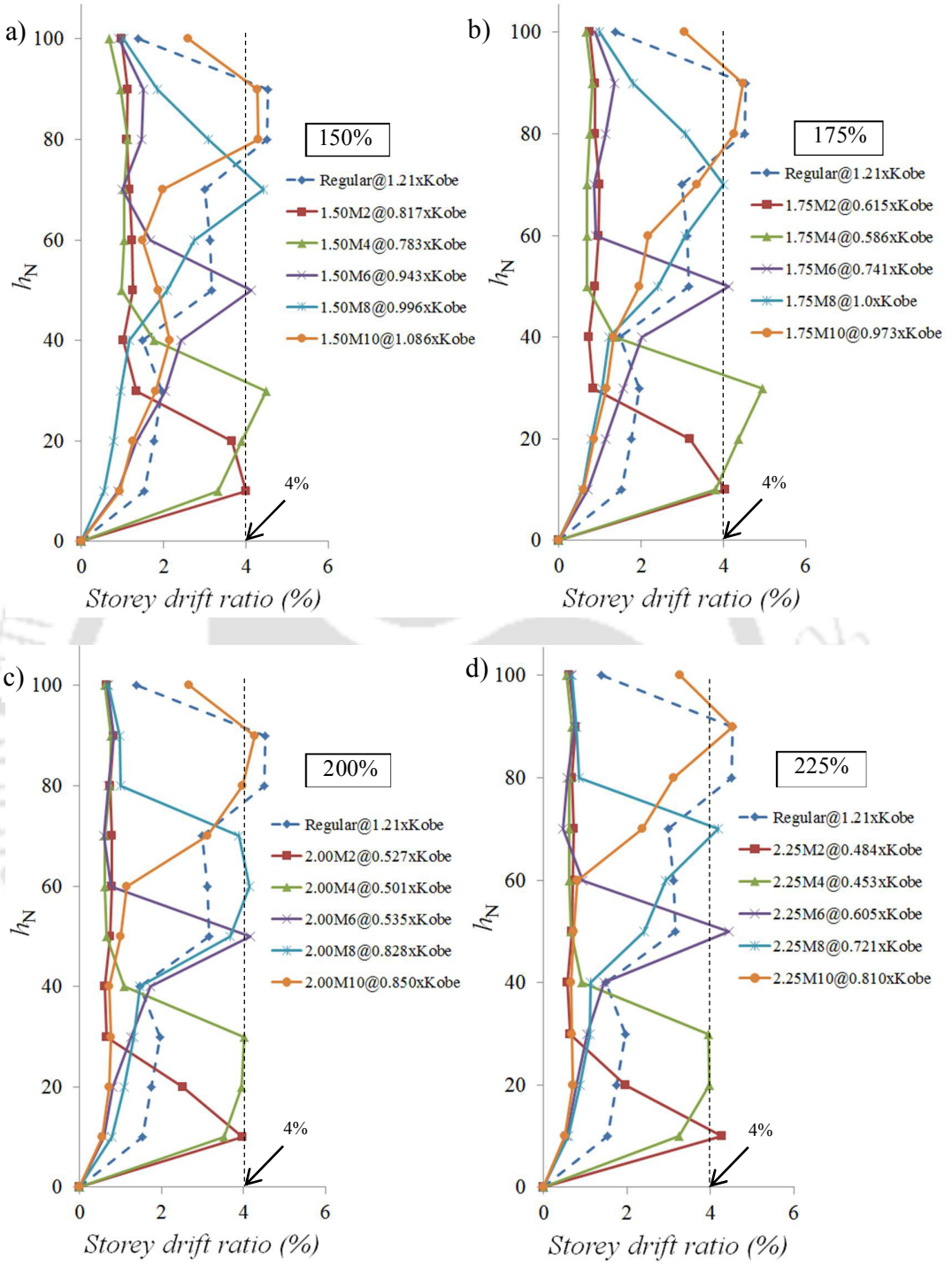

Figure 4.12: Storey drift ratio showing scale values at un-functional state for all frames of a) 150%, b) 175%, c) 200% and d) 225% single floor mass irregular frames.

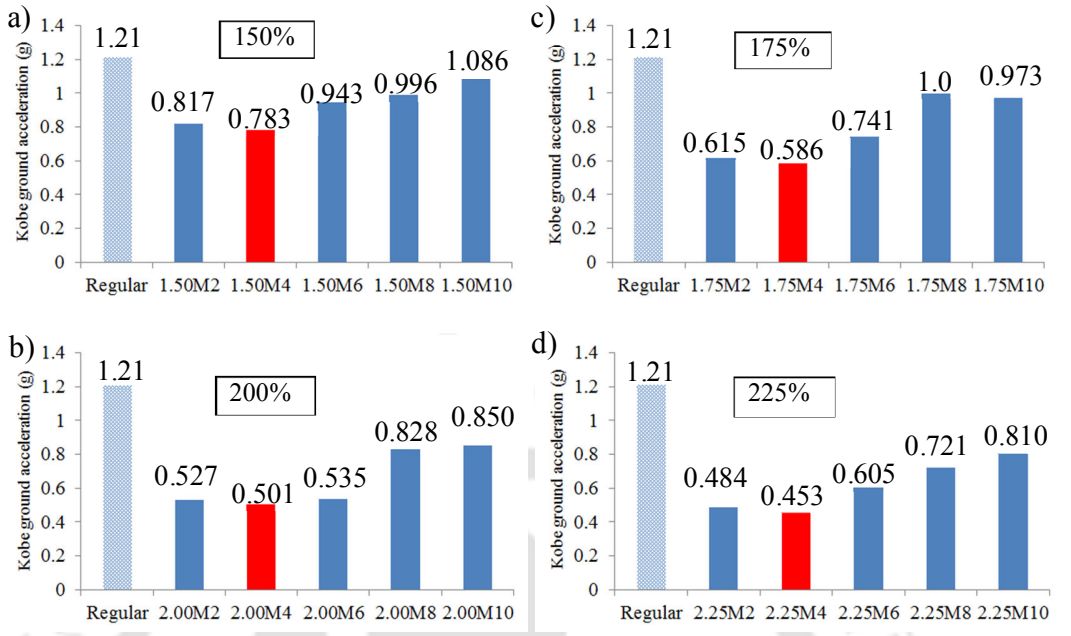

Figure 4.13: Bar charts of scale values at un-functional state for a) 150% b) 175% c) 200% and d) 225% single floor mass irregular frames.

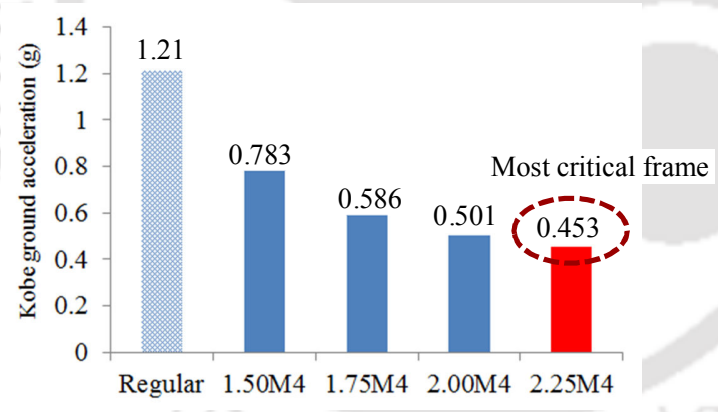

Figure 4.14: Comparison of criticality among the most critical frames of each group

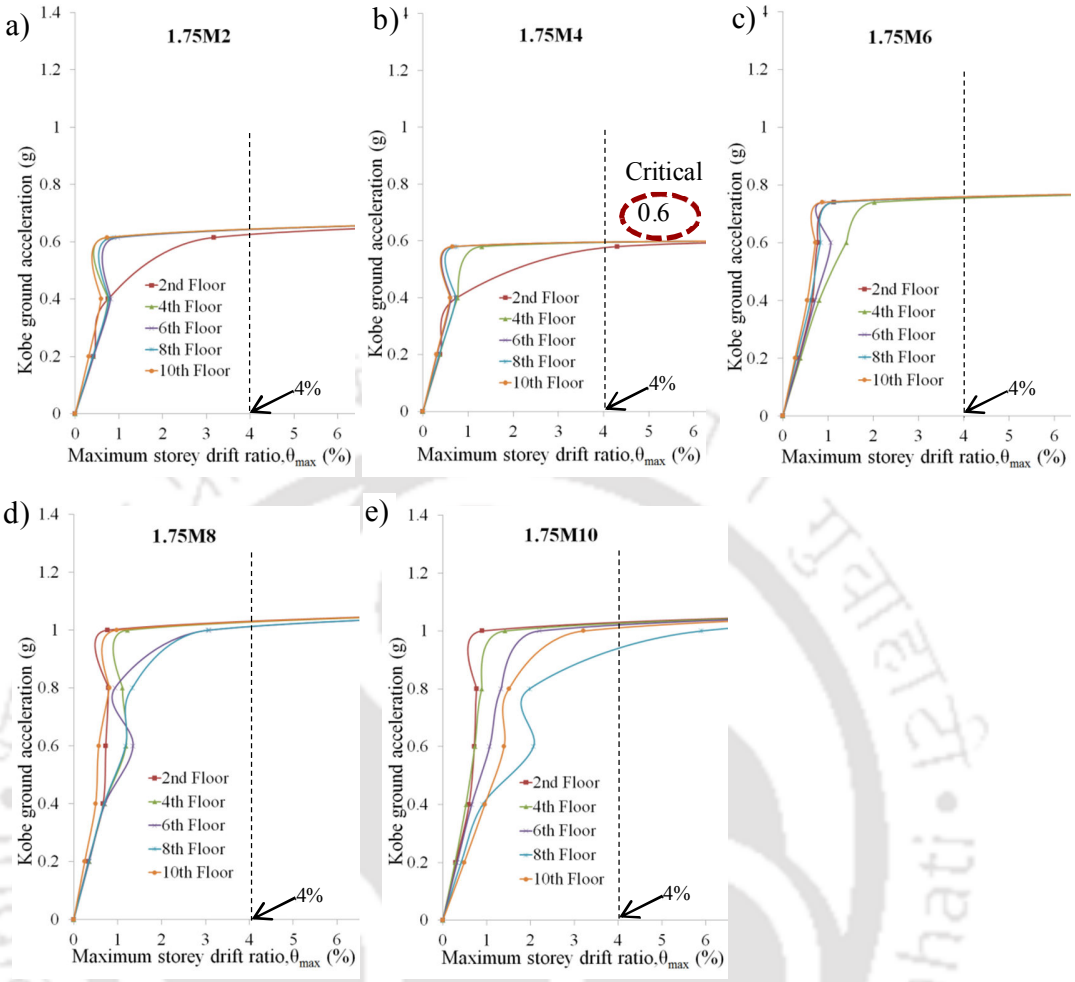

Figure 4.15: Storey-wise IDA curves for 175% mass irregular frames

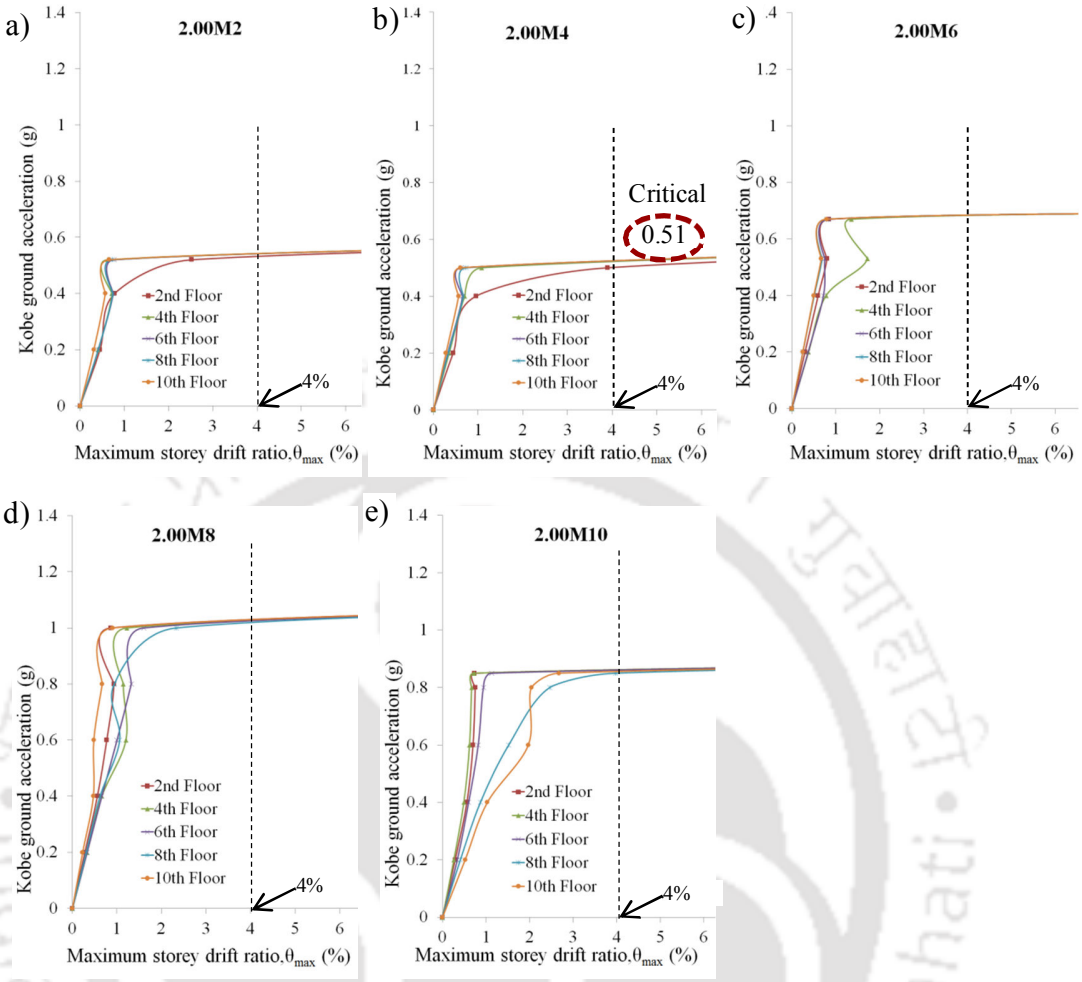

Figure 4.16: Storey-wise IDA curves for 200% mass irregular frames

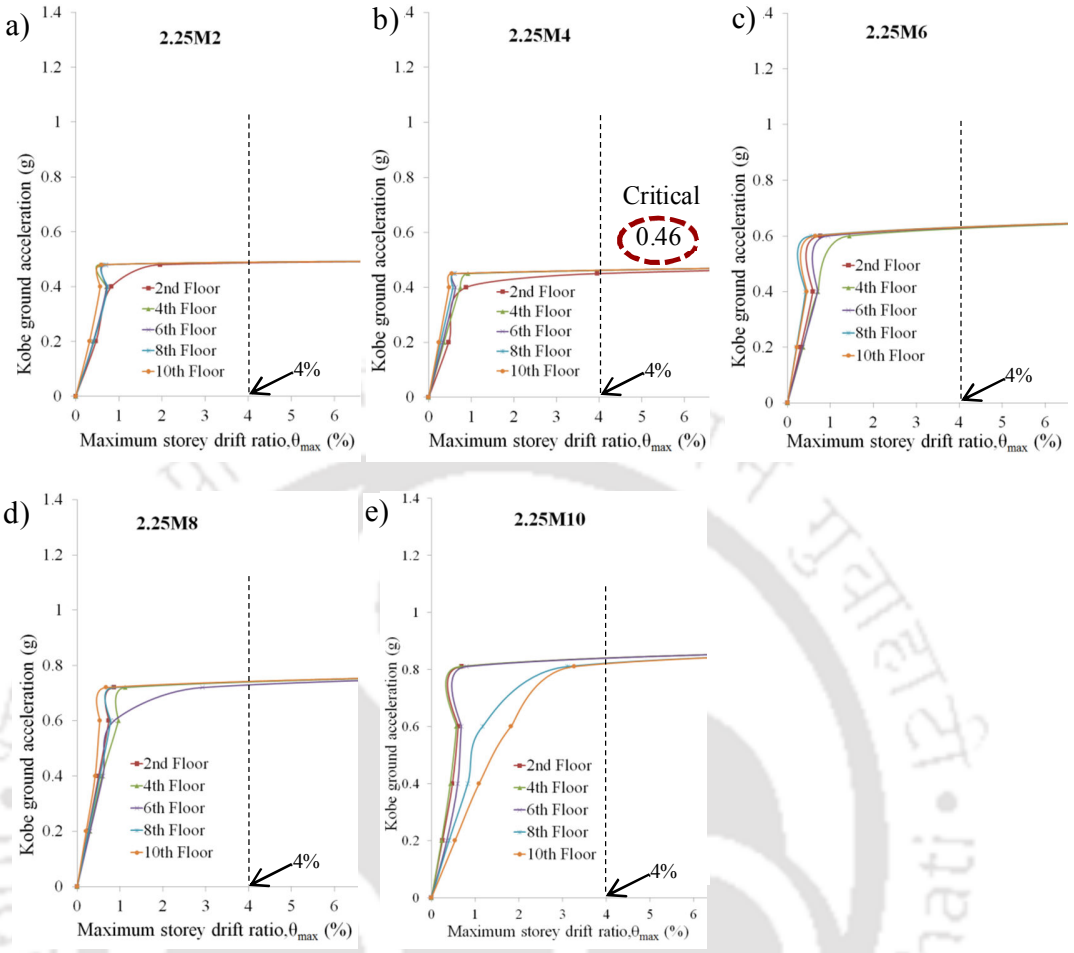

Figure 4.17: Storey-wise IDA curves for 225% mass irregular frames

CHAPTER 5

NONLINEAR TIME HISTORY ANALYSIS OF MULTI-FLOOR MASS IRREGULAR MOMENT RESISTING STEEL FRAME USING FAM

5.1 Introduction

Effect of single floor mass irregularity on seismic behaviours of moment resisting steel frame structures has been presented in Chapter 4. However, it may also be possible that multiple floors in a building frame can also be converted into multi-floor mass irregular frames as seen in many residential cum commercial multi-storeys building frames (see Figure 1.1 of chapter 1). Thus, in this chapter, Nonlinear Time History Analysis (NTHA) of multi-floor mass irregular (i.e. non-uniform distribution of multi-floor mass along the building height) (e.g. Le-Trung *et al.*, 2012; Pirizadeh and Shakib, 2013) moment resisting steel frame is presented. From the literature review in Chapter 2, it has been observed that location of multi mass irregular floors in moment resisting steel frame has been found to confine at some storey levels only along the building height (e.g. lower 3 storeys and upper 3 storeys of 20-storey building (Le-Trung *et al.*, 2012); lower half storeys of 10-storey building (Pirizadeh and Shakib, 2013). Most studies on multi-floor mass irregular frames have been reported especially looking at maximum seismic responses in terms of story drift ratios, without considering full range dynamic behaviours. Thus, in this chapter, an attempt has been made to conduct a detailed systematic Nonlinear Time History Analysis (NTHA) of multi-floor mass irregular moment resisting steel frames considering both material and geometric nonlinearities using FAM methodology, to assess full range dynamic behaviours ensuring maximum coverage of multi-mass irregular floors throughout the building height. Interaction effect due to different locations of multi mass irregular floors (e.g. double and single floor) along the building height will also be investigated. The sequence of criticality of multi-floor

mass irregular frames due to various locations of mass irregular floors along the building height will also be addressed by collapse analysis using IDA study.

The same 10-storey moment resisting steel frame considered in Chapters 3 and 4 (see Figure 3.2) has been considered as the reference regular frame in this chapter also to make relative comparison with both regular and single floor mass irregular frames. For investigating the effect of location of multi-floors mass irregularity on seismic behaviours of building frame; the reference regular frame has been converted into a number of consecutive double floors and consecutive triple floors mass irregular frames by locating multi mass irregular floors at different floor levels along the building height, thus ensuring that the location of multi-floor mass irregularity covers most of the building height. Further, interaction study of location of two equal mass irregular floors as well as the effect of two unequal mass irregular floors has been assessed. Mass irregularity intensity of 150% has been considered for the analysis of multi-floor mass irregular frames in this chapter since mass irregularity of higher intensity (i.e. greater than 150%) may result in immediate collapse (refer Figures 4.16-17-18 of Chapter 4) soon after the end linear elastic behaviour. Further, it has also been observed in Chapter 3 that Kobe earthquake (1995) has been found to give the maximum seismic responses to the 10-storey steel reference frame, and thus Kobe earthquake (1995) has again been adopted as a typical strong input ground motion for the analysis of multi-floor mass irregular 10-storey moment resisting frame. In the next section, a typical detail analysis of consecutive double floors and consecutive triple floors mass irregular frames will be presented. The analysis is further extended by performing interaction study among various mass irregular floors.

5.2. Analysis of multi-floors mass irregular frames

Schematic diagram showing multi-floors (i.e. consecutive double and triple floors) mass irregular frames are shown in Figure 5.1. Typical nomenclature of the frame would take the form XMY, where X indicates the intensity of mass irregularity, M indicates regular floor mass and Y indicates the floor levels at which mass irregularities are located. Thus in irregular frame 1.50M1-2, 1.50 indicates 150%

mass irregularity; M indicates regular floor mass and 1-2 indicate that mass irregularities are located at 1st and 2nd floor levels. In order to cover all ranges of building height, consecutive double floors mass irregular frames are developed by locating two consecutive mass irregular floors at different floor levels (i.e. 1st-2nd, 3rd-4th, 5th-6th, 7th-8th and 9th-10th floors) of the building frame (see Table 5.1); whereas consecutive triple floors mass irregular frames are developed by locating three consecutive mass irregular floors at different floor levels (i.e. 1st-2nd-3rd, 3rd-4th-5th, 5th-6th-7th, 7th-8th-9th and 8th-9th-10th floors) of the building frame (see Table 5.1). Thus there are a total of five consecutive double floors mass irregular frames and five consecutive triple floors mass irregular frames.

As in the case of single mass irregular frame (see Chapter 4), scaling of amplitude of input ground motion (Kobe earthquake, 1995) has been performed to find a suitable amplitude scale value, by trail, so as to have the abovementioned multi-floor mass irregular frames to be in working conditions i.e. within the permissible codal storey drift ratio of 4% (ASCE 7, 2016), similar to the approach followed in the literature (e.g. Pirizadeh and Shakib, (2013); Tremblay and Poncet, (2005); Wong and Speicher, (2015)). The multi-floor mass irregular frame analyses results have been grouped into 1) consecutive double floors, 2) consecutive double floors, 3) interaction for equal intensity of mass irregular floors, and 4) interaction for unequal intensity of mass irregular floors, and are presented in the following sections.

5.2.1 Consecutive double floors mass irregular frames

As per EDP based method of collapse analysis (Vamvatsikos and Cornell, 2002; Wong and Zhao, 2007), it has been observed from Figure 5.2a that the consecutive double floors irregular frame 1.50M3-4 becomes un-functional (exceeding allowable storey drift ratio of 4%, ASCE 7, 2016) early at the lowest scale value (0.513) of amplitudes of Kobe earthquake. At this scale value, the remaining consecutive double floors mass irregular frames have been observed to be still in working condition i.e. within the codal permissible storey drift ratio of 4%, (ASCE 7, 2016). Large floor displacements of consecutive double floors mass irregular frame 1.50M3-4 has been seen as compared to other consecutive double floors mass irregular frames at 0.513

scale value as shown in Figure 5.2b. This may be related to the criticality of the storeys near 40% building height of reference regular as observed in Chapter 3 (refer Figure 3.14). Similarly the scale values of amplitudes of Kobe earthquake at which other consecutive double floors mass irregular frames (i.e.1.50M1-2, 1.50M5-6, 1.50M7-8 and 1.50M9-10) become un-functional are found to be 0.682, 0.667, 0.790 and 1.086 respectively (see Figure 5.3a) as compared to that of the corresponding scale value (i.e. 1.2) of reference regular frame. Maximum floors' displacements of all consecutive double floors mass irregular frames at their corresponding scale values of un-functional states have been shown in Figure 5.3b. It has also been observed that maximum storey drift ratio and maximum floor displacement have been found to occur at the storey level below the location of consecutive double mass irregular floors (see Figures 5.3a-b). Such observations of occurrence of maximum storey drift ratio near the location of mass irregular floor has been reported in the literatures (Choi, 2004 and Le-Trung *et al.*, 2012). Total floor displacement time histories of all the consecutive double floors mass irregular frames at their corresponding un-functional states have been shown in Figure 5.4. Large inter-floor displacements have been observed between the floors levels located below the floor level where consecutive double mass irregular floors is located (see Figure 5.4). The sequence of consecutive double floors mass irregular frames in decreasing order of criticality are found to be 1.50M3-4, 1.50M1-2, 1.50M5-6, 1.50M7-8 and 1.50M9-10 (see Figure 5.5); i.e. consecutive double floors mass irregularity near top storeys of the building frame are much safer than that of consecutive double floors mass irregularity near bottom storeys of the building frame. The criticality of locating multi-mass irregular floors near the bottom storeys of the building has been reported by the following researchers Le-Trung *et al.*, (2012); Pirizadeh and Shakib, (2013) and Varadharajan *et al*., (2014).

A comparative study has been carried out between single floor mass irregular frames of higher intensity of mass irregularity (i.e. 200%) and consecutive double floors mass irregular frames of lower intensity of mass irregularity (i.e. 150%) at equivalent storey height. Scale values of amplitudes of Kobe earthquake at which 150%

consecutive double floors mass irregular frames and 200% single floor mass irregular frames become un-functional state are shown in Figures 5.6a (refer Figure 5.3a) and 5.6b (from Chapter 4; see Figure 4.13c) respectively. It has been observed that consecutive double floors mass irregular frames 1.50M1-2, 1.50M3-4, 1.50M5-6, 1.50M7-8 and 1.50M9-10 are found to be become un-functional at scale values of 0.682, 0.513, 0.667, 0.790 and 0.865 respectively (see Figure 5.6a); whereas 200% single floor mass irregular frames 2.00M2, 2.00M4, 2.00M6, 2.00M8 and 2.00M10 are found to be become un-functional at scale values of 0.527, 0.501, 0.535, 0.828 and 0.850 respectively (see Figure 5.6b). It has been seen that the scale values to be become un-functional for 150% consecutive double floors mass irregular frames are generally found to be more than that of the corresponding 200% single floor mass irregular frames except when mass irregular floors are located at 80% of building height where slight decrease in scale values has been observed (see Figure 5.7). Thus, it has been shown that concentrating higher intensity of mass irregularity at single floor level is found to be more critical than distributing the intensity of mass irregularity to consecutive double floor levels at equivalent storey height. For example single floor mass irregular frame 2.00M2 can handle mass irregularity of 200% at scale value of 0.527, whereas the corresponding consecutive double floors mass irregular frame 1.50M1-2 can handle more mass irregularity of 300% at even more higher scale value of 0.682 (see Figure 5.7). Thus consecutive double floors mass irregular frame 1.50M1-2 can handle 50% more intensity of mass irregularity than single floor mass irregular frame 2.00M2. Hence, it has been found that distribution of intensity of mass irregularity to different floor levels is found to be more beneficial than concentrating at equivalent single floor level.

5.2.2 Consecutive triple floors mass irregular frames

Similar to the responses of consecutive double floors mass irregular frames, it has also been observed that the consecutive triple floors mass irregular frame 1.50M3-4-5 becomes (exceeding allowable storey drift ratio of 4%, ASCE 7, 2016) early at the lowest scale value (0.474) of amplitudes of Kobe earthquake (see Figure 5.8a). At this scale value, the remaining consecutive triple floors mass irregular frames have

been observed to be still in working i.e. within the codal permissible storey drift ratio of 4%, (ASCE 7, 2016). Large floor displacements of consecutive triple floors mass irregular frame 1.50M3-4-5 has been seen as compared to other consecutive triple floors mass irregular frames at 0.474 scale value (see Figure 5.8b). This again, may be related to the criticality of the storey near 40% building height of reference regular as observed in Chapter 3. Similarly the scale values of amplitudes of Kobe earthquake at which other consecutive triple floors mass irregular frames (i.e.1.50M1-2-3, 1.50M5-6-7, 1.50M7-8-9 and 1.50M8-9-10) become un-functional are found to be 0.488, 0.580, 0.701 and 0.920 respectively (see Figure 5.9a). Maximum floor displacements of all consecutive triple floors mass irregular frames at their corresponding scale values of un-functional states have been shown in Figure 5.9b. It has also been observed that maximum storey drift ratio and maximum floor displacement are found to occur at the storey level below the location of consecutive triple mass irregular floors (see Figures 5.9a-b). Total floor displacement time histories of all the consecutive triple floors mass irregular frames at their corresponding un-functional states have been shown in Figure 5.10. As similar to that of consecutive double floors mass irregular frames, large inter-floor displacements have been observed between the floors levels located below the consecutive triple mass irregular floors in total floor displacement time histories (see Figure 5.10). The sequence of consecutive triple floors mass irregular frames in decreasing order of criticality are seen to be 1.50M3-4-5, 1.50M1-2-3, 1.50M5-6-7, 1.50M7-8-9 and 1.50M8-9-10 (see Figure 5.11); i.e. consecutive triple floors mass irregularity located near top storeys of the building frame are safer than that of consecutive triple floors mass irregularity located near bottom storeys of the building frame. Criticality of locating consecutive triple floors mass irregularity near the bottom storeys has also been reported by Le-Trung *et al*., (2012).

A comparative study between single floor mass irregular frames of higher intensity of mass irregularity (i.e. 225%) and consecutive triple floors mass irregular frames of lower intensity of mass irregularity (i.e. 150%) at equivalent median storey level has been studied. Scale values of amplitudes of Kobe earthquake at which 150%

consecutive triple floors mass irregular frames and 225% single floor mass irregular frames become un-functional are shown in Figures 5.12a (refer Figure 5.9a) and 5.12b (from chapter 4; see Figure 4.13d) respectively. It has been observed that consecutive triple floors mass irregular frames 1.50M1-2-3, 1.50M3-4-5, 1.50M5-6-7, 1.50M7-8-9 and 1.50M8-9-10 are found to be become un-functional at scale values of 0.488, 0.474, 0.580, 0.701 and 0.920 respectively (see Figure 5.12a); whereas 200% single floor mass irregular frames 2.25M2, 2.25M4, 2.25M6, 2.25M8 and 2.25M10 are found to be become un-functional at scale values of 0.484, 0.454, 0.605, 0.721 and 0.810 respectively (see Figure 5.12b). It has been seen that the scale values to be become un-functional state for 150% consecutive triple floors mass irregular frames are generally found to be more than that of corresponding 225% single floor mass irregular frames except when mass irregular floors are located at 60% and 80% building height where slight decrease in scale values have been observed (see Figure 5.13). Thus, it has again been shown that concentrating higher intensity of mass irregularity at single floor is found to be more critical than distributing the mass irregularity to consecutive triple floor levels at equivalent median storey height. For example single floor mass irregular frame 2.25M2 can handle mass irregularity of 225% at scale value of 0.484, whereas corresponding consecutive triple floors mass irregular frame 1.50M1-2-3 can handle more mass irregularity of 450% at even more higher scale value of 0.488 (see Figure 5.13). Thus consecutive triple floors mass irregular frame 1.50M1-2-3 can handle 100% more mass irregularity than single floor mass irregular frame 2.25M2. Hence, it has been again found that distribution of mass irregularity to different floor levels is found to be more beneficial than concentrating at single floor level.

5.2.3 Interaction study between equal intensity of mass irregularity

Seismic interaction study between equal intensity of mass irregular floors has been performed by locating equal mass irregular floors at various possible combinations of floors along the building height. Combination of equal mass irregular floors has been performed only in alternate even floor numbers of the building to avoid clumsiness while presenting analysis results. The combination has been conducted in such a way

that the location of one mass irregular floor is kept fix while the other mass irregular floor of same intensity is kept changing along the building height, e.g. one mass irregular floor is kept fixed at 2nd floor while the other is kept changing at 4th, 6th, 8th and 10th floors. Various possible combinations of two equal mass irregular floors have been divided into two groups (i.e. Group 1 and 2) in order to bring clarity in representing results, where each group contains five double floors (i.e. non-consecutive) mass irregular frames (see Figure 5.14). Group 1 consists of double floors irregular frames 1.50M2-4, 1.50M2-6, 1.50M2-8, 1.50M2-10 and 1.50M4-6; whereas as Group 2 consists of double floors irregular frames 1.50M4-8, 1.50M4-10 1.50M6-8, 1.50M6-10 and 1.50M8-10. The scale values of amplitudes of Kobe earthquake at which all the combination of double floors mass irregular frames becomes un-functional (i.e. storey drift ratio > 4%, ASCE 7, 2016) have been determined. It has been found that the scale values of double floors mass irregular frames (Group 1) 1.50M2-4, 1.50M2-6, 1.50M2-8, 1.50M2-10 and 1.50M4-6 to become un-functional states are found to be 0.570, 0.890, 0.950, 1.01 and 0.680 respectively (see Figure 5.15a); whereas that of double floors mass irregular frames (Group 2) 1.50M4-8, 1.50M4-10, 1.50M6-8, 1.50M6-10 and 1.50M8-10 to become un-functional states are found to be 0.780, 0.870, 0.770, 1.00 and 1.04 respectively (see Figure 5.15b).

It has been observed that among the double floors mass irregular frames, irregular frame 1.50M2-4 has been found to be the most critical frame since it becomes un-functional at the lowest scale value of 0.570 (see Figure 5.16a). Thus, double floors mass irregular frames has been found to be the most critical when closely spaced equal intensity of mass irregular floors is located at the lower storey levels of the building. It has also been seen that the criticality of double floors mass irregular frames decreases as the location of two equal intensity of mass irregular floors move away from each other. For example, the criticality of double floors mass irregular frames decreases in the following sequence 1.50M2-4, 1.50M2-6, 1.50M2-8 and 1.50M2-10 as the corresponding scale values to become un-functional state increases in the following sequence 0.570, 0.890, 0.950 and 1.01 (see Figures 5.16a and 5.17).

Similarly, the criticality decreases for the remaining double floors mass irregular frames in the following sequence as 1.50M4-6, 1.50M4-8, 1.50M4-10; and 1.50M6-8, 1.50M6-10 (sees Figure 5.17). Irregular frame 1.50M8-10 has been found to be the least critical among all the double floors mass irregular frames since it becomes un-functional state at the highest scale value of 1.04 (see Figure 5.16b). Thus, double floors mass irregular frames has been found to be the least critical when closely spaced equal intensity of mass irregular floors is located at the highest storey levels of the building. It has also been found that the criticality of closely spaced equal intensity of mass irregular floors increases on moving towards the base of the building. For example, criticality of closely spaced equal intensity of mass irregular floors increases in the following sequence 1.50M8-10, 1.50M6-8, 1.50M4-6 and 1.50M2-4 as the corresponding scale values to become un-functional state decreases in the following sequence 1.04, 0.770, 0.680 and 0.570 (see Figure 5.16). Thus, it has been observed that double floors mass irregular frames 1.50M2-4 and 1.50M8-10 becomes the most critical (scale value, 0.513) and the least critical (scale value, 1.04) respectively.

Further a comparative study between consecutive double floors mass irregular frames and alternate double floors mass irregular frames has also been conducted. Scale values of amplitude of Kobe earthquake at which consecutive double floors mass irregular frames 1.50M3-4, 1.50M5-6, 1.50M7-8 and 1.50M9-10 become un-functional state are 0.513, 0.667, 0.790 and 0.865 respectively (see Figure 5.3a); whereas that of alternate double floors mass irregular frames 1.50M2-4, 1.50M4-6, 1.50M6-8 and 1.50M8-10 to become un-functional state are 0.570, 0.680, 0.770 and 1.04 respectively (see Figure 5.18). It has been seen that the scale values to be become un-functional state for alternate double floors mass irregular frames are generally found to be more than that of the consecutive double floors mass irregular frames except at location where mass irregular floors are located between 60% and 80% building height (see Figure 5.18). Thus, it has been shown that locating mass irregular floors together at consecutive double floors is found to be more critical than distributing the same mass irregular floors at alternate double floors along the

building height. For example consecutive double floors mass irregular frame 1.50M9-10 has been found to be more critical by 17% than that of alternate double floors mass irregular frame 1.50M8-10 (see Figure 5.18).

Maximum floor displacements of all the double floors mass irregular frames at their corresponding scale values of un-functional states have been shown in Figure 5.19. It has also been observed that maximum storey drift ratio and maximum floor displacement are found to occur at the storey level below the location of either of the mass irregular floor.

5.2.4 Interaction study between unequal intensity of mass irregularity

Interaction study between two unequal intensity of mass irregularity (i.e. 150% consecutive double floors and 150% single floor) has been conducted in such a way that the most critical frame of consecutive double floors mass irregular frames (i.e. 1.50M3-4) (see Figure 5.5) is kept fix whereas the other 150% single mass irregular floor is kept changing along the height of the building. In order to bring clarity to the discussion, the interaction study has been carried out into two groups. In Group 1, the location of the addition 150% single mass irregular floor has been kept changing at 1^{st}, 2^{nd}, 5^{th} and 6^{th} floor levels; whereas in Group 2, the location of the addition 150% single mass irregular floor has been kept changing at 7^{th}, 8^{th}, 9^{th} and 10^{th} floor levels (see Figure 5.20). The scale values of amplitudes of Kobe earthquake have been determined for the interacted irregular frames formed by the combination of the critical double floors (1.50M3-4) and the addition 150% single mass irregular floor to becomes un-functional (i.e. exceeding allowable storey drift ratio of 4% (ASCE 7, 2016)). It has been found that the scale values of interacted unequal intensity of mass irregular frames (Group 1) 1.50M1-3-4, 1.50M2-3-4, 1.50M3-4-5 and 1.50M3-4-6 to become un-functional states are found to be 0.487, 0.426, 0.474 and 0.450 respectively (see Figure 5.21a); whereas that of the scale values of interacted unequal intensity of mass irregular frames (Group 2) 1.50M3-4-7, 1.50M3-4-8, 1.50M3-4-9 and 1.50M3-4-10 to become un-functional states are found to be 0.542, 0.566, 0.625 and 0.532 respectively (see Figure 5.21b).

The most critical frame of consecutive double floors mass irregular frames (i.e. 1.50M3-4) has been considered as the reference frame to investigate the interaction effect with the addition of another 150% single mass irregular floor. It has been observed that the criticality increases with respect to reference frame (1.50M3-4) when the addition 150% single mass irregular floor is kept below at first floor level (see Figure 5.22). The criticality has been found to increase further when the addition 150% single mass irregular floor is kept closer at second floor level and this combination becomes the most critical (see Figure 5.22); then the criticality has been found to decrease gradually when the location of the addition 150% single mass irregular floor moves upwards from 5^{th} floor along the building height. However, a slight increase of criticality has been observed when the addition 150% single mass irregular floor has been kept at 10^{th} floor level. Thus, interaction of unequal intensity of mass irregular frames has been found to be the most critical when unequal intensity of mass irregular floors are located close to each other at lower storey levels of the building (i.e. 1.50M2-3-4 attains un-functional state at lowest scale value 0.426) (see Figure 5.22). The sequence of criticality in decreasing order for the interaction of unequal intensity of mass irregular floors has been observed as follow 1.50M2-3-4, 1.50M3-4-5, 1.50M1-3-4, 1.50M3-4-10, 1.50M3-4-6, 1.50M3-4-7, 1.50M3-4-8 and 1.50M3-4-9 (see Figures 5.22 and 5.23). It has also been found that interacted unequal intensity mass irregular frames 1.50M1-3-4, 1.50M2-3-4 and 1.50M3-4-5 have been found to be more critical than the reference frame 1.50M3-4; whereas the rest of the interacted unequal intensity mass irregular frames 1.50M3-4-6, 1.50M3-4-7, 1.50M3-4-8, 1.50M3-4-9 and 1.50M3-4-10 have been found to be less critical than the reference frame 1.50M3-4. Thus, it has been observed that the criticality of the most critical consecutive double floors mass irregular frame 1.50M3-4 has been found to increase when the addition 150% single mass irregular floor is located at lower floors levels, whereas the criticality decreases when the addition 150% single mass irregular floor is located at upper floor levels starting from 6^{th} floor level onwards. Thus, interacted unequal intensity mass irregular frames (i.e. 1.50M3-4-6, 1.50M3-4-7, 1.50M3-4-8, 1.50M3-4-9 and 1.50M3-4-10) can

handle ~33% more mass irregularity even at lower earthquake forces than the consecutive double floors mass irregular frame 1.50M3-4.

Maximum floors' displacement of all the interacted unequal intensity of mass irregular frames at their corresponding scale values of un-functional states have been shown in Figure 5.24. It has also been observed that maximum storey drift ratio and maximum floor displacement are found to occur at lower storey levels below the location of consecutive double mass irregular floors (see Figures 5.21 and 5.24).

5.3 Conclusion

This chapter presents a parametric study of multi-floors mass irregular steel building frames to investigate the seismic behaviours of the irregular building frame when the location of multi-floor mass irregularity changes along the height of the building frame. Multi-floor mass irregular building frames have been divided into consecutive double floors and consecutive triple floors mass irregular frames with mass irregularity intensity of 150%. Interaction study between equal and unequal intensities of mass irregularity have also been conducted. The results are presented in the form of total floor displacements and storey drift ratios. The following conclusions are drawn from the above analysis.

1. The criticality (i.e. storey drift ratio > 4% (ASCE 7, 2016)) of multi-floor mass irregular frames has been found to depend on the criticality of the storey levels in reference regular frame. Multi-floor mass irregular frame has been found to be the most critical when mass irregular floors are located near 40% building height.
2. The criticality of multi-floor mass irregular frames have generally been found to decrease as the location of multi-mass irregular floors moves away from the base towards the top of the building height. Thus, multi-mass irregular floors located at upper storey levels are found to be safer than those located at lower storeys of the building.

3. Distribution of mass irregular intensity at adjacent floor levels has been found to be less critical than concentrating the entire intensity of mass irregularity at equivalent single floor level.
4. Criticality of multi-floors mass irregular frame has been found to increase as the locations of mass irregular floors approaches each other and vice-versa.
5. Criticality of multi-floors mass irregular frame has also been found to increase as the location of closely spaced mass irregular floors moves downwards along the building height and vice-versa.

Table 5.1: Nomenclature of multi-floor mass irregular frames

1	**Consecutive Double-floors mass irregular frames**
	1.50M1-2, 1.50M3-4, 1.50M5-6, 1.50M7-8 and 1.50M9-10
2	**Consecutive Triple-floors mass irregular frames**
	1.50M1-2-3,1.50M3-4-5, 1.50M5-6-7, 1.50M7-8-9 and 1.50M8-9-10
3	**Interaction for equal intensity of mass irregular floor (Group1)**
	1.50M2-4, 1.50M2-6, 1.50M2-8, 1.50M2-10 and 1.50M4-6
4	**Interaction for equal intensity of mass irregular floor (Group2)**
	1.50M4-8, 1.50M4-10, 1.50M6-8, 1.50M6-10 and 1.50M8-10
5	**Interaction for unequal intensities of mass irregular floor (Group1)**
	1.50M2-3-4, 1.50M3-4-6, 1.50M3-4-8 and 1.50M3-4-10
6	**Interaction for unequal intensities of mass irregular floor (Group2)**
	1.50M2-9-10, 1.50M4-9-10, 1.50M6-9-10 and 1.50M8-9-10

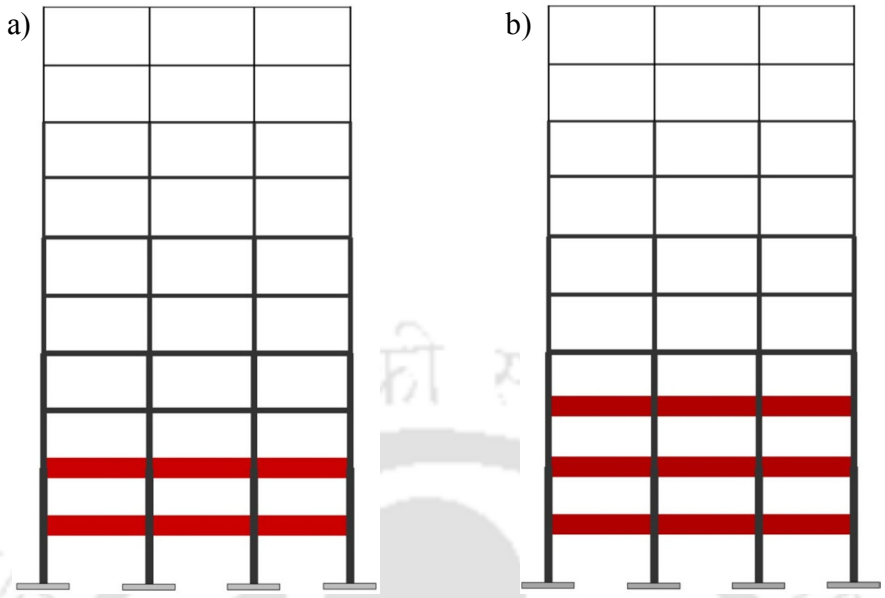

Figure 5.1: Multi-floor mass irregular frames a) 150% consecutive double floors and b) 150% consecutive triple floors

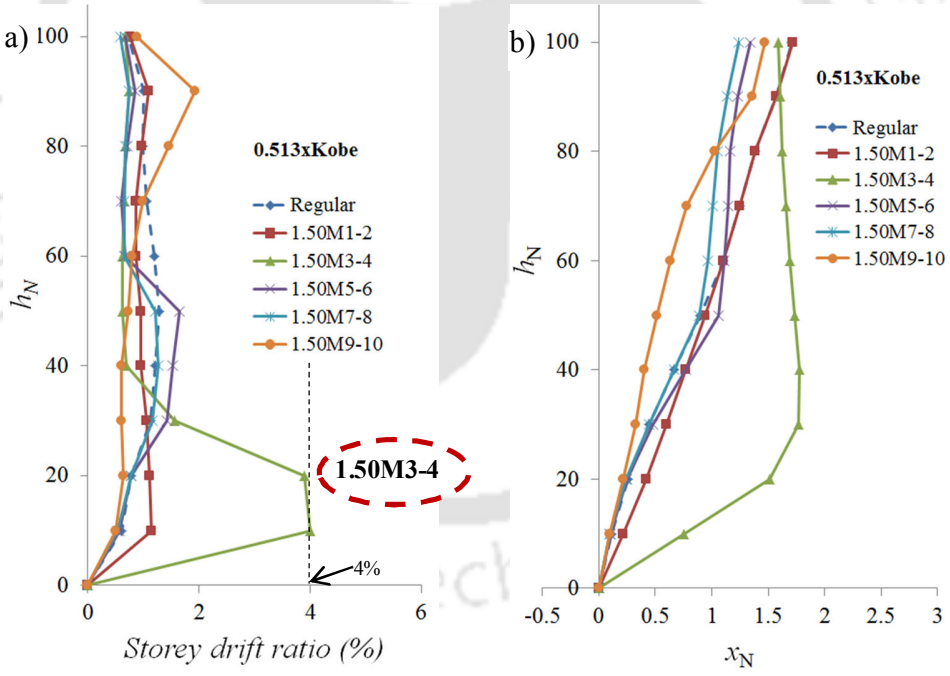

Figure 5.2: a) Storey drifts ratio and b) Maximum floor displacement for 150% consecutive double floors mass irregular frames at 0.513xKobe

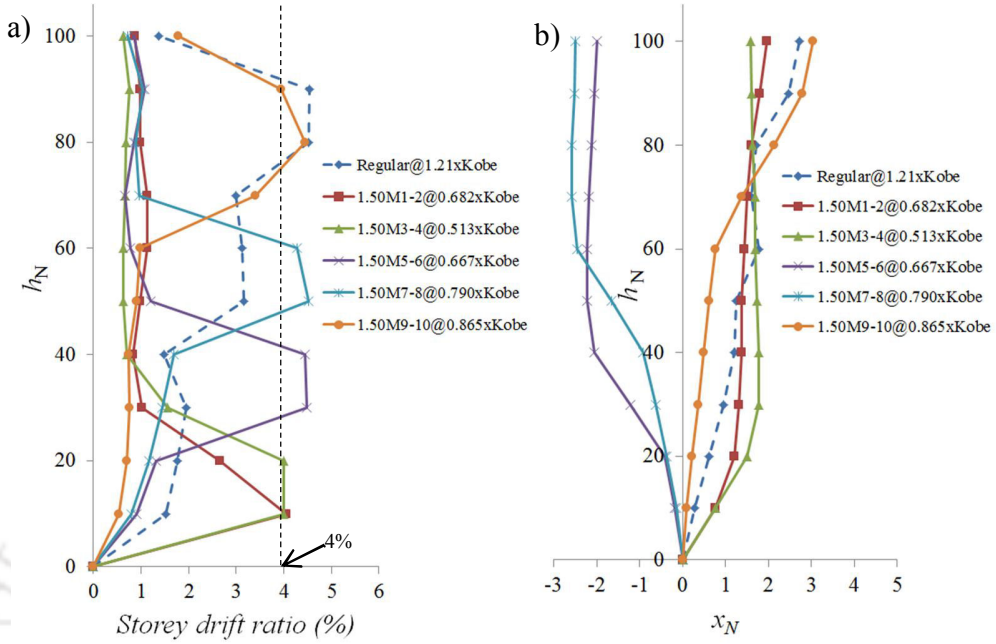

Figure 5.3: a) Storey drift ratio at collapse states and b) Total floor displacements for 150% consecutive double floors mass irregular frames

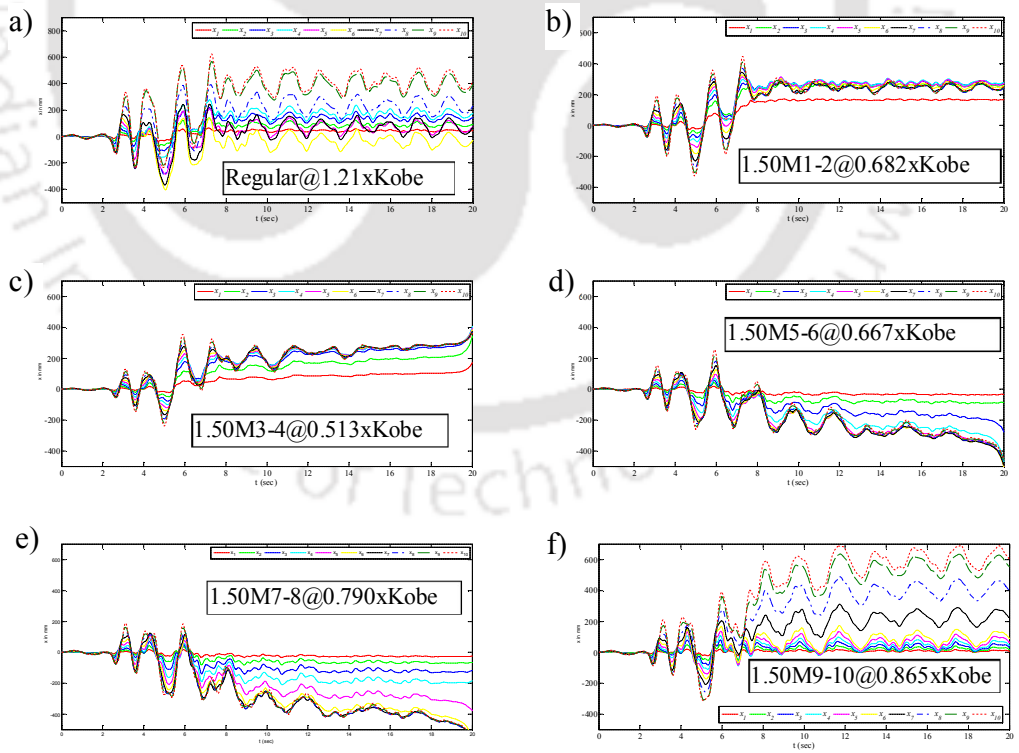

Figure 5.4: Total floor time histories at collapse state for a) Regular b) 1.50M1-2 and c) 1.50M3-4 d) 1.50M5-6 e) 1.50M7-8 and f) 1.50M9-10

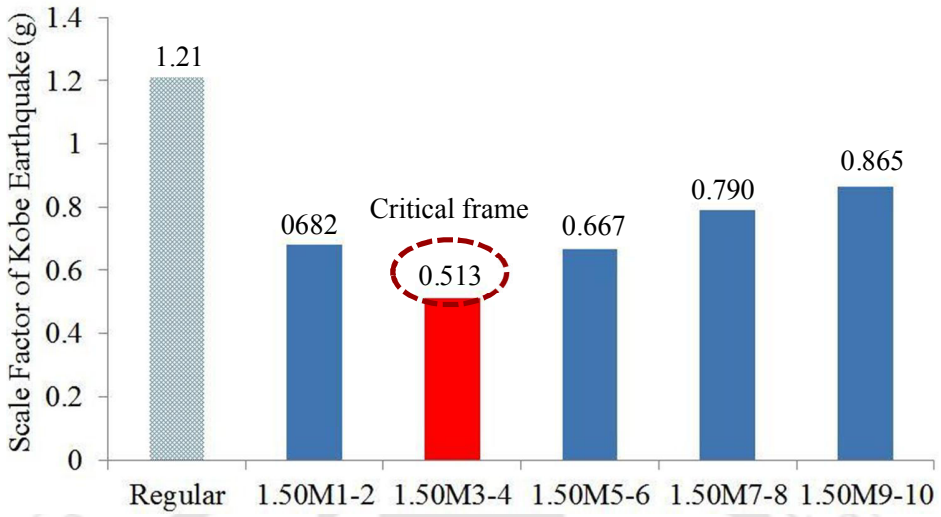

Figure 5.5: Bar chart of scale values at collapse state for 150% consecutive double floors mass irregular frames

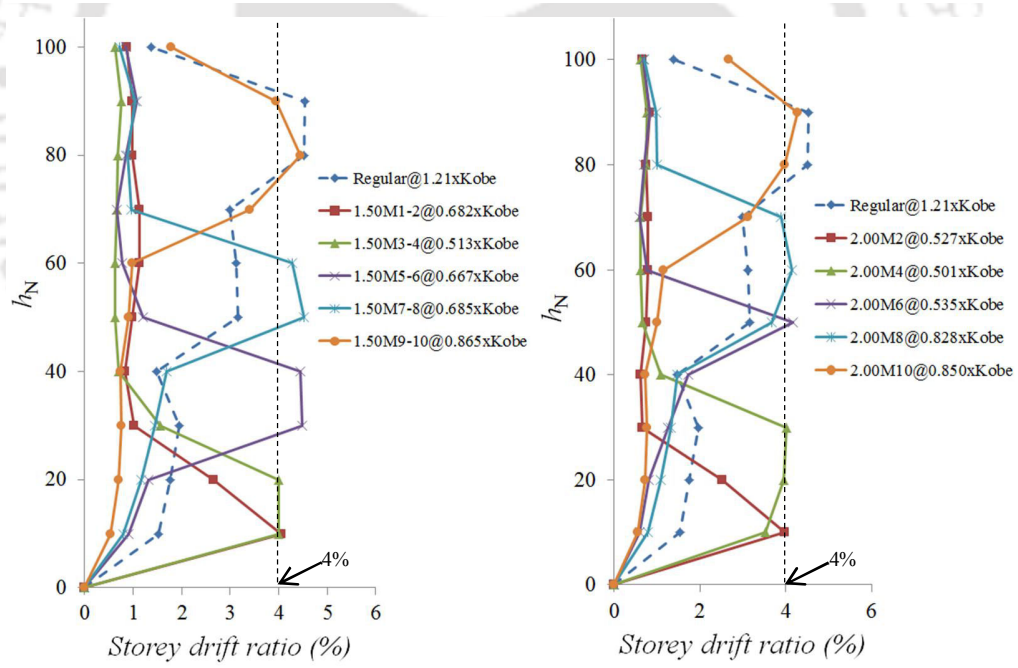

Figure 5.6: Storey drift ratio at collapse state for a) 150% consecutive double floors mass irregular frames and b) 200% single floor mass irregular frames

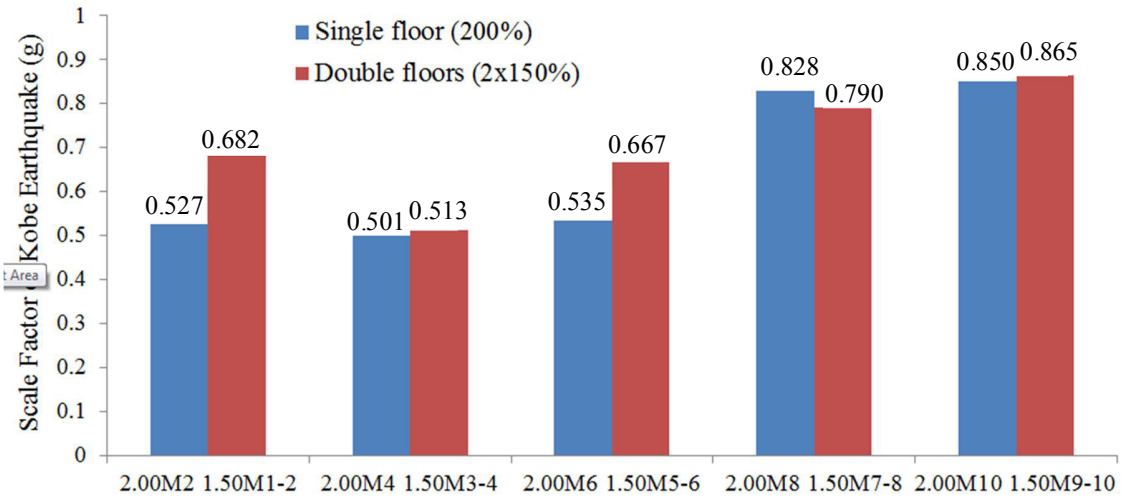

Figure 5.7: Comparison of criticality between 150% consecutive double floors and 200% single floor mass irregular frames

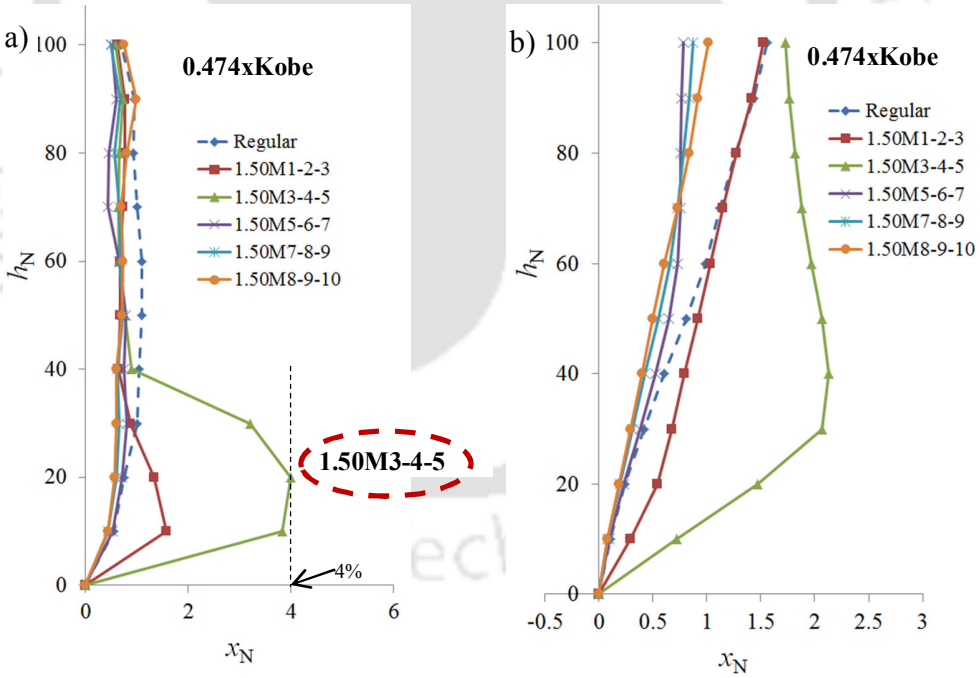

Figure 5.8: a) Storey drifts ratio and b) Maximum floor displacement for 150% consecutive triple floors mass irregular frames at 0.474xKobe

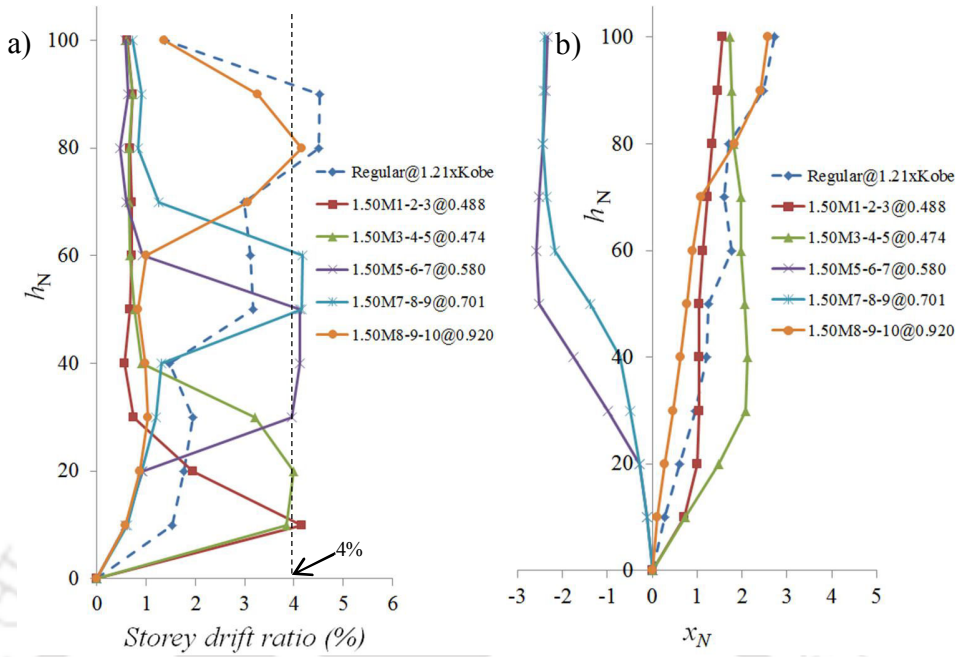

Figure 5.9: a) Storey drift ratio at collapse states and b) Total floor displacements for 150% consecutive triple floors mass irregular frames

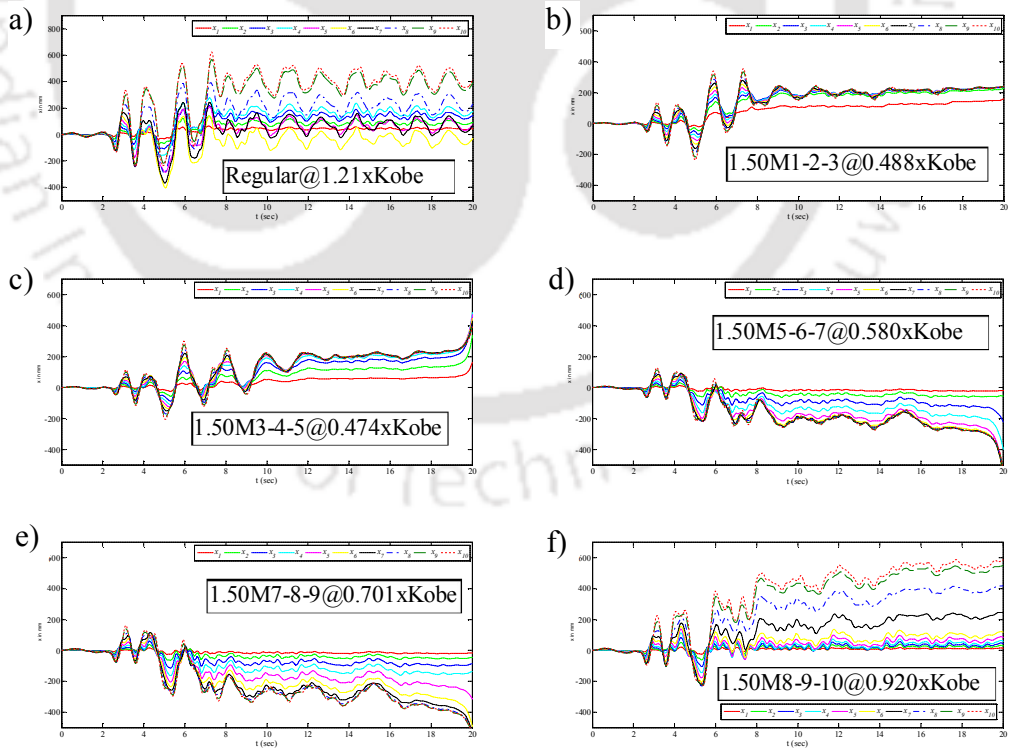

Figure 5.10: Total floor time histories at collapse state for a) Regular b) 1.50M1-2-3 and c) 1.50M3-4-5 d) 1.50M5-6-7 e) 1.50M7-8-9 and f) 1.50M8-9-10

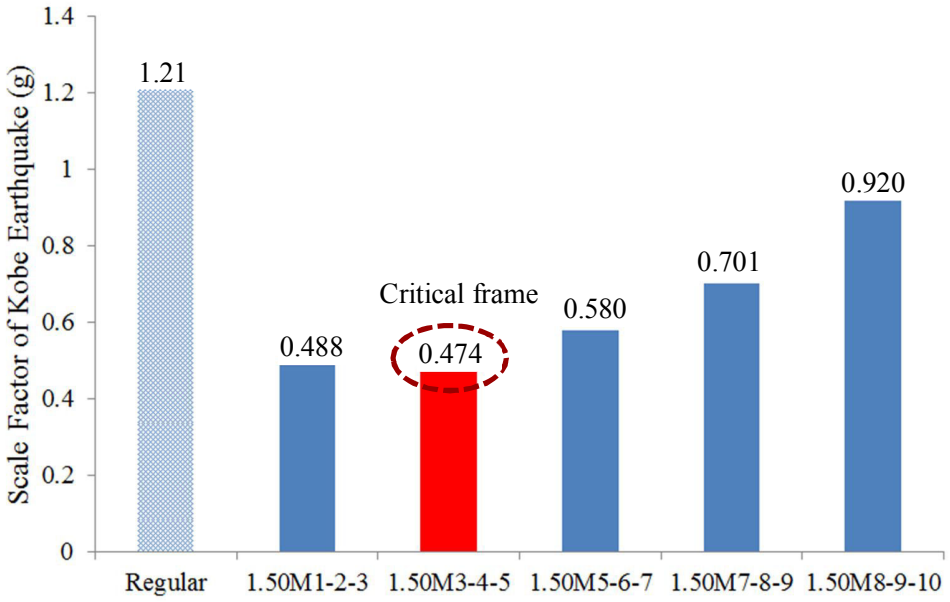

Figure 5.11: Bar chart of scale values at collapse state for 150% consecutive triple floors mass irregular frames

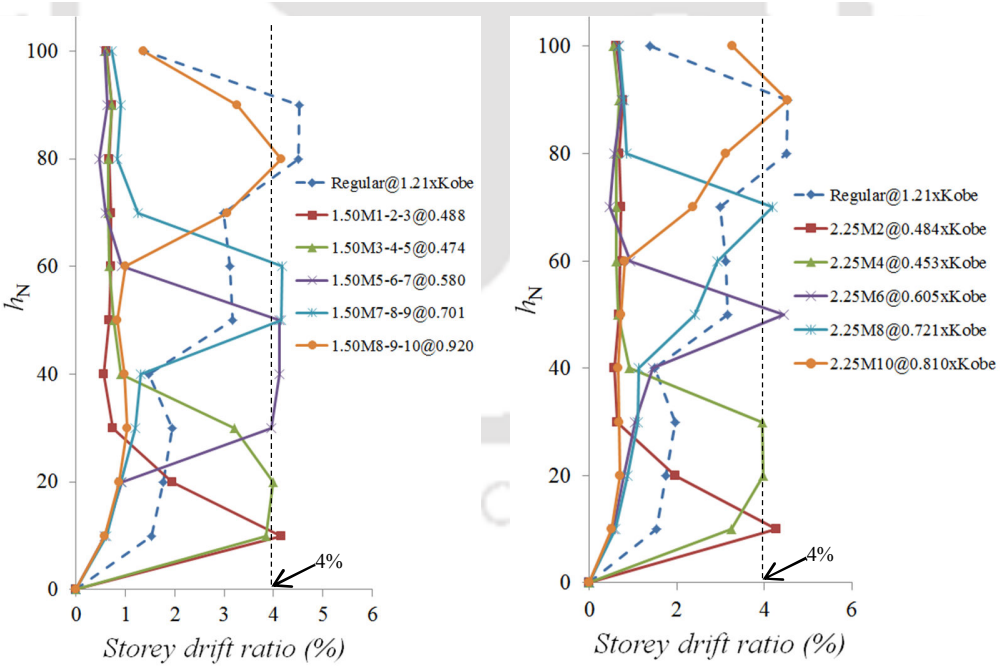

Figure 5.12: Storey drift ratio at collapse state for a) 150% consecutive triple floors mass irregular frames and b) 225% single floor mass irregular frames

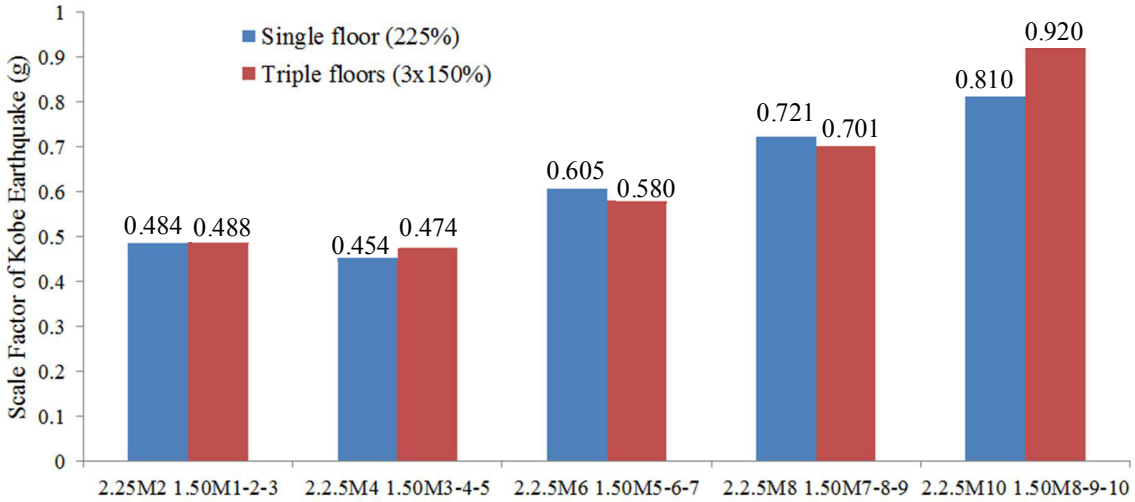

Figure 5.13: Comparison of criticality between 150% consecutive triple floors and 225% single floor mass irregular frames

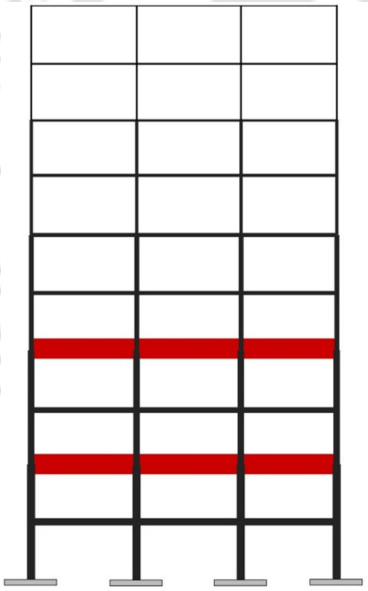

Frame configuration

Group 1:	**Group 2:**
1.50M**2**-4,	1.50M**4**-8,
1.50M**2**-6,	1.50M**4**-10,
1.50M**2**-8,	1.50M**6**-8,
1.50M**2**-10,	1.50M**6**-10,
1.50M**4**-6	1.50M**8**-10

Figure 5.14: Frame configuration for interaction study between mass irregular floors of equal intensity

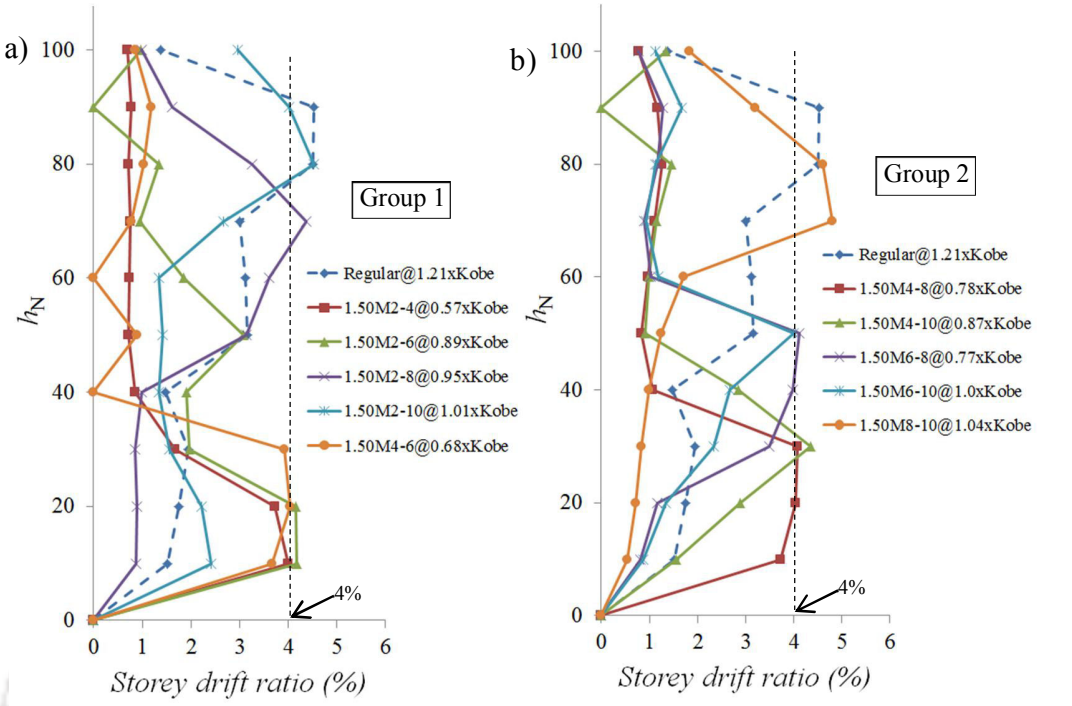

Figure 5.15: Storey drift ratio at collapse state for interaction study between mass irregular floors of equal intensity

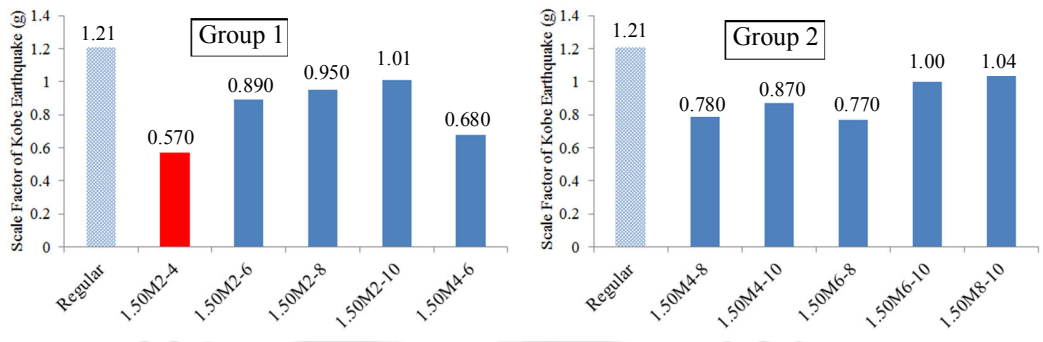

Figure 5.16: Bar charts of scale values at collapse state for interaction study between mass irregular floors of equal intensity

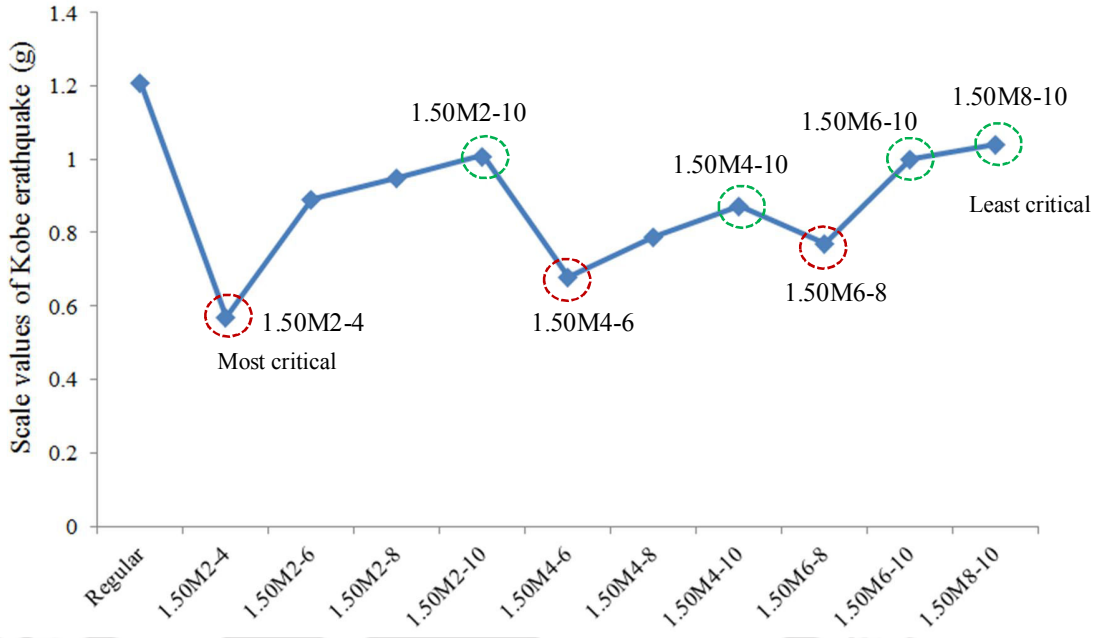

Figure 5.17: Criticality plot for interaction study between mass irregular floors of equal intensity

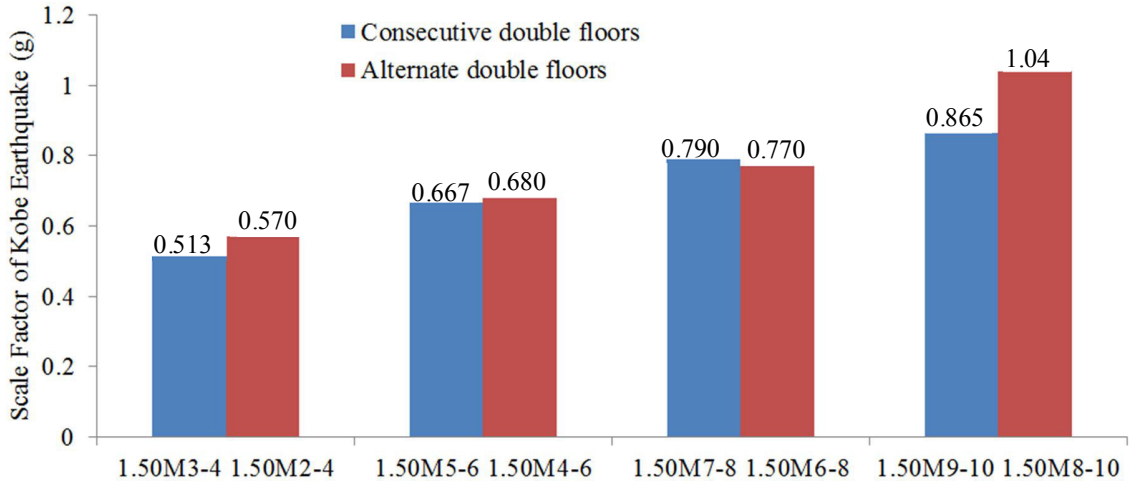

Figure 5.18: Comparison of criticality between consecutive double floors and non-consecutive double floors mass irregular frames

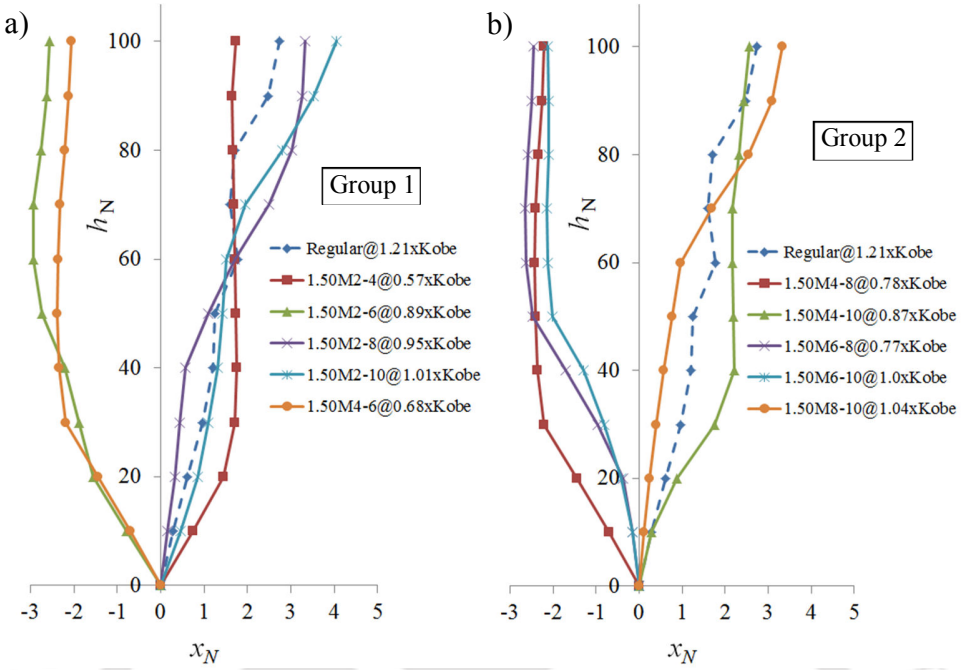

Figure 5.19: Maximum floor displacements at collapse state for interaction study between mass irregular floors of equal intensity

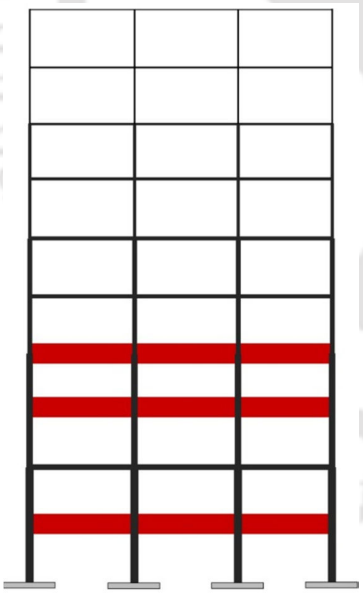

Frame configuration

Group 1:
1.50M1-**3-4**,
1.50M2-**3-4**,
1.50M**3-4**-5,
1.50M**3-4**-6

Group 2:
1.50M**3-4**-7,
1.50M**3-4**-8,
1.50M**3-4**-9,
1.50M**3-4**-10

Figure 5.20: Frame configuration for interaction study between mass irregular floors of unequal intensities

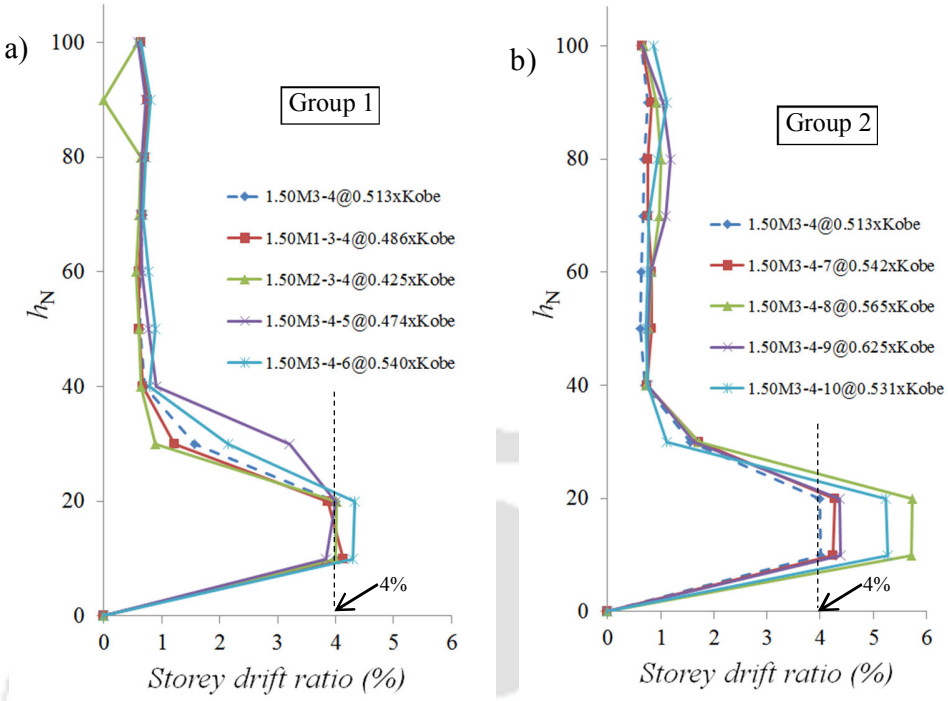

Figure 5.21: Storey drift ratio at collapse state for interaction study between mass irregular floors of unequal intensities

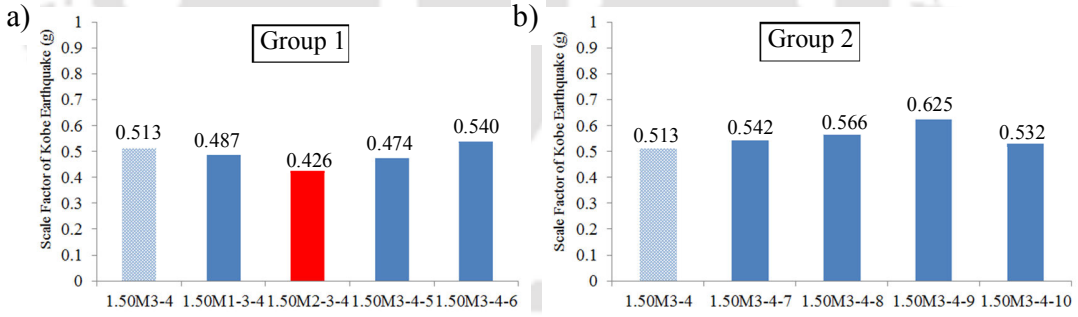

Figure 5.22: Bar charts of scale values at collapse state for interaction study between mass irregular floors of unequal intensities

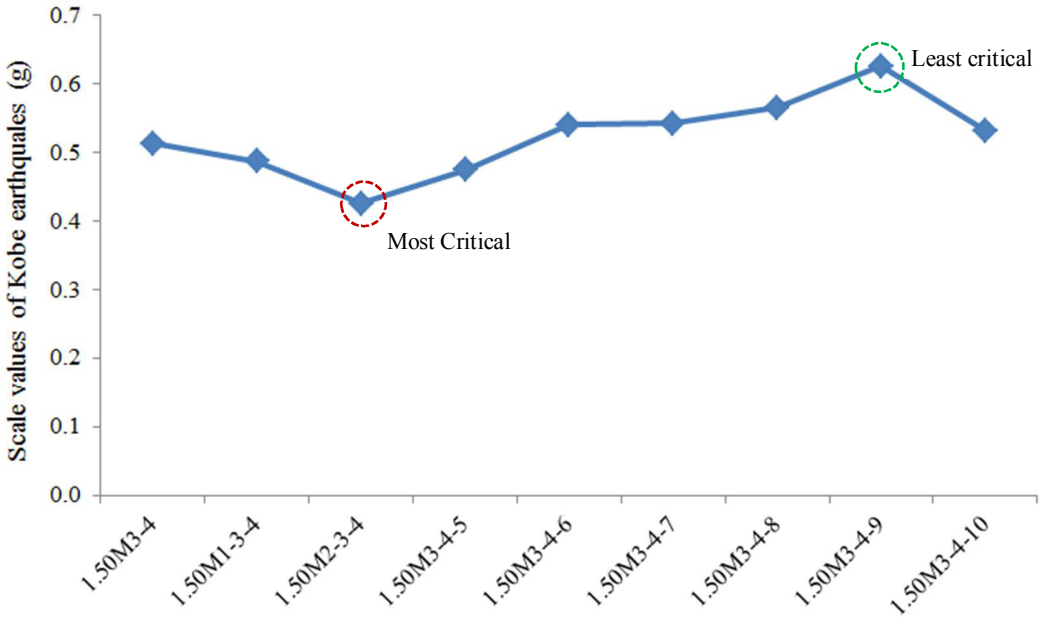

Figure 5.23: Criticality plot for interaction study between mass irregular floors of unequal intensities

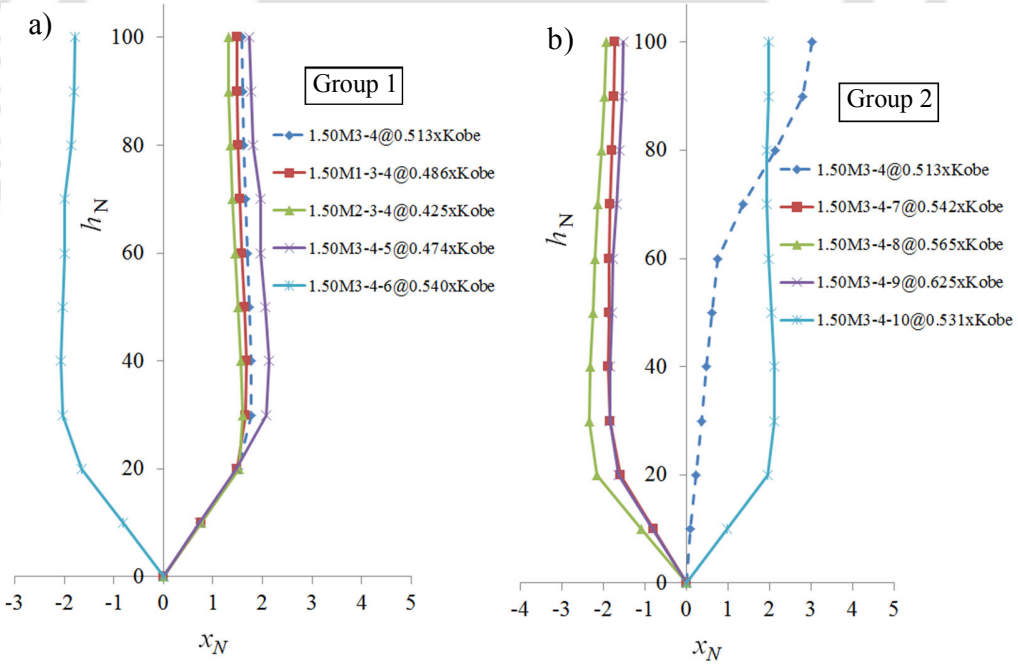

Figure 5.24: Maximum floor displacements at collapse state for interaction study between mass irregular floors of unequal intensities

CHAPTER 6

CONCLUSION

6.1 Introduction

In this thesis, a detailed systematic investigation on seismic behaviours of mass regular and mass irregular 2D multi-storied moment resisting steel frame has been performed by conducting Nonlinear Time History Analysis (NTHA) considering both material and geometric nonlinearities using Force Analogy Method (FAM). The thesis has been divided into six chapters. Chapter 1 represents a brief introduction on different methods of seismic analysis with their advantages and disadvantages. Chapter 2 shows a detailed literature review pertaining to Nonlinear Time History Analysis (NTHA) of moment resisting steel framed buildings. Chapter 3 consists of a detail systematic investigation on mass regular mid-rise (6, 8 and 10-storey) moment resisting steel frames by performing NTHA using implemented FAM code in Matlab, considering seven real earthquake acceleration records as input ground motions. The results are presented in the form of displacement-based (floor displacements, storey drift ratio) and energy-based (plastic energy) responses. Chapter 4 presents a parametric study of single floor mass irregular building frame to investigate the seismic behaviours of the irregular building frame when intensity as well as location of mass irregularity changes along the height of the building frame. Chapter 5 presents an extension of the single floor mass irregularity (Chapter 4) to multi-floor mass (double and triple floors) irregular building frames, considering two different location patterns *viz.* mass irregularities being located at i) consecutive floors, and ii) interaction of equal and unequal mass irregular floors. Chapter 6 represents the overall conclusions of the thesis. Based on the investigation the following chapter-wise conclusions are made.

6.2 Mass regular building frame (Chapter 3)

1. Elastic component of floor displacements has been observed to exhibit uniform (linear) variation and whereas inelastic component of floors' displacement has been found to exhibit non-uniform variation (i.e. maximum around 20% to 40% building height) along the building height.
2. Maximum amount of plastic energy has been found to dissipate at the location of maximum storey drift ratio along the building height.
3. Maximum seismic responses of the building frame has been observed when the input ground motion has critical characteristics like maximum PGA and PGV values, periods of ground excitation close to building fundamental period and large duration of strong motion.
4. For short period ground excitation, it has been observed that seismic response of the building frame is found to increase when the height of the building frame decreases; whereas the seismic response has been found to decrease when the height of the building frame decreases for long period ground excitation.
5. It has been observed in general that lower storey (e.g. 4^{th} storey of 10-storey steel frame) becomes critical at lower scale values (i.e. less than 1.0) of amplitude of ground motion based on IDA study; however the same storey may or may not be critical at upper scale values of amplitudes of ground motion.

6.3 Single floor mass irregular building frames (Chapter 4)

1. The criticality (i.e. becoming un-functional state by exceeding allowable storey drift ratio of 4% (ASCE 7, 2016) or dynamic instability/collapse) of single floor mass irregular frames may be related to the criticality of the storey levels in the reference regular frame.
2. It has been observed that single floor mass irregular frame is found to be the most critical when mass irregular floor is located at 40% building height, and

the criticality decreases as the location of single mass irregular floor moves away from the base towards the top of the building frame.

3. It has also been observed that maximum storey drift ratio or maximum floor displacement has been found to occur at the storey level just below the storey where mass irregular floor is located.
4. The criticality of single floor mass irregular frames has been found to increase as the intensity of mass irregularity increases, and the intensity of plastic energy dissipation has been found to concentrate only near the location of mass irregular floor.
5. Irregular frames of higher intensity of mass irregularity at lower storey levels (e.g. 2.25M2, 2.2.5M4) are found to be highly critical since they become collapse/dynamic instability immediately at the onset of nonlinear behaviour.

6.4 Multi-floor mass irregular building frames (Chapter 5)

1. As similar to single mass irregular frames, the criticality of multi-floor mass irregular frames become the most critical when mass irregular floors are located near 40% building height, and the criticality decreases as the location of multi-mass irregular floors moves away from the base towards the top of the building frame.
2. Mass irregular frame has been found to be less critical if the intensity of mass irregularity is distribution at adjacent floors instead of concentrating to a single floor at equivalent storey height.
3. Criticality of multi-floor mass irregular frame has been found to increase as the location of mass irregular floors approaches each other and vice-versa.
4. Criticality of multi-floor mass irregular frame has also been found to increase as the location of closely spaced mass irregular floors moves downwards along the building height and vice-versa.

6.5 Recommendation for future work

1. Analysis of mass irregular building frame can be extended by including different ranges of the building height to determine the effect of height on the seismic behaviours of mass irregular building frames.
2. Damping used for the dynamic analysis was restricted to Rayleigh-type damping. Other types of nonlinear damping model may be implemented to simulate more realistic behaviours of the building at the time of earthquake.
3. Elastic perfectly plastic behaviour of the steel member has been considered for simplicity in the thesis. More advanced nonlinear material behaviours of steel member with appropriate hysteric loops may be incorporated to give more realistic behaviours of steel frame buildings.
4. Only moment resisting frames are considered in the present work, so the analysis of mass irregularity can be extended to brace frame.
5. For simplicity rigid connection and rigid foundation are considered in the model, hence the model can be updated with semi-rigid connection and soil-structure interaction for foundation.

REFERENCES:

AGC. (2012). Avalon Garden City, https://archinect.com, Retrived in June 2019.

Akbas, B., Shen, J., & Hao, H. (2001). Energy approach in performance-based seismic design of steel moment resisting frames for basic safety objective. *Structural Design of Tall Buildings*, *10*, 193–217.

Antoniou, S., & Pinho, R. (2004). Advantages and limitations of adaptive and non-adaptive force-based pushover procedures. *Journal of Earthquake Engineering*, *2469*, 497–522.

ASCE 7-16. (2016). *Minimum design loads for buildings and other structures*. *ASCE standard*.

ASTM A6/A6M-07. (2007). *Standard Specification for General Requirements for Rolled Structural Steel Bars, Plates, Shapes, and Sheet Piling, ASTM International, West Conshohocken, PA, 2007*.

Chao, S.-H., & Loh, C.-H. (2007). Inelastic response analysis of reinforced concrete structures using modified force analogy method. *Earthquake Engineering and Structural Dynamics*, *36*, 1659–1683.

Choi, B. J. (2004). Hysteretic energy response of steel moment-resisting frames with vertical mass irregularities. *Structural Design of Tall and Special Buildings*, *13*, 123–144.

Chopra, A. K., & Goel, R. K. (2002). A modal pushover analysis procedure for estimating seismic demands for buildings. *Earthquake Engineering and Structural Dynamics*, *31*, 561–582.

Chou, C., & Uang, C. (2003). A procedure for evaluating seismic energy demand of framed structures. *Earthquake Engineering and Structural Dynamics*, *244*, 229–244.

Computers and Structures Inc. (2011). SAP2000, Integrated Software for Structural Analysis and Design. Berkeley, California.

Das, S., & Nau, J. M. (2003). Seismic Design Aspects of Vertically Irregular Reinforced Concrete Buildings. *Earthquake Spectra*, *19*, 455–477.

De Domenico, D., Falsone, G., & Ricciardi, G. (2018). Improved response-spectrum analysis of base-isolated buildings: A substructure-based response spectrum method. *Engineering Structures*, *162*, 198–212.

Di Cuia, A., Lombardi, L., De Luca, F., De Risi, R., Caprili, S., & Salvatore, W. (2017). Linear Time-History Analysis for EC8 design of CBF structures. *Procedia Engineering*, *199*, 3522–3527.

Domizio, M., Ambrosini, D., & Curadelli, O. (2015). Experimental and numerical analysis to collapse of a framed structure subjected to seismic loading. *Engineering Structures*, *82*, 22–32.

Eads, L., Miranda, E., Krawinkler, H., & Lignos, D. G. (2013). An efficient method for estimating the collapse risk of structures in seismic regions. *Earthquake Engineering and Structural Dynamics*, *42*, 25–41.

Eurocode 8. (2004). *Design of structures for earthquake resistance - Part 1: General rules, seismic actions and rules for buildings*.

FEMA-350. (2000). Recommended Seismic Design Critria for New Steel Moment-Frame Buildings Fema 350. *FEMA-350, Washington, DC*.

FEMA-356. (2000). Prestandard and Commentary for the Seismic Rehabilitation of Buildings. *FEMA-356, Washington, DC*.

Hariri-ardebili, M. A., Zarringhalam, Y., Estekanchi, H. E., & Yahyai, M. (2013). Nonlinear seismic assessment of steel moment frames using time-history , incremental dynamic , and endurance time analysis methods. *Scientia Iranica*, *20*, 431–444.

ICC. (2000). International Building Code.

IS 1893 (Part 1). (2016). *Criteria for Earthquake Resistant Design of Structures*. *Bureau of Indian Standards*.

Kalkan, E., & Kunnath, S. K. (2004). Method of modal combinations for pushover analysis of buildings. In *13 th World Conference on Earthquake Engineering, August 1-6, Vancouver, B.C., Canada*.

Kalkan, E., & Kunnath, S. K. (2006). Adaptive Modal Combination Procedure for Nonlinear Static Analysis of Building Structures. *Journal of Structural Engineering*, *132*, 1721–1731.

Karavasilis, T. L., Bazeos, N., & Beskos, D. E. (2008). Estimation of seismic inelastic deformation demands in plane steel MRF with vertical mass irregularities. *Engineering Structures*, *30*, 3265–3275.

Kim, K. D., & Engelhardt, M. D. (2005). Beam-Column Element for Nonlinear Seismic Analysis of Steel Frames. *Journal of Structural Engineering*, *131*, 715–724.

Krawinkler, H., & Seneviratna, G. D. P. K. (1998). Pros and cons of a pushover analysis of seismic performance evaluation. *Engineering Structures*, *20*, 452–464.

Krishnan, S., Ji, C., Komatitsch, D., & Tromp, J. (2006). Performance of Two 18-Story Steel Moment-Frame Buildings in Southern California During Two Large Simulated San Andreas Earthquakes. *Earthquake Spectra*, *22*, 1035–1061.

Krishnan, S., & Muto, M. (2013). Sensitivity of the Earthquake Response of Tall Steel Moment Frame Buildings to Ground Motion Features. *Journal of Earthquake Engineering*, *17*, 673–698.

Le-Trung, K., Lee, K., Lee, J., & Lee, D. H. (2012). Evaluation of seismic behaviour of steel special moment frame buildings with vertical irregularities. *The Structural Design of Tall and Special Buildings*, *21*, 215–232.

Li, G., & Li, H.-N. (2011). Seismic response analysis of structure with energy dissipation devices using force analogy method. *The Structural Design of Tall and Special Buildings*, *20*, 291–313.

Li, G., & Wong, K. K. F. (2014). *Theory of Nonlinear Structural Analysis : The Force Analogy Method for Earthquake Engineering*. John Wiley & Sons, Singapore Pte. Ltd.

Li, G., Yu, Z., & Hong-Nan, L. (2014). Nonlinear Seismic Analysis of Reinforced Concrete Bridges Using the Force Analogy Method. *Journal of Bridge Engineering*, *20*, 1–12.

Li, G., Zhang, F., Zhang, Y., & Li, H.-N. (2015). Nonlinear hysteretic behavior simulation of reinforced shear walls using the force analogy method. *The Structural Design of Tall and Special Buildings*, *24*, 504–520.

Li, G., Zhang, Y., & Li, H.-N. (2014). Nonlinear seismic analysis of reinforced concrete frames using the force analogy method. *Earthquake Engineering & Structural Dynamics*, *43*, 2115–2134.

Li, G., Zhang, Y., & Li, H. (2013). Seismic Damage Analysis of Reinforced Concrete Frame

Using the Force Analogy Method. *Journal of Engineering Mechanics*, *139*, 1780–1789.

Lin, T. H. (1968). *Theory of Inelastic Structures*. Wiley, New York.

Liu, S. W., Bai, R., & Chan, S. L. (2016). Dynamic Time-history Elastic Analysis of Steel Frames Using One Element per Member. *Structures*, *8*, 300–309.

Mahin, S. A., & Bertero, V. V. (1981). An evaluation of inelastic seismic design spectra. *Journal of the Structural Division*, *107*, 1777–1795.

Meyer, C. (1974). Inelastic dynamic analysis of tall buildings. *Earthquake Engineering and Structural Dynamics*, *2*, 325–342.

Mokarram, V., & Banan, M. R. (2018). An improved multi-objective optimization approach for performance-based design of structures using nonlinear time-history analyses. *Applied Soft Computing Journal*, *73*, 647–665.

Moschen, L., Adam, C., & Vamvatsikos, D. (2016). A response spectrum method for peak floor acceleration demands in earthquake excited structures. *Probabilistic Engineering Mechanics*, *46*, 94–106.

Mulas, M. G. (2004). A structural model for panel zones in non linear seismic analysis of steel moment-resisting frames. *Engineering Structures*, *26*, 363–380.

Pang, M., & Wong, K. K. F. (2006). Predictive instantaneous optimal control of inelastic structures based on ground velocity. *Structural Design of Tall and Special Buildings*, *15*, 307–324.

Papanikolaou, V. K., Elnashai, A. S., & Pareja, J. F. (2005). *Limits of applicability of conventional and adaptive pushover analysis for seismic response assessment*. Mid-America Earthquake Center, University of Illinois at Urbana-Champaign.

Pinho, R. U. I., Antoniou, S., Casarotti, C., & Lopez, M. (2006). A displacement-based adaptive pushover for assessment of buildings and bridges. In *Advances in Earthquake Engineering for Urban Risk Reduction* (pp. 79–94).

Pirizadeh, M., & Shakib, H. (2013). Probabilistic seismic performance evaluation of non-geometric vertically irregular steel buildings. *Journal of Constructional Steel Research*, *82*, 88–98.

Sucuoğlu, H., & Nurtuğ, A. (1995). Earthquake ground motion characteristics and seismic energy dissipation. *Earthquake Engineering & Structural Dynamics*, *24*, 1195–1213.

SW. (2019). Spacewizard.in, Retrived in June 2019.

The MathWorks Inc. (2012). MATLAB R2012b. Natick, Massachusetts, United States.

Tremblay, R., & Poncet, L. (2005). Seismic Performance of Concentrically Braced Steel Frames in Multistory Buildings with Mass Irregularity. *Journal of Structural Engineering*, *131*, 1363–1375.

Uang, C., Yu, Q.-S., Sadre, A., Bonowitz, D., Youssef, N., & Vinkler, J. (1997). Siesmic Responses of an Instrumented 13-Story Steel Frame Building Damaged in the 1994 Northridge Earthquake. *Earthquake Spectra*, *13*, 131–149.

UBC. (1997). Uniform Building Code. In *International Conference of Building Official*. Whittier, California, 1997.

Valmundsson, E. V., & Nau, J. M. (1997). Seismic Response of Building Frames with Vertical Structural Irregularities. *Journal of Structural Engineering*, *123*, 30–41.

Vamvatsikos, D., & Allin Cornell, C. (2002). Incremental dynamic analysis. *Earthquake*

Engineering and Structural Dynamics, *31*, 491–514.

Varadharajan, S., Sehgal, V. K., & Saini, B. (2014). Seismic response of multistory reinforced concrete frame with vertical mass and stiffness irregularities. *The Structural Design of Tall and Special Buildings*, *23*, 362–389.

VDC. (2012). Strong-Motion Virtual Data Center, http://strongmotioncenter.org/vdc/scripts/default.plx.

Ventura, C. E., & Ding, Y. (2000). Linear and Nonlinear Seismic Response of a 52-Storey Steel Frame Building. *The Structural Design of Tall and Special Buildings*, *45*, 25–45.

Wilkinson, S. M., & Hiley, R. A. (2006). A non-linear response history model for the seismic analysis of high-rise framed buildings. *Computers and Structures*, *84*, 318–329.

Wong, K K F. (2008). Seismic Energy Dissipation of Inelastic Structures with Tuned Mass Dampers. *Journal of Engineering Mechanics*, *134*, 163–172.

Wong, Kevin K. F., & Zhao, D. (2007). Uncoupling of Potential Energy in Nonlinear Seismic Analysis of Framed Structures. *Journal of Engineering Mechanics*, *133*, 1061–1071.

Wong, Kevin K F. (2005). Predictive Optimal Linear Control of Elastic Structures during Earthquake. Part II. *Journal of Engineering Mechanics*, *131*, 142–152.

Wong, Kevin K F. (2011). Seismic energy analysis of structures with nonlinear fluid viscous dampers-algorithm and numerical verification. *The Structural Design of Tall and Special Buildings*, *20*, 482–496.

Wong, Kevin K F. (2014). A new analytical method for solving nonlinear stability problems of framed structures. In *Proceedings of the Annual Stability Conference Structural Stability Research Council*. Toronto, Canada, March 25-28, 2014.

Wong, Kevin K F, & Johnson, J. (2009). Seismic Energy Dissipation of Inelastic Structures with Multiple Tuned Mass Dampers. *Journal of Engineering Mechanics*, *135*, 265–275.

Wong, Kevin K F, & Speicher, M. S. (2015). Dynamic effects of geometric nonlinearity on inelastic frame behavior for seismic applications. In *Proceedings of the Annual Stability Conference Structural Stability Research Council*. Nashville, Tennessee, March 24-27, 2015.

Wong, Kevin K F, & Wang, Y. (2003). Energy-based design of structures using modified force analogy method. *Structural Design of Tall and Special Buildings*, *12*, 393–407.

Wong, Kevin K F, & Wang, Z. H. E. (2007a). Seismic analysis of inelastic moment-resisting frames part I: Modified force analogy method for end offsets. *Structural Design of Tall and Special Buildings*, *16*, 267–282.

Wong, Kevin K F, & Wang, Z. H. E. (2007b). Seismic analysis of inelastic moment-resisting frames part II: Energy dissipation in deformable panel zones. *Structural Design of Tall and Special Buildings*, *16*, 283–299.

Wong, Kevin K F, & Yang, R. (1999). Inelastic dynamic response of structures using force analogy method. *Journal of Engineering Mechanics*, *125*, 1190–1199.

Wong, Kevin K F, & Yang, R. (2002). Earthquake Response and Energy Evaluation of Inelastic Structures. *Journal of Engineering Mechanics*, *128*, 308–317.

Zareian, F., & Krawinkler, H. (2010). Structural System Parameter Selection Based on Collapse Potential of Buildings in Earthquakes. *Journal of Structural Engineering*, *136*, 933–943.

Zareian, F., Krawinkler, H., Ibarra, L., & Lignos, D. (2010). Basic Concepts and Performance Measures in Prediction of Collapse of Buildings under Earthquake Ground Motions. *The Structural Design of Tall and Special Buildings*, *181*, 167–181.

Zhang, X., Wong, K. K. F., & Wang, Y. (2007). Performance assessment of moment resisting frames during earthquakes based on the force analogy method. *Engineering Structures*, *29*, 2792–2802.

Zhao, D., & Wong, K. K. F. (2006). New Approach for Seismic Nonlinear Analysis of Inelastic Framed Structures. *Journal of Engineering Mechanics*, *132*, 959–966.

APPENDIX A

FORCE ANALOGY METHOD

A.1 Introduction

The Force Analogy Method (FAM) is an algorithm to study the inelastic behaviour of structural system using only the initial stiffness matrix. It was proposed by Wong and Yang in 1999. The algorithm is based on inelastic displacement concept proposed by Lin in 1968 where inelastic behaviour of structural member is determined by changing the structural displacement field which is different from the conventional method of changing stiffness. Lin used this inelastic displacement concept for the application of stress and strain in continuum mechanics where the inelastic behaviour was defined by plastic strain. In FAM, all the inelastic behaviours of the structural system are represented by a single equation since each inelastic deformation of the structure is considered as a degree of freedom in the formulation.

A.2 Nonlinear static analysis in FAM

The concept of inelastic displacement in FAM can be briefly described with the help of Figure A.1.

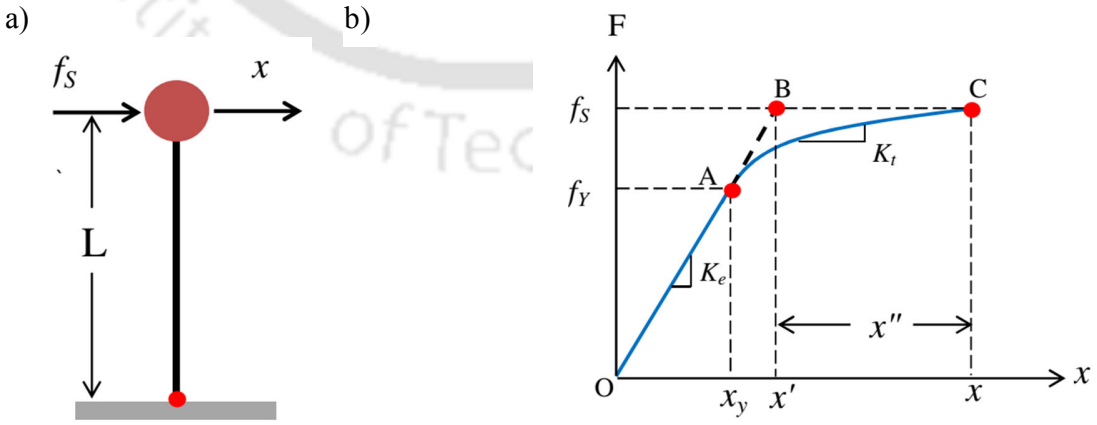

Figure A.1 (a) Single degree of freedom (SDOF) system and (b) force-displacement relationship

Figure A.1a indicates an SDOF system where a static force (f_S) is applied only in the degree of freedom (DOF) x. Figure A.1b indicates force versus displacement relationship where K_e denotes the initial elastic stiffness and K_t denotes the varying post-yield stiffness. The lateral deformation (x) of SDOF system is represented by point C. The basic concept of FAM is to extend the initial stiffness line OA until it reaches the force f_S level at point B. The displacement corresponding to point B is defined as elastic displacement (x') and the difference between the total displacement (x) and elastic displacement (x') is defined as the inelastic displacement (x''). Hence,

$$x = x' + x'' \Rightarrow x' = x - x'' \qquad (A.1)$$

Force in the system (f_S) at any displacement (x) is given by

$$f_S = K_e x' \qquad (A.2)$$

In elastic range (i.e. $x \leq x_y$),

$$f_S = K_e x' = K_e(x - x'') = K_e(x - 0) = K_e x \qquad (A.3)$$

Whereas, in inelastic range (i.e. $x > x_y$),

$$f_S = K_e x' = K_e(x - x'') \qquad (A.4)$$

Application of FAM on SDOF system can be described with the help of Figures A.2 and A.3

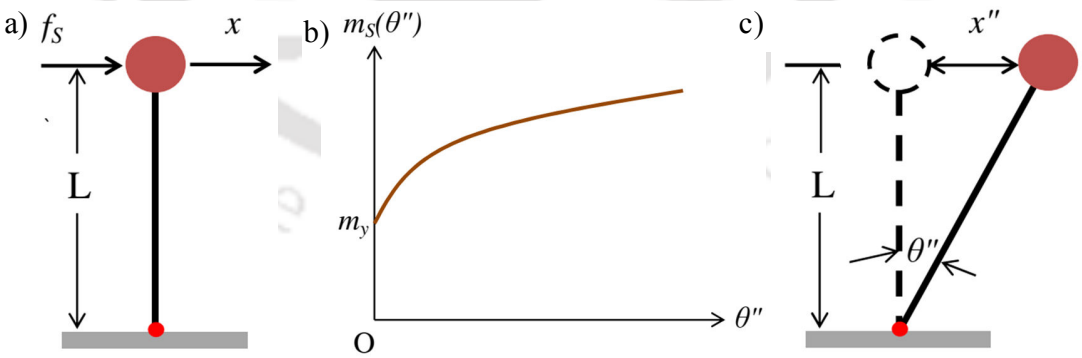

Figure A.2: Framework of the FAM: (a) SDOF system, (b) moment-plastic rotation relationship and (c) plastic rotation-inelastic displacement relationship

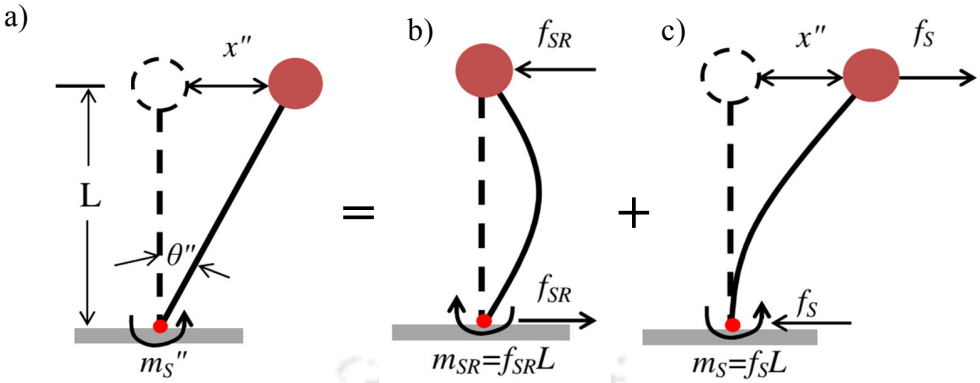

Figure A.3: Framework of the FAM: (a) plastic rotation-inelastic displacement relationship, (b) force apply to satisfy compatibility condition and (c) equivalent force applied to satisfy equilibrium condition

The displacement and moment relationships for an SDOF system with a single plastic location (PHL) based on FAM are

$$x = x' + x'' \tag{A.5}$$

$$m_S = m_S' + m_S'' \tag{A.6}$$

Considering purely inelastic behaviour (i.e. plastic rotation occurs after the load is removed), as shown in Figure A.3a, is separated into two parts (Figures A.3b and A.3c). In Figure A.3b, a restoring force f_{SR} is applied on the column to give a zero displacement to restore back the column into its original position as if the column is connected to other parts of the structure in a multi-degree-of-freedom system. Applying restoring force f_{SR} would result in satisfying the compatibility condition. This applied restoring force is given by

$$f_{SR} = -\left(\frac{3EI}{L^2}\right)\theta'' = K'\theta'' \tag{A.7}$$

$$m_{SR} = -f_{SR}L = -\left(\frac{3EI}{L}\right)\theta'' = -K''\theta'' \tag{A.8}$$

Where K' denotes the stiffness that relates the plastic rotation (θ'') with the restoring force (f_{SR}) and K'' denotes the stiffness that relates the plastic rotation (θ'') with the residual moment (m_{SR}). Since f_{SR} is not present actually and hence equal and opposite force f_S must be applied to satisfy equilibrium condition as shown in Figure A.3c.

$$f_S = -f_{SR} = \left(\frac{3EI}{L^2}\right)\theta'' = K'\theta'' \tag{A.9}$$

Also by traditional stiffness method of structural analysis in Figure A.3c,

$$f_S = \left(\frac{3EI}{L^3}\right)x'' = Kx'' \tag{A.10}$$

Where, K is the global stiffness matrix of the structure. Equating f_S in Equations A.9 and A.10 we have,

$$x'' = L\theta'' \tag{A.11}$$

This is the kinematic relation between inelastic displacement (x'') and plastic rotation (θ''). In addition, applying the equivalent force f_S causes induced moment m_S at the PHL.

$$m_S = Lf_S = \left(\frac{3EI}{L}\right)\theta'' \tag{A.12}$$

Inelastic moment (m_S'') shown in Figure A.3a can be computed as

$$m_S'' = m_{SR} + m_S = -\left(\frac{3EI}{L}\right)\theta'' + \left(\frac{3EI}{L}\right)\theta'' = 0 \tag{A.13}$$

This means that plastic rotation (θ'') will not induce any inelastic moment (m_S'') on this column since the column is free to displace laterally.

A relationship can be obtained between the elastic moment (m_S'), the elastic displacement (x') and the external applied force (f_S) as

$$f_S = Kx' = \left(\frac{3EI}{L^3}\right)x' = \left(\frac{3EI}{L^3}\right)[x - x''] = \left(\frac{3EI}{L^3}\right)[x - L\theta''] \tag{A.14}$$

$$m_S' = K'x' = \left(\frac{3EI}{L^2}\right)x' = \left(\frac{3EI}{L^2}\right)[x - x''] = \left(\frac{3EI}{L^2}\right)[x - L\theta''] \tag{A.15}$$

Simplifying equation A.14 gives the first governing equation of FAM as

$$\left(\frac{3EI}{L^3}\right)x-\left(\frac{3EI}{L^2}\right)\theta''=f_S \tag{A.16}$$

Also,

$$m_S=m_S'+m_S''=m_S'+0=m_S'$$
$$\Rightarrow\left(\frac{3EI}{L^2}\right)x-\left(\frac{3EI}{L}\right)\theta''=m_S \tag{A.17}$$

Equation A.17 is the second governing equation of FAM. Representing the governing equations of FAM in matrix form as

$$\begin{bmatrix}\frac{3EI}{L^3} & \frac{3EI}{L^2}\\ \frac{3EI}{L^2} & \frac{3EI}{L}\end{bmatrix}\begin{Bmatrix}x\\ -\theta''\end{Bmatrix}=\begin{Bmatrix}f_S\\ m_S\end{Bmatrix}$$
$$\Rightarrow\begin{bmatrix}K & K'\\ K' & K''\end{bmatrix}\begin{Bmatrix}x\\ -\theta''\end{Bmatrix}=\begin{Bmatrix}f_S\\ m_S\end{Bmatrix} \tag{A.18}$$

A.3 Dynamic analysis in FAM with material nonlinearity

For a moment-resisting frame with *n* Degrees Of Freedoms (DOFs) and *p* Plastic Hinge Locations (PHLs), the total displacement *x(t)* at each DOF is given by the summation of elastic displacement *x′(t)* and inelastic displacement *x″(t)*

$$x(t)=x'(t)+x''(t) \tag{A.19}$$

Similarly, the total moment, $m_S(t)$ at Plastic Hinge Location (PHL) is given by the summation of elastic moment $m_S'(t)$ due to elastic displacement *x′(t)* and inelastic (residual) moment $m_S''(t)$ due to inelastic displacement *x″(t)*.

$$m_S(t)=m_S'(t)+m_S''(t) \tag{A.20}$$

The displacements in Equation (A.19) and moments in Equation (A.20) are inter-related by the following expressions (Wong and Speicher, 2015):

$$m'(t) = K'(t)^T x'(t) \tag{A.21}$$

$$m''(t) = -[K''(t) - K'(t)^T K(t)^{-1} K'(t)]\theta''(t) \tag{A.22}$$

where, $K(t)$ is $n \times n$ global stiffness matrix, $K'(t)$ is $n \times p$ stiffness matrix formed by relating plastic rotations at the PHLs with the restoring forces at the DOFs, $K''(t)$ is the $p \times p$ stiffness matrix formed by relating plastic rotations with corresponding residual moments at the PHLs and $\theta''(t)$ is the plastic rotation at each PHL.

Putting Equations (A.21) and (A.22) into Equation (A.20) and rearranging the terms gives the first governing of FAM for dynamic analysis as:

$$m_S(t) = K'(t)^T x(t) - K''(t)\theta''(t) \tag{A.23}$$

The second governing equation of FAM relates the inelastic displacements $x''(t)$ with the plastic rotation $\theta''(t)$ as:

$$x''(t) = K(t)^{-1} K'(t)\theta''(t) \tag{A.24}$$

A.4 Geometric nonlinearity in FAM

In FAM, the stiffness force in equation of motion is calculated by multiplying the stiffness matrix $K(t)$ with the elastic displacement $x'(t)$. For an n-DOFs system, the equation of motion subjected to earthquake ground motions can be expressed as

$$M\ddot{x}(t) + C\dot{x}(t) + K(t)x'(t) = -M\ddot{g}(t) - F_a(t) \tag{A.25}$$

where, M is $n \times n$ invertible mass matrix, C is $n \times n$ damping matrix, $\dot{x}(t)$ is $n \times 1$ velocity vector, $\ddot{x}(t)$ is $n \times 1$ acceleration vector, $\ddot{g}(t)$ is $n \times 1$ earthquake ground acceleration vector, and $F_a(t)$ is $n \times 1$ additional force vector imposed on the frame due to geometric nonlinearity (mainly due to P-Δ effect). The relationship between this additional force vector $F_a(t)$ and the lateral displacement vector $x(t)$ can be expressed as:

$$F_a(t) = K_a x(t) \tag{A.26}$$

where, K_a is $n \times n$ stiffness matrix which is a function of the gravity loads on the leaning column and the corresponding storey height but not a function of time. For a

two-dimensional structural frame with horizontal degrees of freedom only, K_a matrix usually takes the form:

$$K_a = \begin{bmatrix} -Q_1/h_1 - Q_2/h_2 & Q_2/h_2 & 0 & \cdots & 0 \\ Q_2/h_2 & -Q_2/h_2 - Q_3/h_2 & \ddots & \ddots & \vdots \\ 0 & \ddots & \ddots & Q_{n-1}/h_{n-1} & 0 \\ \vdots & \ddots & Q_{n-1}/h_{n-1} & -Q_{n-1}/h_{n-1} - Q_n/h_n & Q_n/h_n \\ 0 & \cdots & 0 & Q_n/h_n & -Q_n/h_n \end{bmatrix} \quad (A.27)$$

where Q_i and h_i are the axial force due to gravity on the leaning column and storey height of the ith floor respectively.

The stiffness matrix $K(t)$ in Equation (A. 25) considers both large P-Δ and small P-Δ effects and it can be represented as:

$$K(t) = K_L + K_G(t) \quad (A.28)$$

where, K_L denotes the elastic stiffness matrix due to the gravity loads only, and $K_G(t)$ denotes the stiffness matrix which changes as the axial load on members changes at the time of earthquake loading. Here the elastic stiffness matrix K_L is constant which is computed once at the initial time of analysis and it can be used throughout the entire nonlinear time history analysis without any changes. This becomes one of the advantages of using Force Analogy Method in structural dynamics.

A.5 Static condensation for state space dynamic analysis

Consider a moment-resisting frame with n DOFs and p PHLs as presented in Equation (A. 25), the equation of motion can be partitioned in the matrix form as

$$\left[\begin{array}{c|c} M_{dd} & 0 \\ \hline 0 & 0 \end{array}\right] \left\{\begin{array}{c} \ddot{x}_d(t) \\ \hline \ddot{x}_r(t) \end{array}\right\} + \left[\begin{array}{c|c} C_{dd} & 0 \\ \hline 0 & 0 \end{array}\right] \left\{\begin{array}{c} \dot{x}_d(t) \\ \hline \dot{x}_r(t) \end{array}\right\} + \left[\begin{array}{c|c} K_{dd}(t) & K_{dr}(t) \\ \hline K_{rd}(t) & K_{rr}(t) \end{array}\right] \left\{\begin{array}{c} x_d'(t) \\ \hline x_r'(t) \end{array}\right\} \quad (A.29)$$

$$= -\left[\begin{array}{c|c} M_{dd} & 0 \\ \hline 0 & 0 \end{array}\right] \left\{\begin{array}{c} \ddot{g}_d(t) \\ \hline 0 \end{array}\right\} - \left\{\begin{array}{c} F_a(t) \\ \hline 0 \end{array}\right\}$$

where M_{dd} and C_{dd} are the mass and damping matrices respectively associated with translational DOFs with mass only, whereas $K_{dd}(t)$, $K_{dr}(t)$, $K_{rd}(t)$ and $K_{rr}(t)$ are the stiffness sub-matrices partitioned according to the DOFs with mass and those with zero mass.

The governing equations of the FAM presented in Equations (A. 23) and (A. 24) can similarly be partitioned as follows:

$$m(t) + K''(t)\theta''(t) = \begin{bmatrix} K_d'(t)^T & K_r'(t)^T \end{bmatrix} \begin{Bmatrix} x_d(t) \\ x_r(t) \end{Bmatrix} \tag{A.30}$$

$$\begin{Bmatrix} x_d''(t) \\ x_r''(t) \end{Bmatrix} = \begin{bmatrix} K_{dd}(t) & K_{dr}(t) \\ K_{rd}(t) & K_{rr}(t) \end{bmatrix}^{-1} \begin{bmatrix} K_d'(t) \\ K_r'(t) \end{bmatrix} \theta''(t) \tag{A.31}$$

A.6 State space methods in FAM for nonlinear dynamic analysis

After applying static condensation to eliminate those DOFs associated with zero mass moment of inertia, the governing equations for nonlinear dynamic analysis with the FAM presented in Equations (A. 23), (A. 24) and (A. 25) are rewritten as (Wong and Speicher, 2015):

$$m(t) + \bar{K}''(t)\theta''(t) = \bar{K}'(t)^T x_d(t) \tag{A.32}$$

$$x_d''(t) = \bar{K}(t)^{-1} \bar{K}'(t)\theta''(t) \tag{A.33}$$

$$M_{dd}\ddot{x}_d(t) + C_{dd}\dot{x}_d(t) + \bar{K}(t)x_d'(t) = -M_{dd}\ddot{g}_d(t) - F_a(t) \tag{A.34}$$

where,

$$\bar{K}(t) = K_{dd}(t) - K_{dr}(t)K_{rr}^{-1}(t)K_{rd}(t) \tag{A.35a}$$

$$\bar{K}'(t) = K_d'(t) - K_{dr}(t)K_{rr}^{-1}(t)K_r'(t) \tag{A.35b}$$

$$\bar{K}''(t) = K''(t) - K_r'(t)^T K_{rr}^{-1}(t)K_r'(t) \tag{A.35c}$$

and Equations (A. 26) and (A. 28) can be written as:

$$F_a(t) = K_a x_d(t), \qquad \bar{K}(t) = \bar{K}_L + \bar{K}_G(t) \tag{A.36}$$

Now Equation (A. 35) can be rewritten as:

$$M_{dd}\ddot{x}_d(t)+C_{dd}\dot{x}_d(t)+\bar{K}(t)[x_d(t)-x_d"(t)]=-M_{dd}\ddot{g}_d(t)-F_a(t)$$
$$\Rightarrow M_{dd}\ddot{x}_d(t)+C_{dd}\dot{x}_d(t)+\bar{K}(t)x_d(t)=-M_{dd}\ddot{g}_d(t)-F_a(t)+\bar{K}(t)x_d"(t) \quad (A.37)$$

Substituting Equation (A. 36) into Equation (A. 37), the equation of motion considering both large P-Δ and small P-δ effects of geometric nonlinearity of the whole structure becomes

$$M_{dd}\ddot{x}_d(t)+C_{dd}\dot{x}_d(t)+\bar{K}_L x_d(t)=-M_{dd}\ddot{g}_d(t)-K_a x_d(t)-\bar{K}_G(t)x_d(t)+\bar{K}(t)x_d"(t) \quad (A.38)$$

Let us define

$$\bar{K}_e=\bar{K}_L+K_a \quad (A.39)$$

where $\bar{K}_e$ represents the elastic stiffness of the whole structure, which is the sum of the linearized elastic stiffness $\bar{K}_L$ of the frame only and the additional stiffness K_a induced by the gravity columns. Substituting Equation (A. 39) into Equation (A. 38), it follows

$$M_{dd}\ddot{x}_d(t)+C_{dd}\dot{x}_d(t)+\bar{K}_e x_d(t)=-M_{dd}\ddot{g}_d(t)-\bar{K}_G(t)x_d(t)+\bar{K}(t)x_d"(t) \quad (A.40)$$

Material nonlinearity term $[\bar{K}(t)x_d"(t)]$ and geometric nonlinearity term $[-\bar{K}_G(t)x_d(t)]$ on the right hand side of Equation (A. 40) can be considered as the equivalent forces applied on the structures. The Equation (A. 40) can now be solved by using state space method as:

$$z(t)=\begin{Bmatrix} x_d(t) \\ \dot{x}_d(t) \end{Bmatrix} \quad (A.41)$$

$$\dot{z}(t)=\begin{Bmatrix} \dot{x}_d(t) \\ \ddot{x}_d(t) \end{Bmatrix}=\begin{bmatrix} 0 & I \\ -M_{dd}^{-1}\bar{K}_e & -M_{dd}^{-1}C_{dd} \end{bmatrix}\begin{Bmatrix} x_d(t) \\ \dot{x}_d(t) \end{Bmatrix}+\begin{bmatrix} 0 \\ j \end{bmatrix}a(t)$$

$$+\begin{bmatrix} 0 \\ M_{dd}^{-1} \end{bmatrix}\{\bar{K}(t)x_d''(t) - \bar{K}_G(t)x_d(t)\} \tag{A.42}$$

where j is an n×3 matrix which relates with the directions of each DOF with the global X-, Y-, and Z- directions, and $a(t)$ is the 3×1 input ground motion vector in the three global directions. The relationship between the input ground motion vector $\ddot{g}_d(t)$ for each DOF in Equation (A. 36) and the three-components input ground motion vector $a(t)$ can be expressed as

$$\ddot{g}_d(t) = ja(t) = j\begin{Bmatrix} \ddot{g}_X(t) \\ \ddot{g}_Y(t) \\ \ddot{g}_Z(t) \end{Bmatrix} \tag{A.43}$$

Let,

$$A = \begin{bmatrix} 0 & I \\ -M_{dd}^{-1}\bar{K}_e & -M_{dd}^{-1}C_{dd} \end{bmatrix}, \quad J = \begin{bmatrix} 0 \\ -j \end{bmatrix}, \quad B = \begin{bmatrix} 0 \\ -M_{dd}^{-1} \end{bmatrix}$$

$$f_G(t) = -\bar{K}_G(t)x_d(t), \quad f_M(t) = -\bar{K}(t)x_d''(t) \tag{A.44}$$

where A is the $2d \times 2d$ state transition matrix, J is the $2d \times 3$ ground motion transition matrix, B is the $2d \times d$ nonlinear transition matrix, all transition matrices are in the continuous form. $f_G(t)$ and $f_M(t)$ are the $d \times 1$ equivalent force vectors due to geometric and material nonlinearities respectively. Now Equation (A. 42) can be represented as

$$\dot{z}(t) = Az(t) + Ja(t) + Bf_G(t) + Bf_M(t) \tag{A.45}$$

Solving the first-order linear differential Equation (A. 45) gives

$$\dot{z}(t) = e^{A(t-t_0)}z(t_0) + e^{At}\int_{t_0}^{t} e^{-As}[Ja(s) + Bf_G(s) + Bf_M(s)]ds \tag{A.46}$$

To integrate Equation (A. 46) numerically, let $t_{k+1} = t$, $t_k = t_0$ and $\Delta t = t_{k+1} - t_k$, where the subscript k denotes the k^{th} time step, Equation (A. 46) becomes

$$z_{k+1} = e^{A\Delta t}z_k + e^{At_{k+1}}\int_{t_k}^{t_{k+1}} e^{-As}[Ja(s) + Bf_G(s) + Bf_M(s)]ds \tag{A.47}$$

Using delta function approximation for the variables in the integral $a(s)$, $f_G(s)$, and $f_M(s)$ take the form

$$a(s) = a_k \delta(s - t_k)\Delta t, \quad t_k \le s \le t_{k+1} \tag{A .48 a}$$

$$f_G(s) = f_{G,k} \delta(s - t_k)\Delta t, \quad t_k \le s \le t_{k+1} \tag{A .48 b}$$

$$f_M(s) = f_{M,k} \delta(s - t_k)\Delta t, \quad t_k \le s \le t_{k+1} \tag{A .48 c}$$

Substituting Equation (A. 48) into Equation (A. 47) and performing integration gives

$$z_{k+1} = e^{A\Delta t} z_k + \Delta t e^{A\Delta t} J a_k + \Delta t e^{A\Delta t} B f_{G,k} + \Delta t e^{A\Delta t} B f_{M,k} \tag{A .49}$$

Let,

$$F_d = e^{A\Delta t}, \quad J_d = e^{A\Delta t} J\Delta t, \quad B_d = e^{A\Delta t} B\Delta t$$

Then Equation (A. 49) becomes

$$z_{k+1} = F_d z_k + J_d a_k + B_d f_{G,k} + B_d f_{M,k} \tag{A .50}$$

Equation (A. 50) represents the recursive equation for calculating the seismic responses of moment-resisting framed structure considering updates on geometric nonlinearity as the axial compressive force in columns changes with time since both the equivalent force terms $f_{G,K}$ and $f_{M,k}$ in Equation (A. 50) are functions of the column axial forces at time step k.

It has been demonstrated that ignoring updates on geometric nonlinearity has resulted negligible responses. Thus, when updates on geometric nonlinearity are ignored, the $\bar{K}_G(t)$ matrix as given in Equation (A. 36) becomes $\bar{K}_G(t) = 0$. Then from the same equation, $\bar{K}_G(t) = \bar{K}_0$. Therefore from Equation (A. 44), it implies that

$$f_G(t) = 0, \quad f_M(t) = \bar{K}_0 x_d''(t)$$

Then Equation (A. 50) becomes

$$z_{k+1} = F_d z_k + J_d a_k + G_d x''_{d,k} \tag{A .51}$$

where, $$G_d = B_d \bar{K}_0 = e^{A\Delta t}\begin{bmatrix} 0 \\ M_{dd}^{-1} \end{bmatrix} \bar{K}_0 \Delta t = e^{A\Delta t}\begin{bmatrix} 0 \\ M_{dd}^{-1}\bar{K}_0 \end{bmatrix} \Delta t = e^{A\Delta t} G \Delta t$$

Equation (A. 51) represents the recursive equation for calculating the seismic responses of moment-resisting framed structure without considering updates on geometric nonlinearity as the axial compressive force in columns changes with time.

In order to perform nonlinear dynamic analysis, the governing equations of FAM (Equations (A. 32) and (A. 33)) can be represented in discretized form as:

$$m_{k+1} + \bar{K}''_{k+1}\Delta\theta'' = \bar{K}'^{T}_{k+1} x_{d,k+1} - \bar{K}''_{k+1}\theta''_k \qquad (A.52)$$

$$x''_{d,k+1} = \bar{K}^{-1}_{k+1}\bar{K}'_{k+1}\theta''_{k+1} \qquad (A.53)$$

However, the axial forces in columns at time step *k+1* is unknown, therefore the stiffness matrices in these two equations can be substituted by those at time step *k* without compromising accuracy, i.e.,

$$m_{k+1} + \bar{K}''_{k}\Delta\theta'' = \bar{K}'^{T}_{k} x_{d,k+1} - \bar{K}''_{k}\theta''_k \qquad (A.54)$$

$$x''_{d,k+1} = \bar{K}^{-1}_{k}\bar{K}'_{k}\theta''_{k+1} \qquad (A.55)$$

Moreover, if update on geometric nonlinearity is ignored, these stiffness matrices become:

$$\bar{K}_k = \bar{K}_0, \quad \bar{K}'_k = \bar{K}'_0, \quad \bar{K}''_k = \bar{K}''_0 \qquad (A.56)$$

Now Equations (A. 54) and (A. 55) become

$$m_{k+1} + \bar{K}''_{0}\Delta\theta'' = \bar{K}'^{T}_{0} x_{d,k+1} - \bar{K}''_{0}\theta''_k \qquad (A.57)$$

$$x''_{d,k+1} = \bar{K}^{-1}_{0}\bar{K}'_{0}\theta''_{k+1} \qquad (A.58)$$

Equations (A.51), (A.57) and (A.58) represent the set of equations for solving the nonlinear dynamic analysis problems when update on geometric nonlinearity is ignored.

Finally, the absolute acceleration vector $[\ddot{y}_d(t) = \ddot{x}_d(t) + \ddot{g}_d(t)]$ can be computed by simplifying Equation (A. 19) in discretized form as:

$$\ddot{y}_{d,k} = -M_{dd}^{-1} C_{dd} \dot{x}_{d,k} - M_{dd}^{-1} \bar{K}_k (x_{d,k} - x''_{d,k}) - M_{dd}^{-1} K_a x_{d,k} \quad (A.60)$$

A.7 Evaluation of energy components in structural dynamic system

Consider the dynamic equilibrium equation of motion as given in Equation (A. 34).

$$M_{dd}\ddot{x}_d(t) + C_{dd}\dot{x}_d(t) + \bar{K}(t)x_d'(t) = -M_{dd}\ddot{g}_d(t) - F_a(t)$$

Define the absolute acceleration $[\ddot{y}_d(t) = \ddot{x}_d(t) + \ddot{g}_d(t)]$

$$M_{dd}\ddot{y}_d(t) + C_{dd}\dot{x}_d(t) + \bar{K}(t)x_d'(t) = -F_a(t) \quad (A.61)$$

Putting $\bar{K}(t) = \bar{K}_L + \bar{K}_G(t)$ from Equation (A. 36), Equation (A. 61) can be rewritten as:

$$M_{dd}\ddot{y}_d(t) + C_{dd}\dot{x}_d(t) + \bar{K}_L x_d'(t) + \bar{K}_G(t)x_d'(t) = -F_a(t) \quad (A.62)$$

Integrating Equation (A. 62) over the path of displacement response gives

$$\int_0^t M_{dd}\ddot{y}_d(t)dx_d + \int_0^t C_{dd}\dot{x}_d(t)dx_d + \int_0^t \bar{K}_L x_d'(t)dx_d + \int_0^t \bar{K}_G(t)x_d(t)dx_d = -\int_0^t F_a(t)dx_d \quad (A.63)$$

Note that $dx_d = dy_d - dg_d$, Equation (A. 63) can be rewritten as:

$$\int_0^t M_{dd}\ddot{y}_d(t)dy_d + \int_0^t C_{dd}\dot{x}_d(t)dx_d + \int_0^t \bar{K}_L x_d'(t)dx_d + \int_0^t \bar{K}_G(t)x_d'(t)dx_d = -\int_0^t F_a(t)dx_d + \int_0^t M_{dd}\ddot{y}_d(t)dg_d \quad (A.64)$$

Also $dx_d = dx'_d + dx''_d$, Equation (A. 64) can be rewritten as:

$$\int_0^t M_{dd}\ddot{y}_d(t)dy_d + \int_0^t C_{dd}\dot{x}_d(t)dx_d + \int_0^t \bar{K}_L x'_d(t)dx'_d + \int_0^t \bar{K}_L x'_d(t)dx''_d + \int_0^t \bar{K}_G(t)x'_d(t)dx_d = -\int_0^t F_a(t)dx_d + \int_0^t M_{dd}\ddot{y}_d(t)dg_d \quad (A.65)$$

Equation (A. 65) shows the different components of energy in the structural system when subjected to earthquake excitation. The different terms in this equation indicate different forms of energy as:

$\int_0^t M_{dd}\ddot{y}_d(t)dy_d$ indicates Kinetic Energy of the system,

$\int_0^t C_{dd}\dot{x}_d(t)dx_d$ indicates Damping Energy of the system,

$\int_0^t \bar{K}_L x_d^{'}(t)dx_d^{'}$ indicates Strain Energy of the system,

$\int_0^t \bar{K}_L x_d^{'}(t)dx_d^{''}$ indicates Plastic Energy of the system,

$\int_0^t \bar{K}_G(t)x_d^{'}(t)dx_d$ indicates energy due to updates on geometric nonlinearity,

$\int_0^t F_a(t)dx_d$ indicates external loads which exclude seismic action induced by ground motion,

$\int_0^t M_{dd}\ddot{y}_d(t)dg_d$ indicates absolute Input Energy of the system based on ground motion.

Thus when the structure is subjected to seismic excitation, the input energy coming from ground motion is transmitted by the structure in the various forms of energy. It has been observed that large portion of input energy (~80)% has been dissipated as plastic energy (PE) with the formation of inelastic deformations at various plastic hinge locations (Wong and Zhao, 2007). The plastic energy is computed in FAM as given below:

$$PE = \int_0^t x_d^{'}(t)\bar{K}_L dx_d^{''} = \int_0^t x_d^{'}(t)K_p d\theta'' = \int_0^t m'(t)d\theta'' = \sum_{k=1}^{t_k} m_{i,k}(\theta_{i,k}^{''} - \theta_{i,k-1}^{''}) \qquad (A.66)$$

The plastic rotation θ'' in Equation (A. 66) indicates the final outcome of plastic rotation at each plastic hinge location during the time span of input ground motion, which means this permanent structural deformation θ'' incorporates both material and geometric nonlinearities. Therefore, Equation (A. 66) gives the plastic energy dissipated at each plastic hinged point of the structure due to both material and geometric nonlinearities when excited to seismic ground motion.

LIST OF PUBLICATIONS

A) CONFERENCES

1. S.S. Ningthoukhongjam, K.D. Singh (2017). Inelastic Time History Analysis of Mass Irregular Moment Resisting Steel Frame using Force Analogy Metho*d*, *Proceedings of 13th International Conference on Vibration Problems*, 29th November - 2nd December, 2017, Paper No: 244, Indian Institute of Technology Guwahati, India. (**Manuscript accepted** for publishing in "Advanced Topics in Structural Vibration" under *Lecture Notes in Mechanical Engineering* by Springer Nature, ISSN 2195-4356).

2. S.S. Ningthoukhongjam, K.D. Singh (2020). Collapse Analysis of Moment Resisting Steel Frame by Performing Nonlinear Time History Analysis using Force Analogy method. (**Abstract accepted** for *Indian Structural Steel Conference, March 25-27, 2020* at Indian Institute of Technology Hyderabad)

3. S.S. Ningthoukhongjam, K.D. Singh (2020). Building Height Effects on Nonlinear Time History Responses of Moment Resisting Steel Frame using FAM. (**Abstract accepted** for *17th World Conference on Earthquake Engineering, September 13-18, 2020* at Sendai International Center, Sendai, Japan).

A) JOURNALS

1. S.S. Ningthoukhongjam, K.D. Singh (2020). Nonlinear Time History Analysis of Moment Resisting Steel Frames Using Force Analogy Method (**Under preparation**)

2. S.S. Ningthoukhongjam, K.D. Singh (2020). Effect of Single Floor Mass Irregularity on Nonlinear Dynamic Behaviours of Moment Resisting Steel Frame using Force Analogy Method (**Under preparation**)

3. S.S. Ningthoukhongjam, K.D. Singh (2020). Interaction Effect of Multi-Floor Mass Irregularity on Nonlinear Dynamic Behaviours of Moment Resisting Steel Frame using Force Analogy Method (**Under preparation**).